CONFORMANCE IMPROVEMENT USING GELS

First Annual Technical Progress Report,
Reporting Period: September 1, 2001 through August 31, 2002

Principal Author: Randall S. Seright
                            (505) 835-5571

Report Date: September 2002

Name and Address of Submitting Organization:
            New Mexico Petroleum Recovery Research Center
            New Mexico Institute of Mining and Technology
            Socorro, New Mexico 87801

NM PRRC Contributors: Richard Schrader,
John Hagstrom II, Ying Wang, Abdullah Al-Dhafeeri, Raven Gary
PDVSA Intevep Contributor: Amaury Marin
SUNY Contributor: Brent Lindquist

PRRC Report 02-15

DISCLAIMER

This report was prepared as an account of work sponsored by an agency of the United States Government. Neither the United States Government nor any agency thereof, nor any of their employees, makes any warranty, expressed or implied, or assumes any legal liability or responsibility for the accuracy, completeness, or usefulness of any information, apparatus, product, or process disclosed, or represents that its use would not infringe privately owned rights. Reference herein to any specific commercial product, process, or service by trade name, trademark, manufacturer, or otherwise does not necessarily constitute or imply its endorsement, recommendation, or favoring by the United States Government or any agency thereof. The views and opinions of authors expressed herein do not necessarily state or reflect those of the United States Government.

DEDICATION

This report is dedicated to the memory of Tom Reid. During his time with the National Petroleum Technology Office, Tom played a very constructive part in overseeing our research. We will miss his insights, his vision, his dedication to advancing petroleum engineering, and his friendship.

ABSTRACT

This report describes work performed during the first year of the project, "Conformance Improvement Using Gels." The project has two objectives. The first objective is to identify gel compositions and conditions that substantially reduce flow through fractures that allow direct channeling between wells, while leaving secondary fractures open so that high fluid injection and production rates can be maintained. The second objective is to optimize treatments in fractured production wells, where the gel must reduce permeability to water much more than that to oil.

The placement and washout properties of formed gels in fractures were studied. Two key parameters that affect the distance of gel penetration along a fracture are the pressure gradient and the degree of water loss exhibited by the gel. The pressure gradient for gel extrusion was insensitive to injection rate, temperature, rock lithology, permeability, and character of the rock face. It varied with the square of polymer content and inversely with the square of fracture width. We now have a fairly clear understanding of the mechanism for gel propagation through fractures. Gel that dehydrates basically becomes immobile in the fracture. The only mobile gel has the same composition as the injected gel. This mobile gel forms wormholes through the concentrated gel.

We examined two promising new ideas to reduce gel washout from fractures. The first concept involved controlling gel injection rate during placement. Gels placed at lower rates experienced greater dehydration and were more resistant to washout. The second method to control gel washout involved use of secondary gelation reactions. The concept is to inject a gel that undergoes two separate crosslinking reactions. The first reaction is timed to take place before entry into the fracture—to prevent gel from entering the porous rock and yet provide low pressure gradients during extrusion. The second reaction occurs after gel placement—to strengthen the gel. Both concepts showed considerable promise during our experiments. We also found that gels in fractures can provide a significant disproportionate permeability reduction.

A Cr(III)-acetate-HPAM gel (containing 5% of a 500,000-Mw HPAM) was considered for plugging pin-hole leaks in casing. We assumed that the gel would stop flow by plugging the sand or rock just outside of the casing leak. In 9.7-20 darcy sandpacks, this gel reduced permeability to 1-2 μd. In the sandpacks, the gel withstood pressure gradients of 3,000 psi/ft with no apparent damage. Calculations indicate that this gel should allow a well to pass a casing integrity test if the gelant penetrates at least 4 inches from the wellbore into porous rock. Since the mechanical strength of the gel is much greater in porous rock than in an open channel, we make no claim about the ability of the gel to plug open channels.

We investigated the ability of an adsorption-based polymer to reduce permeability to water more than that to oil. With this polymer, a significant variability existed for oil and water residual resistance factors. As with any material used for disproportionate permeability reduction, understanding and controlling performance variability will be key to successful applications.

A methodology is presented for optimizing the volume of gelant injected in naturally fractured production wells. With this method, we demonstrated the connection between laboratory measurements and field results from the Motatan field in Venezuela. Accurate pressure drops before, during, and after gelant placement were particularly important in the methodology.

TABLE OF CONTENTS

TABLE OF FIGURES

LIST OF TABLES

ACKNOWLEDGMENTS

EXECUTIVE SUMMARY

This report describes work performed during the first year of the project, "Conformance Improvement Using Gels." This three-year research project has two objectives. The first objective is to identify gel compositions and conditions that substantially reduce flow through fractures that allow direct channeling between wells, while leaving secondary fractures open so that high fluid injection and production rates can be maintained. This goal will be reached by (1) characterizing gel propagation through fractures as a function of fracture width, length, and height, injection rate, gel composition, and temperature, (2) correlating rheology in fractures with that in a viscometer, and (3) using the experimental results to develop an appropriate model for gel placement and treatment sizing.

The second objective is to optimize treatments in fractured production wells, where the gel must reduce permeability to water much more than that to oil. Within this objective, the specific goals are to (1) determine the correct mechanism(s) for the disproportionate permeability reduction, (2) identify conditions that maximize the phenomenon, (3) find materials and methods that make the phenomenon predictable and controllable, and (4) establish a methodology to determine how much gelant should be injected in a given fractured production well.

Gel Extrusion And Washout In Fractures
In many cases where fractures are responsible for excess water production, the most effective treatment involves extruding formed gels into the fracture or fracture system. Chapter 2 describes the placement and washout properties of gels in fractures. During the placement process, two key parameters that affect the distance of gel penetration along a fracture are the pressure gradient and the degree of water loss exhibited by the gel. We characterized these properties as a function of fracture width, injection rate, gel composition, temperature, and rock properties. The pressure gradient for gel extrusion was insensitive to injection rate, temperature, rock lithology, permeability, and character of the rock face. It varied with the square of polymer content and inversely with the square of fracture width. We now have a fairly clear understanding of the mechanism for gel propagation through fractures. Gel that dehydrates basically becomes immobile in the fracture. The only mobile gel has the same composition as the injected gel. This mobile gel forms wormholes through the concentrated gel.

After formed gels are extruded into fractures, we wish to minimize gel washout when the well is returned to service. In fractures that were 1-mm wide or less, the pressure gradient for gel washout during brine injection was about the same as the pressure gradient observed during gel placement. However, in fractures wider than 2 mm, the pressure gradient for washout can be significantly less that the pressure gradient during gel placement. The mechanism of gel failure appears to involve the displacement of relatively mobile gel from wormholes. Generally, only a small fraction of the gel was displaced during the washout process. Resistance to washout can be increased by injection of more concentrated gels or by incorporation of particulate matter into the gel. However, these approaches are accompanied by significantly higher pressure gradients during the gel placement process. Also, with these approaches, the pressure gradients for washout were less than or equal to the pressure gradients during gel placement.

We examined two promising new ideas to reduce gel washout from fractures. The first concept involved controlling gel injection rate during placement. Gels placed at lower rates experienced greater dehydration and were more resistant to washout. The second method to control gel washout involved use of secondary gelation reactions. The concept is to inject a gel that undergoes two separate crosslinking reactions. The first reaction is timed to take place before entry into the fracture—to prevent gel from entering the porous rock and yet provide low pressure gradients during extrusion. The second reaction occurs after gel placement—to strengthen the gel. Both concepts showed considerable promise during our experiments.

The extrusion and washout behavior in fractures contained by strongly oil-wet polyethylene cores were not significantly different than those in strongly water-wet Berea sandstone. We also found that gels in fractures could provide a significant disproportionate permeability reduction—i.e., reducing permeability to water much more that that to hydrocarbon. This result was unexpected, since based on a limited earlier study, we believed that attaining disproportionate permeability reduction required that the gel reside in a porous medium. Consequently, these new findings will receive close examination and further testing in our future work.

Plugging Pinhole Leaks Using Gels
Many old wells exist where corrosion leads to casing leaks. For medium to large leaks, cement squeezes are commonly used for remedial treatment. However, when the leaks are very small (i.e., "pinhole leaks"), difficulty may exist in finding the holes. Also, even when the leaks are located, cement may be ineffective as a plugging agent because of difficulty in penetrating into small holes. In these cases, gelants may provide a viable alternative to cement.

Cements exhibit much greater (~1 million times greater) mechanical strength than gels. Consequently, concern exists about the ability of gels to withstand high pressure gradients when plugging casing leaks. In Chapter 3, we consider the plugging abilities of a Cr(III)-acetate-HPAM gel. The gel contained 5% Alcoflood 254S HPAM™ (nominally 500,000 MW and 5% hydrolyzed), 0.417% Cr(III)-acetate, 1% NaCl, and 0.1% $CaCl_2$. In 9.7-20 darcy sandpacks, this gel reduced permeability to 1-2 μd. In the sandpacks, the gel withstood pressure gradients of 3,000 psi/ft with no apparent damage. Calculations indicate that this gel should allow a well to pass a casing integrity test if the gelant penetrates at least 4 inches from the wellbore into porous rock. Since the mechanical strength of the gel is much greater in porous rock than in an open channel, we make no claim about the ability of the gel to plug open channels. Also, we make no judgment about potential toxicity and environmental issues that might be associated with the Cr(III)-acetate-HPAM gel (e.g., contamination of fresh-water aquifers).

Adsorption-Based Disproportionate Permeability Reduction
Adsorbed polymers have been advocated to produce a disproportionate permeability reduction. In concept, this method could provide more reproducible residual resistance factors if all water-wet surfaces became coated with a uniform layer of adsorbed polymer. Chapter 4 describes an investigation of the polymer, AquaCon™. With this polymer, a significant degree of variability exists for the oil and water residual resistance factors. The variations did not correlate with whether (a) the core was Berea sandstone or polyethylene, (b) the polymer concentration was 900 or 1,800 ppm, (c) preflushes and postflushes were used, or (d) the first fluid injected after polymer placement was oil or water. As with any material used for disproportionate permeability

reduction, understanding and controlling this performance variability will be key to the successful application of this polymer in production wells.

For most cores, the disproportionate permeability reduction was not large—F_{rrw} /F_{rro} was less than 3 for more than 80% of the cores. This level of disproportionate permeability reduction would be unacceptably low for most field applications—either in unfractured or fractured production wells. The polymer did provide acceptable ratios for F_{rrw} /F_{rro} in a few cases—leaving hope that the polymer may be valuable if a controlled disproportionate permeability reduction can be attained.

Oil and water residual resistance factors typically decreased with increased oil or water throughput. For the water residual resistance factors, evidence of washout was noted for some cores. However, washout did not adequately explain the decrease in oil residual resistance factors with increased throughput.

For a given throughput value (above 1 PV), oil residual resistance factors were similar through multiple cycles of oil and water injection (i.e., F_{rro1} and F_{rro2} values were generally similar). In contrast, the F_{rrw1} and F_{rrw2} values were similar for only half of the cores.

Gelant Treatments In Fractured Production Wells
Chapter 5 demonstrates the connection between laboratory measurements and field results from gelant treatments in production wells at the naturally fractured Motatan field in Venezuela. Using a HPAM polymer with an organic crosslinker, laboratory corefloods revealed that under reservoir conditions, the gel provided oil and water residual resistance factors of 20 and 200, respectively. This gel was placed in several production wells in the Motatan field. In Well P-47, 1,000 bbl of this gel reduced the water cut from 97% to 64% and increased the oil production rate by 36%. The success of these treatments depends on the distance of gelant leakoff from the fracture face and the *in situ* residual resistance factors in the oil and water zones. Analyses were performed to determine these parameters, based on formation permeabilities, porosities, fluid saturations, fluid properties, fluid production rates, and pressure drops before, during, and after gelant placement. Accurate pressure drops before, during, and after gelant placement were particularly important. Sensitivity studies were performed to demonstrate their significance and the impact of measurement errors. A methodology is presented for optimizing the volume of gelant injected for these applications.

XMT Studies Of Disproportionate Permeability Reduction
During recent presentations of our studies using X-ray computed microtomography, several issues were raised that we address in Chapter 6. These issues included (1) relatively high residual oil saturations in the smallest observable pores in Berea sandstone, (2) a wide range of saturations for any given pore size, (3) high coordination numbers for a few large pores, (4) capillary end effects, (5) representative elementary volumes, and tortuosity measurements.

Technology Transfer
Technology transfer efforts for the project are listed in Appendix A.

1. INTRODUCTION

On average in the United States, more than seven barrels of water are produced for each barrel of oil.[1,2] Worldwide, an average of three barrels of water are produced for each barrel of oil.[3] The annual cost of disposing of this water is estimated to be 5-10 billion dollars in the US and around 40 billion dollars worldwide.[3] Reduced water production would result directly in improved oil recovery (IOR) efficiency in addition to reduced oil production costs. A substantial positive environmental impact could also be realized if significant reductions are achieved in the amount of water produced during oilfield operations.

Fractures (either naturally or artificially induced) often cause excess water production and reduced oil recovery efficiency, especially during waterfloods and IOR projects. Fractures constitute a channeling and water production problem that has a high potential for successful treatment by gels and certain other chemical blocking agents. Especially in fractured production wells, gels can substantially diminish water production if the gel can reduce permeability to water much more than that to oil.

This report describes work performed during the first year of the project, "Conformance Improvement Using Gels."

Objectives
This research project has two objectives. The first objective is to identify gel compositions and conditions that substantially reduce flow through fractures that allow direct channeling between wells, while leaving secondary fractures open so that high fluid injection and production rates can be maintained. This goal will be reached by (1) characterizing gel propagation through fractures as a function of fracture width, length, and height, injection rate, gel composition, and temperature, (2) correlating rheology in fractures with that in a viscometer, and (3) using the experimental results to develop an appropriate model for gel placement and treatment sizing.

The second objective is to optimize treatments in fractured production wells, where the gel must reduce permeability to water much more than that to oil. Within this objective, the specific goals are to (1) determine the correct mechanism(s) for the disproportionate permeability reduction, (2) identify conditions that maximize the phenomenon, (3) find materials and methods that make the phenomenon predictable and controllable, and (4) establish a methodology to determine how much gelant should be injected in a given fractured production well.

Report Content
This report describes work performed during the first year of the project. Chapter 2 examines the placement and washout properties of gels in fractures. Chapter 3 considers the use of gels to plug pinhole leaks. In Chapter 4, we study disproportionate permeability reduction provided by a relatively new adsorption-based polymer. In Chapter 5, a field application is analyzed where disproportionate permeability reduction was utilized to reduce water production from a naturally fractured production well. Chapter 6 discusses the use of X-ray computed microtomography to identify the mechanism responsible for gels reducing the permeability to water more than that to oil. Finally, technology transfer activities are described in Appendix A.

2. GEL EXTRUSION AND WASHOUT IN FRACTURES

Gel treatments currently provide the most effective means to reduce channeling through fractures.[3-10] Except in narrow fractures, extruded gels have a placement advantage over conventional gelant treatments. To explain, during conventional gel treatments, a fluid gelant solution typically flows into a reservoir through porous rock and fractures. After placement, chemical reactions (i.e., gelation) cause an immobile gel to form. During gelant injection, fluid velocities in the fracture are usually large enough that viscous forces dominate over gravity forces.[11] Consequently, for small-volume treatments, the gelant front is not greatly distorted by gravity during gelant injection. However, after gelant injection stops, even a small density difference (e.g., 1%) between the gelant and the displaced reservoir fluids allows gravity to rapidly drain gelant from at least part of the fracture.[11] Generally, gelation times cannot be controlled well enough to prevent gravity segregation between gelant injection and gelation.

Alternative to conventional gelant treatments, formed gels can be extruded into fractures. Since these gels are 10^3 to 10^6 times mores viscous than gelants,[12] gravity segregation is much less important than for gelants. In fact, for the most successful treatments in fractured reservoirs, formed gels were extruded through fractures during most of the placement process.[4-10] This chapter examines two topics: (1) properties of formed gels during extrusion through fractures, and (2) gel washout from fractures after placement.

Gel Extrusion During Placement
The gel compositions that are used for conformance control usually contain more than 90% water—and frequently more than 99% water. For example, much of our research has focused on an aqueous gel that contained 0.5% Ciba Alcoflood 935™ HPAM (molecular weight ≈$5x10^6$ daltons; degree of hydrolysis 5% to 10%), 0.0417% Cr(III) acetate, 1% NaCl, and 0.1% CaCl$_2$. The gelation time for this formulation is about 5 hours at 41°C. In this report, we call this formulation (after aging 24 hours) our standard 1X Cr(III)-acetate-HPAM gel.

Formed Gels Dehydrate During Extrusion Through Fractures. This point is made in Figs. 1-3, which show results when the above Cr(III)-acetate-HPAM gel was aged for one day (about 5 times the gelation time) and forced through a 48x1.5x0.04-in. (1-mm wide) fracture in a 48x1.5x1.5-in. Berea sandstone core using an injection rate of 200 cm^3/hr (413 ft/d).[13] At the end of the 4-ft long fracture, a special outlet fitting segregated the effluent from the fracture and that from the porous rock. This fractured core was initially saturated with brine only. During subsequent gel injection, Fig. 1 plots the fraction of the effluent that was produced from the fracture versus from the porous rock. During the first 15 fracture volumes (700 cm^3) of gel injection, virtually 100% of the flow occurred in the fracture. This result was expected. Before gel injection, the calculated flow capacity of the fracture was 3,400 times greater than the flow capacity of the porous rock. Gel arrived at the fracture outlet after injecting 15 fracture volumes of gel. Coincident with gel arrival, flow from the fracture abruptly stopped for a period of 1 to 2 fracture volumes of gel injection. (So, 100% of the effluent was produced from the matrix during this time.) Subsequently, the fraction of flow from the fracture increased, while flow from the porous rock decreased. After injecting 80 fracture volumes of gel, flow from the fracture accounted for 65% of the total flow, while flow from the matrix accounted for 35% of the total flow.
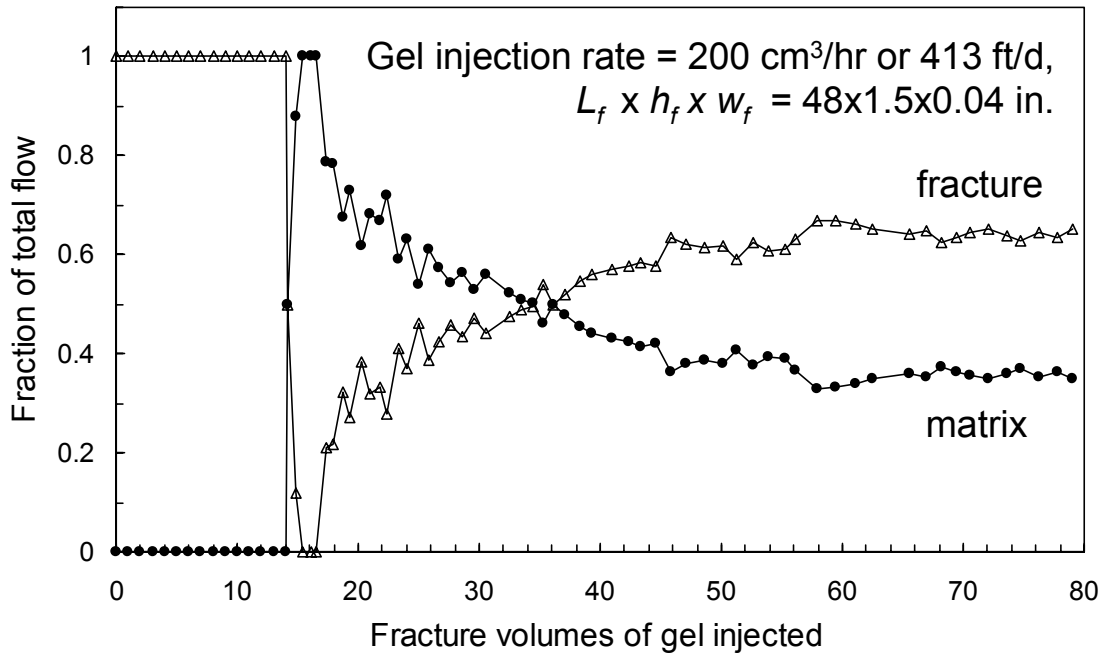
Fig. 1—Fractional flow measured at the core outlet.
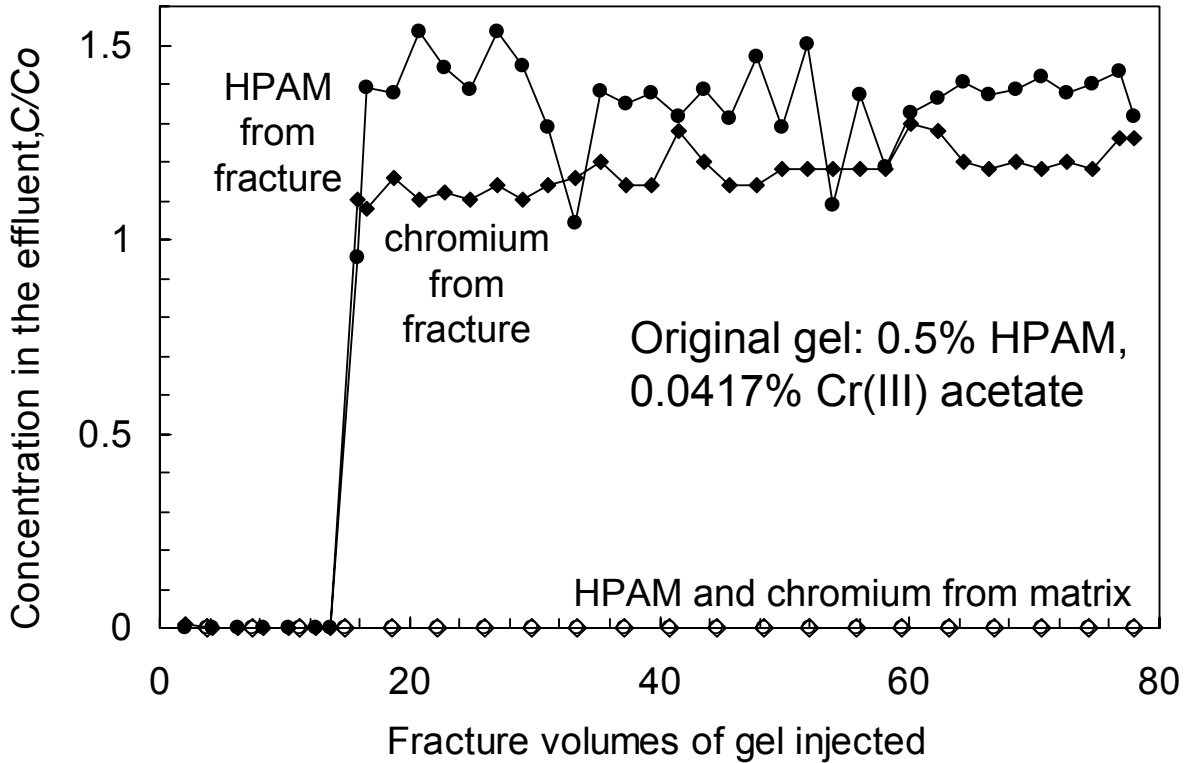
Fig. 2—Chromium and HPAM concentrations in the effluent: fracture versus matrix.
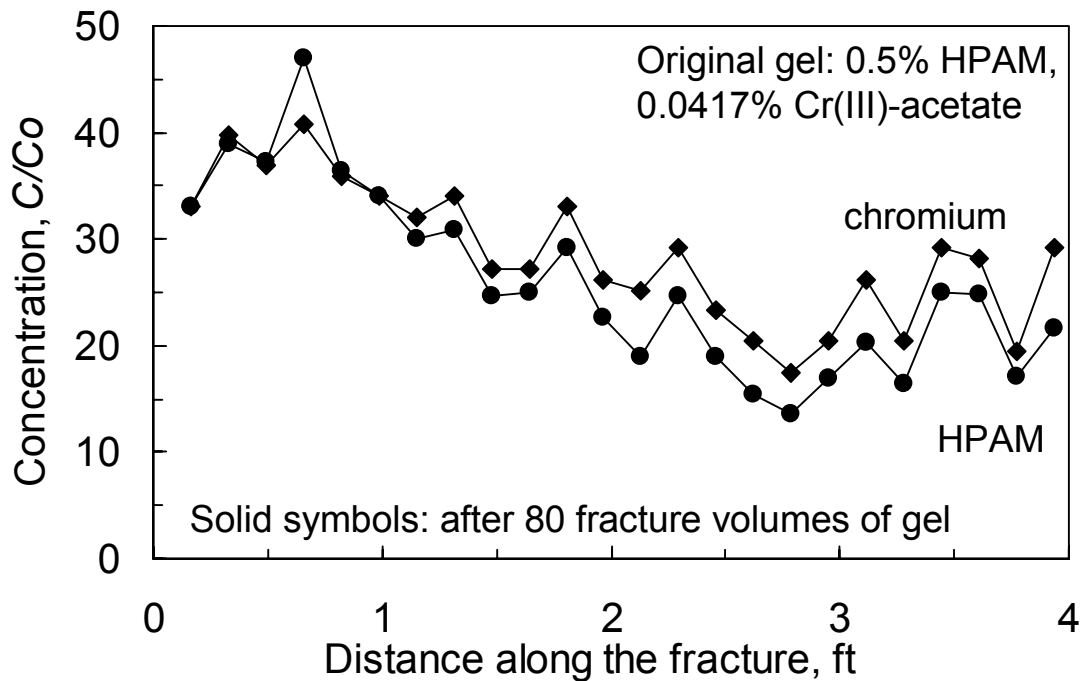
Fig. 3—Composition of gel in the fracture (relative to the injected gel).

Mobile Gel Has Basically The Same Composition As The Injected Gel. The physical appearance of the gel from the fracture outlet was the same as that of the injected gel. Also, the composition of the gel from the fracture outlet was similar to that of the injected gel. The chromium and HPAM concentrations are plotted in Fig. 2 for effluent samples from the fracture and the matrix. This figure confirms that the fracture provided the only conduit for the gel. After gel breakthrough, the chromium concentration averaged 1.17 times that of the injected gel, while the polymer concentration averaged 1.35 times that of the injected gel. Based on this and many other experiments, we conclude that the only gel that actually moves through the fracture has basically the same composition as the injected gel. Chromium and polymer concentrations for the matrix effluent were negligible.

Dehydrated Gel Is Immobile. After gel injection, the fracture was opened to reveal a rubbery gel that completely filled the fracture. This gel (after 80 fracture volumes of gel injection) was analyzed for chromium and HPAM as a function of length along the fracture (Fig. 3). The chromium and HPAM concentrations in the fracture averaged 28.7 and 26.0 times those for the injected gel, respectively. The gel became somewhat less concentrated with increased distance along the fracture. In the first 25% of the fracture, the gel was about 50% more concentrated than in the final 25% of the fracture. Since the effluent from the fracture had basically the same composition as the injected gel, we conclude that the dehydrated or concentrated gel is basically immobile. (Although we do recognize the possibility that some of the concentrated immobile gel can be eroded and produced in small quantities.)

4

Gels Do Not Flow Through Porous Rock After Gelation. This fact is demonstrated in Fig. 2. During extrusion of the formed Cr(III)-acetate-HPAM gel through the fracture, no crosslinked polymer was detected in the effluent from the matrix—only brine was produced. This behavior is advantageous since the gel is confined to the fractures—it does not enter or damage the porous rock. Thus, after gel placement, water, oil, or gas can flow unimpeded through the rock, but flow through the fracture is reduced substantially.

Useful Gels Do Not Show Progressive Plugging In Fractures. The pressure gradients required to extrude gels through fractures are greater than those for gelant flow. Depending on conditions, the effective viscosity of formed gels in fractures are typically between 10^3 and 10^6 times greater than those for gelants.[14] However, useful gels do not show progressive plugging during extrusion through fractures. This point is illustrated in Fig. 4, where 75 fracture volumes of Cr(III)-acetate-HPAM gel were extruded through a fracture using a fixed rate of 2,000 cm^3/hr (4,130 ft/d). After gel breakthrough at the end of the 4-ft long fracture, the pressure gradient was stable at 13.5 psi/ft. In other experiments with this gel, the pressure gradients sometimes showed greater variations than those illustrated in Fig. 4.[13] These variations may result from temporary gel screenouts that form and break during the extrusion process. However, in general, the pressure gradients do not steadily increase with increased time and gel throughput. This behavior is necessary to propagate gels deep into a fracture or fracture system. Of course, the presence or absence of this desirable behavior depends on the gel and the extrusion conditions. We have examined gels that do show dramatic screenouts and progressive plugging.[11]
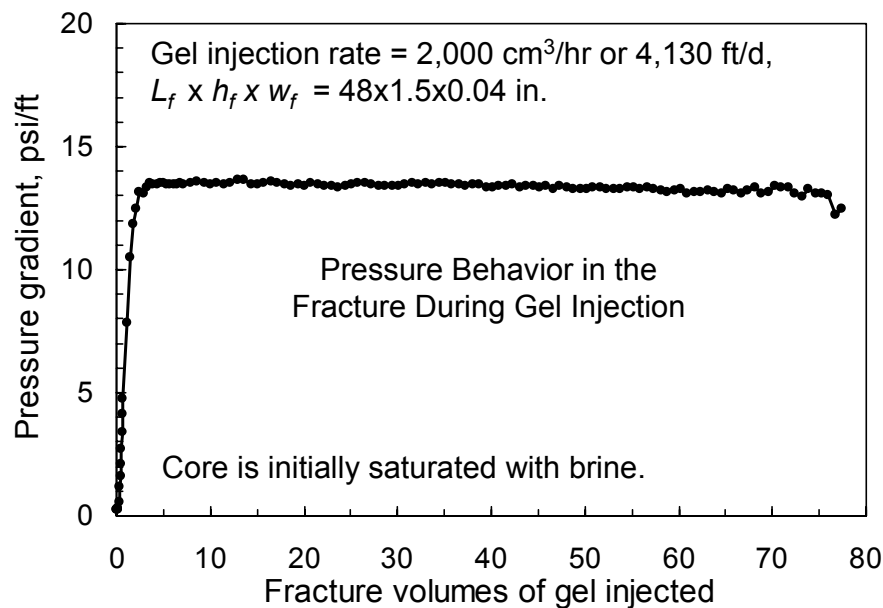
Fig. 4—Pressure gradients during gel extrusion.

Pressure Gradient Is Insensitive To Flow Rate. Previously,[11-15] we demonstrated that a minimum pressure gradient was required to extrude a given gel through a fracture. Once this minimum pressure gradient was exceeded, the pressure gradient during gel extrusion was insensitive to the flow rate. This point can be appreciated from Table 1 for extrusion experiments

with our standard one-day-old Cr(III)-acetate-HPAM gel in 48x1.5x0.04-in. (1-mm wide) fractures in 48x1.5x1.5-in. Berea sandstone cores. The average pressure gradients (Row 4 of Table 1) ranged from 18 to 40 psi/ft for estimated gel velocities ranging from 413 to 33,100 ft/d. We suspect the pressure-gradient variations in Table 1 were caused by differences in the actual fracture width rather than by velocity differences. In contrast, a Newtonian fluid would be expected to experience an 80-fold increase in pressure gradient as the fluid velocity increased from 413 to 33,100 ft/d.

Table 1—Effect of injection rate on gel propagation
during injection of 80 fracture volumes of gel.

1	Fracture dimensions ($L_f \times h_f \times w_f$)	48×1.5×0.04 in.			
2	Injection rate, cm^3/hr	200	500	2,000	16,000
3	Estimated velocity in the fracture, ft/d	413	1,030	4,130	33,100
4	Average pressure gradient, psi/ft	28	29	40	18
5	Gel front arrival at core end, fracture volumes	15	6.0	4.0	1.7
6	Average C/C_o in fracture at end of experiment	27	17	11	4

To Maximize Gel Penetration Along A Fracture, Maximize Injection Rate. The rate of gel front propagation increased significantly with increased injection rate (Row 5 of Table 1). For 413 ft/d, gel arrival at the end of a 4-ft long fracture occurred after 15 fracture volumes of gel injection. Only 1.7 fracture volumes of gel were required when the velocity was 33,100 ft/d. Evidently, the gel had less time to dehydrate as the injection rate increased. With a lower level of gel dehydration (concentration), the gel propagated a greater distance for a given total volume of gel injection. This result has important consequences for field applications. It suggests that gels should be injected at the highest practical rate in order to maximize penetration into the fracture system. On the other hand, in wide fractures or near the end of gel injection, gel dehydration may be desirable to form rigid gels that are less likely to washout after placement. In these applications, reduced injection rates may be appropriate.

Pressure Gradient Varies Inversely With The Square Of Fracture Width. For a Cr(III)-acetate-HPAM gel, the pressure gradient required for extrusion varied inversely with the square of fracture width (Fig. 5 and Eq. 1).

$$dp/dl = 0.02 / (w_f)^2,..(1)$$

where pressure gradient, dp/dl, has units of psi/ft, and fracture width, w_f, has units of inches. In contrast, a force balance during gel extrusion predicts that the pressure gradient should vary linearly with fracture width.[16] Although we have not definitively identified the origin of this behavior, we have demonstrated that it is directly linked to the extremely strong apparent shear-thinning behavior during extrusion.[16] Note from Fig. 5 that the pressure gradient for gel extrusion is not sensitive to the permeability of the rock that contains the fracture (i.e., from 1.5 to 10,000 md).
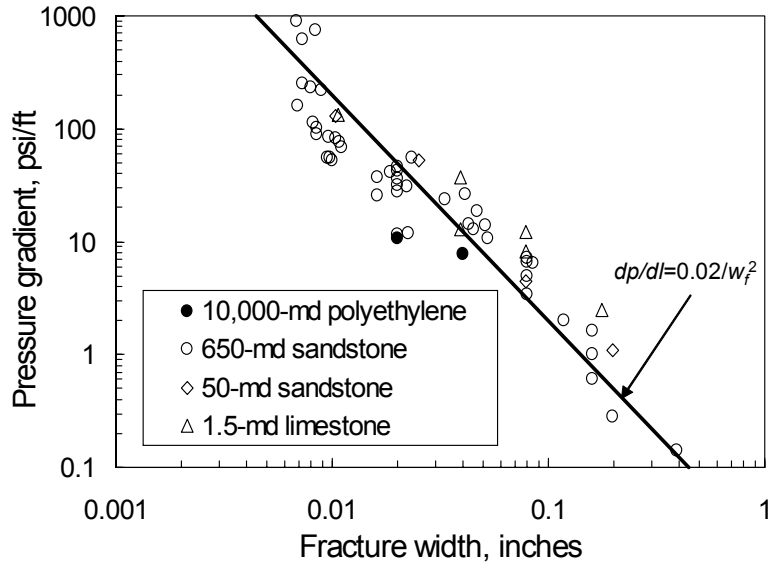
Fig. 5—Pressure gradients required for gel extrusion through open fractures.

Gel Dehydration Rate Varies Inversely With The Square Root Of Time. As mentioned earlier, the effluent from our extrusion experiments is collected both from the fracture and from the matrix. While gel is produced from the fracture, only brine is produced from the matrix. The rate of water production from the matrix divided by the total fracture area gives the rate of water leakoff (in units of leakoff volume per fracture area per time) or the rate of gel dehydration. Based on several experiments in 0.04-in. (1-mm) wide fractures, Fig. 6 shows that the gel dehydration rate for our standard Cr(III)-acetate-HPAM gel varied inversely with the square root of time. Fig. 7 shows that this same trend was followed over a wide range of conditions, including fracture widths from 0.02 to 0.16 in. (0.5 to 4 mm), fracture lengths from 0.5 to 32 ft, fracture heights from 1.5 to 12 inches, and injection fluxes from 129 to 66,200 ft/d. Although greater data scatter was observed in Fig. 7 than in Fig. 6, the average rate of gel dehydration and leakoff (u_l, in ft/d or ft^3/ft^2/d) was described reasonably well using Eq. 2.

$$u_l = 0.05 \, t^{-0.55}, \dots\dots\dots\dots\dots\dots\dots\dots\dots\dots\dots\dots\dots\dots\dots\dots\dots\dots\dots\dots\dots\dots\dots\dots\dots\dots\dots(2)$$

where t is time in days.

Time Dependence Matches Expectations From The Conventional Filtration Model. On first consideration, Eq. 2 and the solid line in Fig. 6 appears to support the conventional view of filter cake formation in hydraulic fractures—because leakoff varies with $t^{-0.5}$. The widely accepted model of filter cake formation was introduced by Carter.[17-19] It assumes that a particulate-laden fluid contacts a rock interface (i.e., a fracture face) and a pressure difference, Δp, exists between the fracture and the porous rock. As the solvent (with viscosity, μ) flows into the porous rock at a velocity, u_l, the particulates form a filter cake of permeability, k, and thickness, L. At any given time, the filtrate velocity (i.e., the leakoff rate) is given by the Darcy equation, and the thickness of an incompressible filter cake grows at a rate that is proportional to the throughput of filtrate. These assumptions lead to Eq. 3.[20]

$$u_l = [\alpha \, k \, \Delta p \, / \, (2 \, \mu)]^{0.5} \, (t - t_{exp})^{-0.5} \quad , \dots\dots\dots\dots\dots\dots\dots\dots\dots\dots\dots\dots\dots\dots\dots\dots\dots\dots\dots(3)$$

where t_{exp} is the time of first exposure to filter cake for the element of fracture face of interest and α indicates the factor by which the particulates are concentrated during the transition from the suspension to the filter cake.. The key result in Eq. 3 is that the leakoff rate is proportional to $t^{-0.5}$. This proportionality was often verified experimentally—especially during static filtration experiments.[17-19]
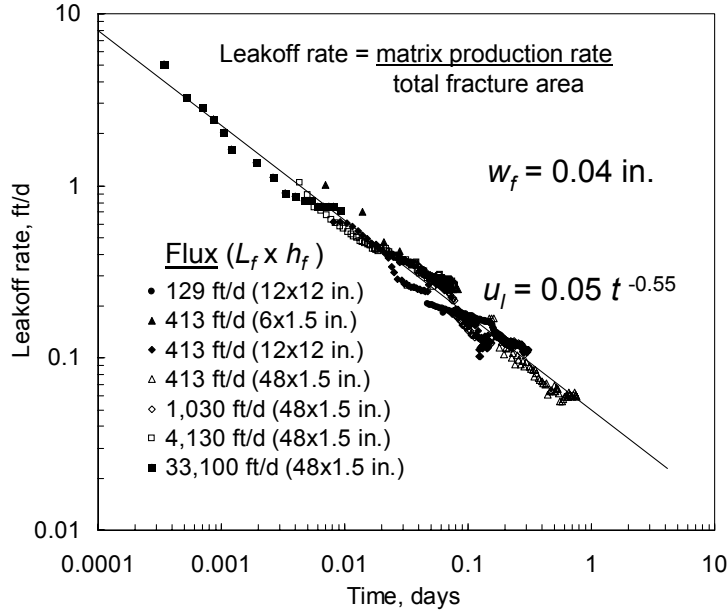
Fig. 6—Leakoff rate versus time in 0.04-in. (1-mm) wide fractures.
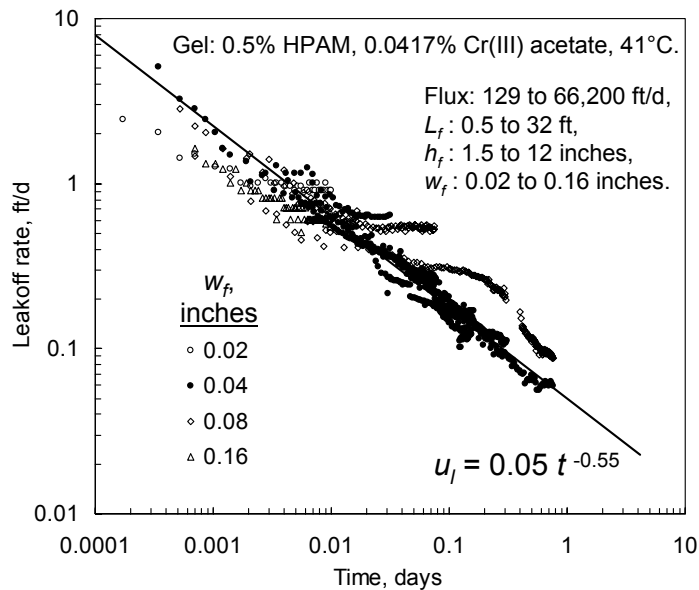
Fig. 7—Summary of leakoff data at 41°C.

Failures Of The Conventional Model. An important assumption in the development of Eq. 3 was that the thickness of the filter cake was uniform at any given time. However, our experiments revealed that fresh gel wormholed through concentrated gel—resulting in a distinctly non-uniform distribution of the filter cake on the fracture faces. Fig. 8 shows the wormhole pattern that developed during one experiment.[20] Early in the process of gel injection, the wormhole pattern was very branched, with a significant fraction of the fracture area contacted by the wormholes (as in Fig. 8).[20] As additional gel volumes were injected, the wormholes became less branched, and a diminished fraction of the fracture area was contacted by the wormholes.[20] This behavior was not surprising since the dehydrated gel became increasingly concentrated and less mobile and the mobility ratio (mobility of fresh gel divided by mobility of concentrated gel) increased with gel throughput.
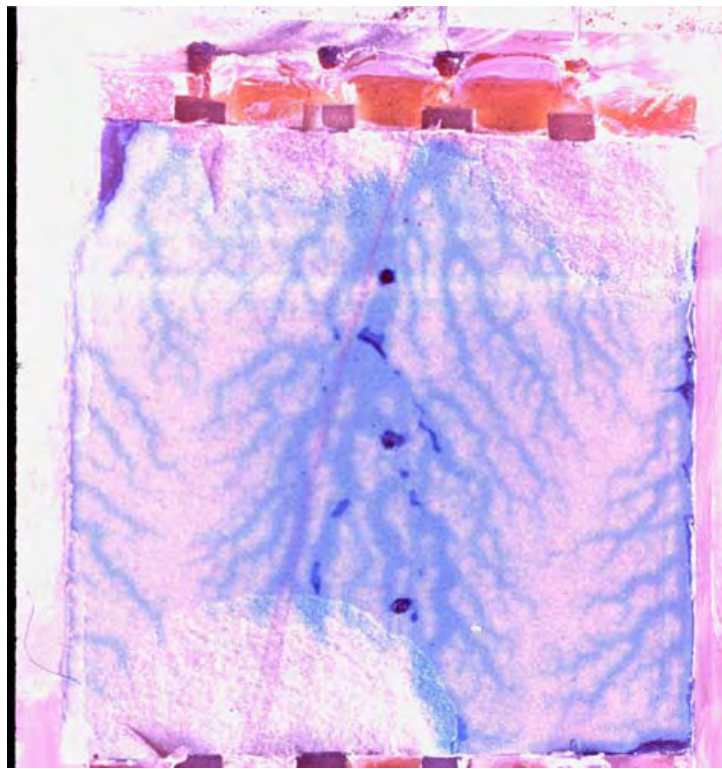
Fig. 8—Wormhole pattern.
[During dyed gel injection following gel of the same composition (not dyed). Fracture dimensions (L_f x h_f x w_f) = 12x12x0.04 in.]

A second failure of the conventional filter cake model occurs with its prediction of pressure behavior versus gel throughput. In particular, the model predicts that the filter cake on the fracture walls should uniformly increase in thickness with time—thereby decreasing the width of the active flow path in the fracture (see Fig. 9, which greatly exaggerates fracture width relative to fracture height). Since the pressure gradient required for gel extrusion increases significantly with decreased channel width (Fig. 5), the conventional model predicts that the pressure gradients during gel extrusion should increase substantially with increased time and gel throughput. Fig. 4 demonstrates that this prediction is incorrect—after gel breakthrough, pressure gradients are reasonably stable during gel extrusion.

9
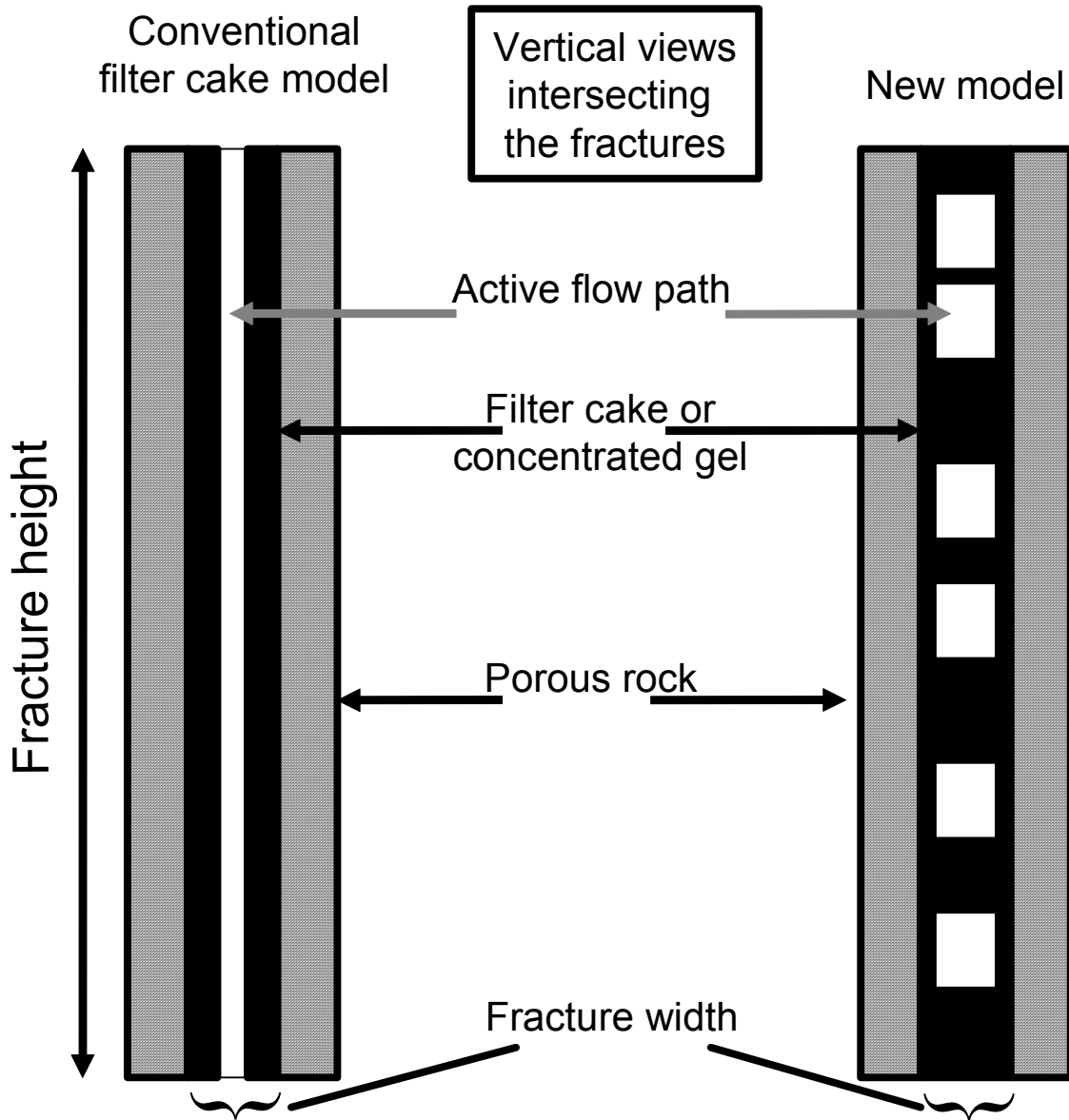
Fig. 9—Illustration of conventional filtration model versus the new model.

New Model. In view of the failures of the conventional filtration model, we developed an alternative model for filter cake formation in fractures.[20] Consistent with our experimental results, this model assumed the following:

1. Water can leave the gel and leakoff through the fracture faces, but crosslinked polymer cannot.
2. The mobile gel has the same composition as the injected gel.
3. When an element of mobile gel dehydrates, that gel becomes immobile. For a given vicinity and time, t, in a fracture of width, w_f, the average gel concentration (C/C_o, which gives the gel concentration, C, relative to the concentration for the injected gel, C_o) is

$$C/C_o = 1 + \int u_l \, dt \, / \, w_f,$$ ....(4)

where u_l is the average leakoff rate for that vicinity.

4. At a given point along the fracture, the fracture surface is covered by either mobile gel (with fractional area, A_m) or immobile gel (with fractional area, A_c) so that

$$A_m + A_c = 1$$ ....(5)

The fraction of surface that contacts mobile gel decreases with time as more immobile gel forms. Based on area and mass balances, the fractional area covered by concentrated gel at a given time and vicinity is approximated by

$$A_c = [\, C/C_o - 1 \,] / [\, C/C_o \,]^n$$ ....(6)

Presumably, as mobile gel in a wormhole dehydrates, a thin layer of concentrated gel forms at the fracture surface. However, this thin layer is continually pushed aside by the leakoff water or mobile gel, and the concentrated gel is added to the accumulation of immobile gel at the sides of the wormhole. Although we use $n=1$, Eq. 6 will work reasonably well when n has any value between 0.25 and 4 (see Fig. 10).

5. Water leakoff from immobile (dehydrated) gel (u_c) is negligible compared to that from the mobile gel (u_m). (The immobile gel continues to concentrate and lose water with time. However, this leakoff rate is small compared to that from the much more permeable mobile gel. The validity of this assumption was demonstrated in Ref. 21. Also, see Fig. 11.)

$$u_m \gg u_c$$ ....(7)

6. The mobile gel has a finite permeability to water (k_{gel}) that provides a fixed local leakoff flux (u_m) for the fracture surface that is in direct contact with mobile gel (i.e., the wormhole area that is in contact with the fracture faces).

$$u_l \approx A_m \, u_m$$ ....(8)

Combining Eqs. 4 to 8 yields Eq. 9, which is the basis of the new model. The model predicts the leakoff rate (i.e., the rate of gel dehydration) at a given time and distance along the gel-contacted portion of a fracture.

$$u_l = u_m / [1 + \int u_l \, dt \, / w_f \,]$$ ....(9)

The denominator of Eq. 9 reflects the rate of loss of fracture surface that is contacted by mobile gel (i.e., the wormhole-contact area). For our 24-hr-old Cr(III)-acetate-HPAM gel, u_m has a value around 4 ft/d, which translates to a k_{gel} value around 1 md. The latter value was confirmed from independent experiments.[22] The fraction of the fracture area that was contacted by concentrated gel versus time is plotted in Fig. 12. This plot indicates that after 0.0007 days (1 minute) of gel contact, at least 50% of the fracture face is covered by concentrated gel rather than fresh gel. Within 0.02 days (30 minutes) of gel contact, more than 90% of the fracture face is covered by concentrated gel.
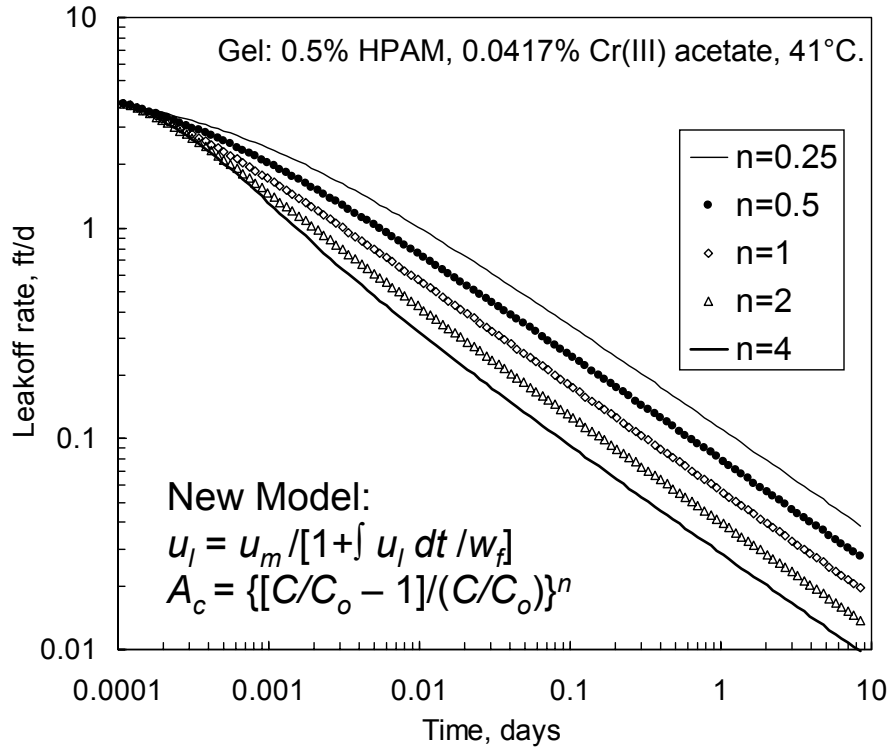
Fig. 10—Effect of exponent, n, in Eq. 6.

New Model:
$$u_l = u_m / [1 + \int u_l \, dt / w_f]$$
$$A_c = \{[C/C_o - 1]/(C/C_o)\}^n$$

Gel: 0.5% HPAM, 0.0417% Cr(III) acetate, 41°C.
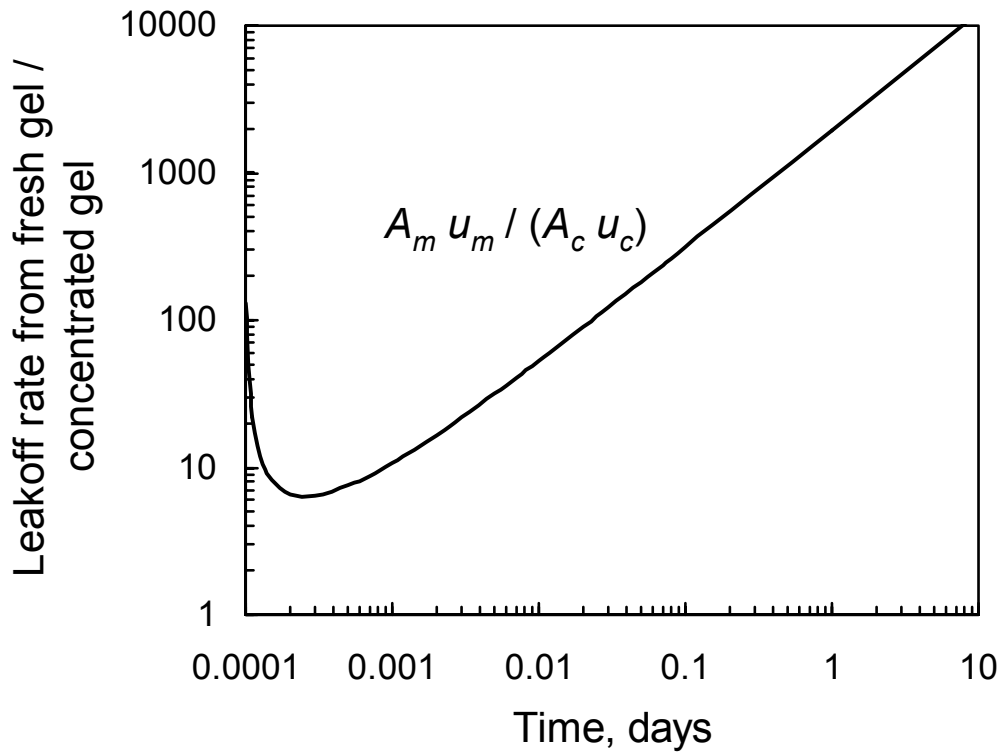
Fig. 11—Leakoff from mobile gel relative to concentrated gel.

$$A_m u_m / (A_c u_c)$$
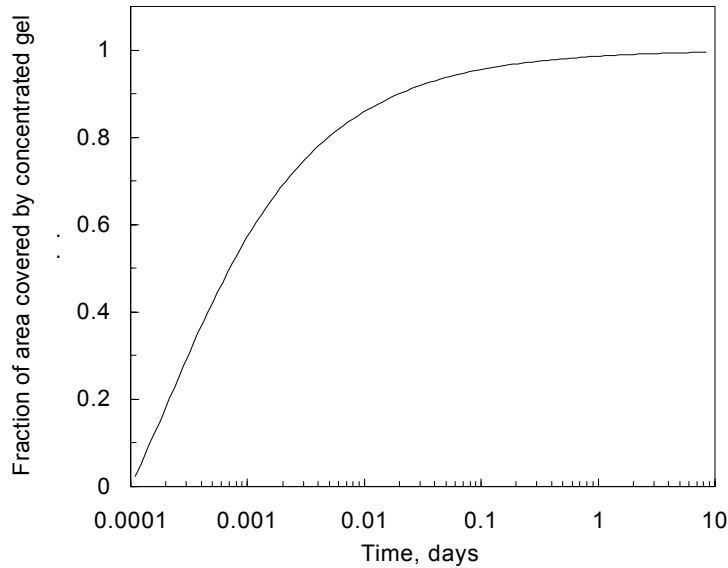
Fig. 12—Predictions of fraction of fracture area contacted by concentrated gel.

Leakoff predictions using Eq. 9 are plotted in Fig. 13 for four fracture widths from 0.02 to 0.16 in. (0.5 to 4 mm). The lowest solid line shows the prediction for 0.02-in. wide fractures, while the curves associated with the wider fractures shift to progressively larger leakoff rates (i.e., are shifted to the right). The predictions are not perfect but still match the experimental data (especially for the 0.04-in. (1-mm) wide fractures) quite well, considering that Eq. 9 was derived strictly from mechanistic considerations.
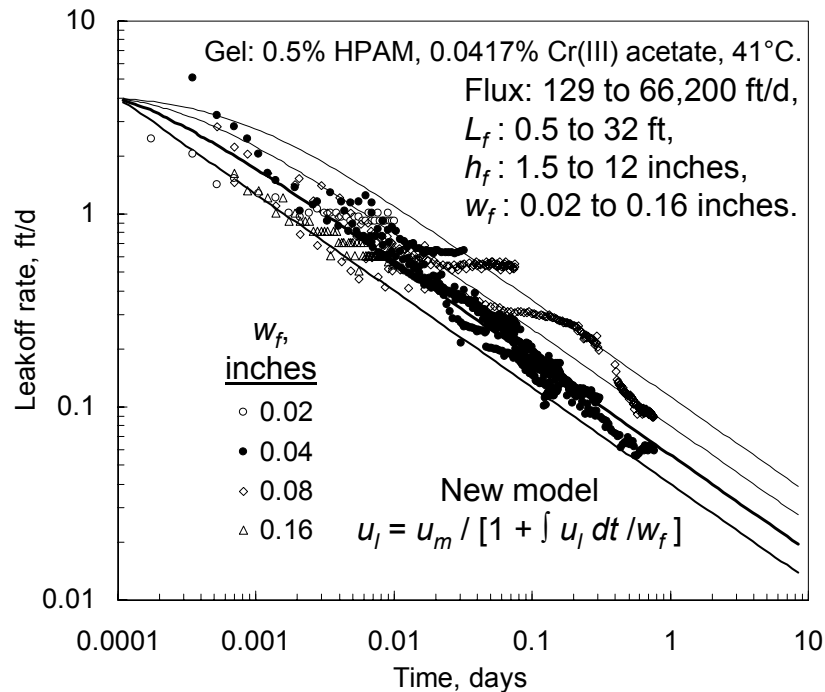
Fig. 13—Leakoff predictions for the new model.

13

Model Differences. The predicted rate of leakoff versus time is about the same for both the new model and the conventional filtration model (Figs. 6, 7, and 13). However, the two models are basically different and predict different behavior for several important properties. In the conventional model, the thickness of the filter cake is areally uniform (at least locally); the entire fracture area continually experiences leakoff; and the leakoff rate decreases because of a steady growth in thickness of the filter cake. In the new model, the filter cake is areally heterogeneous; leakoff is significant only on the fracture area that is contacted by wormholes; and the global leakoff rate decreases because of a continual loss of fracture area that is contacted by wormholes. As mentioned earlier, our observations of wormhole behavior during gel extrusion through fractures is consistent with the new model, but inconsistent with the conventional filter cake model.

In the conventional model, a single opening to flow exists that has a width that is equal to the fracture width minus twice the thickness of the filter cake at that point. The height of this opening is basically as high as the fracture. Thus, the flow opening is extremely high and narrow. In contrast, in the new model, for a given distance along the fracture, multiple flow channels exist (corresponding to the wormholes), the width of each channel could be only slightly less than the original fracture width, and the "height" of each channel is small compared to the total fracture height (but generally large compared to the fracture width). As mentioned earlier, the conventional model incorrectly predicts that the width of the active flow path in the fracture decreases with increasing gel throughput (left side of Fig. 9) so that pressure gradients increase significantly with time. In contrast, in the new model, the width of the active flow path stays fairly constant with gel throughput and time (right side of Fig. 9), so the pressure gradient is independent of throughput and time—which is consistent with observations (Fig. 4).

The two models predict significantly different flow and leakoff patterns and shear rates and stress levels within a fracture. These differences have important consequences for erosion of the filter cake, propagation of gels and particulates along fractures, transmission of pressures along fractures, fracture extension, and gel washout after placement. For a fixed pressure gradient, the new model predicts higher shear rates and shear stresses at the wall and much higher average fluid velocities than the conventional model.[20] Consequently, greater erosion of the filter cake is predicted in the new model than in the conventional model.

Potential Use In Hydraulic Fracturing. We wondered whether our new model might be a viable alternative to the conventional filter cake model used in hydraulic fracturing. As mentioned, the new model quantitatively described leakoff for Cr(III)-acetate-HPAM gels quite well over a wide range of conditions. We examined whether the new model would work as well for a guar-borate gel that was commonly used during hydraulic fracturing. The gel (components provided by Prentice Creel of Halliburton) contained 0.36% guar, 0.018% $NaBO_2$, 0.24% tallow soap, and 0.1% surfactant. This gel was aged for 1 day at 40°C and injected at 4,130 ft/d through a 6-in. long, 0.04-in. wide fracture. The experimental leakoff rates (Fig. 14) were matched very well using our new model, even though the new model was developed to match the behavior of Cr(III)-acetate-HPAM gels.

14
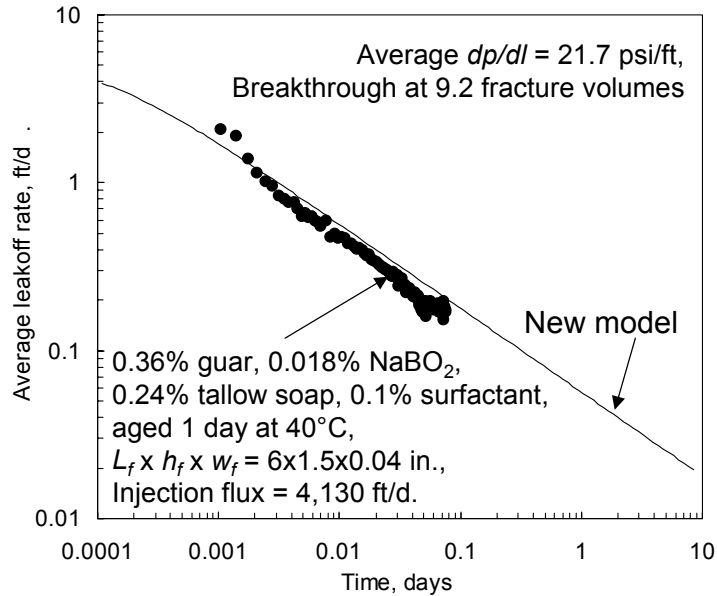
Fig. 14—Leakoff results for a guar-borate gel.

Of course, the time dependence of leakoff behavior in Fig. 14 does not prove that the new model is superior to the conventional model for guar-borate gels. Consequently, we performed an extrusion experiment using the guar-borate gel in a fracture where L_f x h_f x w_f = 12x12x0.04 in. After performing an experiment similar to that associated with Fig. 8, the fracture was opened to view the wormhole pattern in Fig. 15. The presence of these wormhole patterns are consistent with our new model and inconsistent with the conventional filter cake model.
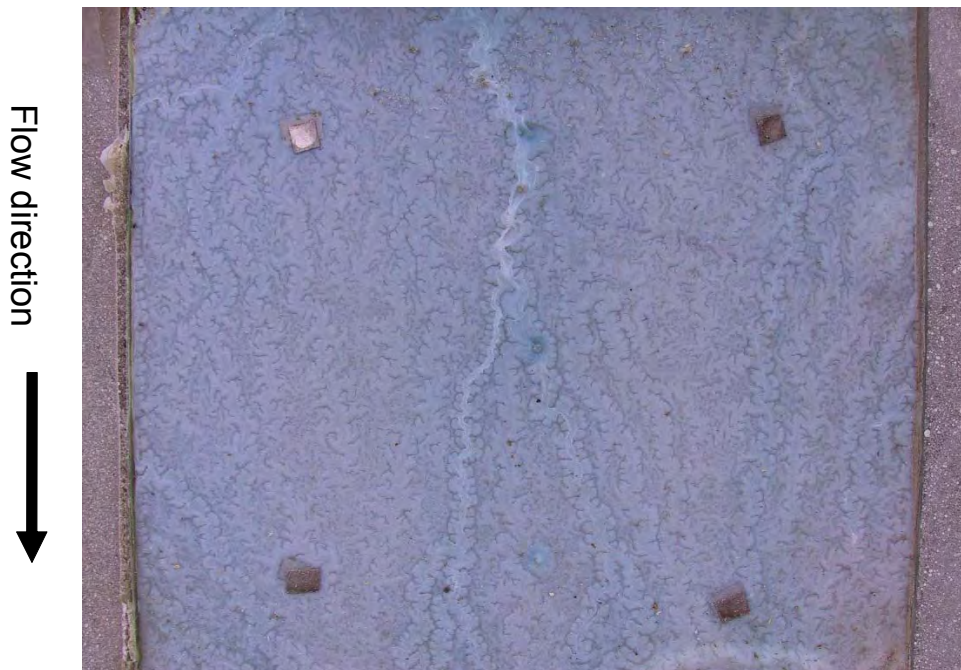
Fig. 15—Wormhole pattern for a guar-borate gel.

Phenol-Formaldehyde-HPAM Gel. We also examined the behavior of a phenol-formaldehyde-HPAM gel. This gel contained 0.51% phenol, 0.74% formaldehyde, and 1.57% HPAM, in a brine that contained 0.3% total dissolved solids. The gelant was prepared at room temperature and then aged for 5 days at 110°C. Then at 40°C, the gel was extruded through a fractured Berea sandstone core that was 6-in. long and 1.5-in. in diameter. Four separate experiments were performed (using four different fractured cores). In two experiments, the fracture width was 0.04-in. (1-mm), while the fracture width was 0.08-in. (2-mm) in the other two experiments. For each fracture width, a high-rate and a low-rate experiment were performed, with the two rates differing by a factor of 10. Fig. 16 shows the leakoff behavior during these four experiments. The leakoff data roughly followed the predictions from the new Cr(III)-acetate-HPAM model, but significant deviations were noted, especially for the high-rate experiments.
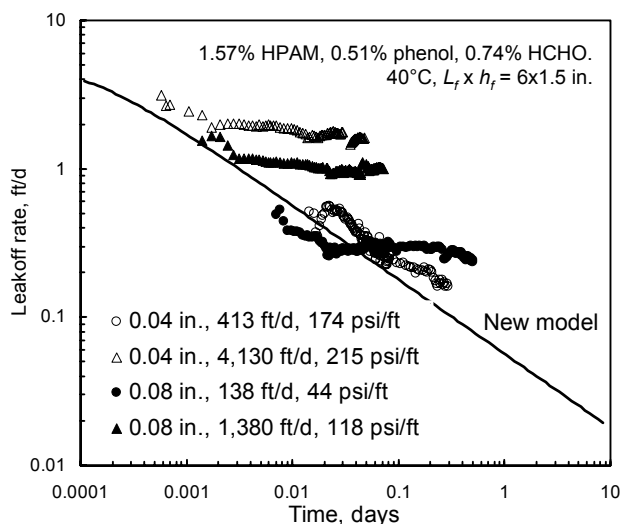
Fig. 16—Leakoff results for a phenol-formaldehyde-HPAM gel.

For the experiments in 0.04-in. wide fractures, the pressure gradient at 4,130 ft/d was only 24% greater than at 413 ft/d (215 versus 174 psi/ft). Thus, consistent with the Cr(III)-acetate-HPAM experiments results, the pressure gradient appeared insensitive to flow rate. However, for the phenol-formaldehyde-HPAM gels in the wider fractures, a greater sensitivity to flow rate was observed. Additional work is needed to characterize this behavior.

Effect Of Temperature. Most of our experiments to date were performed at 41°C. Of course, many reservoirs and field applications exist at other (mostly higher) temperatures. Therefore, a need exists to determine gel extrusion and dehydration properties at other temperatures. Using temperatures ranging from 20°C to 80°C, extrusion experiments were performed using 650-md Berea sandstone cores that had lengths of either 6 or 48 in. (15 or 122 cm). In each case, the fracture width was 0.04 in. and the fracture height was 1.5 in. (3.9 cm). We used our standard Cr(III)-acetate-HPAM gel (0.5% Alcoflood 935 HPAM, 0.0417% Cr(III) acetate) that was aged for 24 hours at 40°C before injection. The fractured core was equilibrated at the test temperature well before gel injection started. During injection of 3.7 liters of gel, the rate was fixed at 2,000 cm^3/hr—translating to a flux in the fracture of 4,130 ft/d. Leakoff results from six sets of experiments are shown in Fig. 17. This figure shows that the leakoff behavior was not sensitive to temperature between 20°C and 80°C.
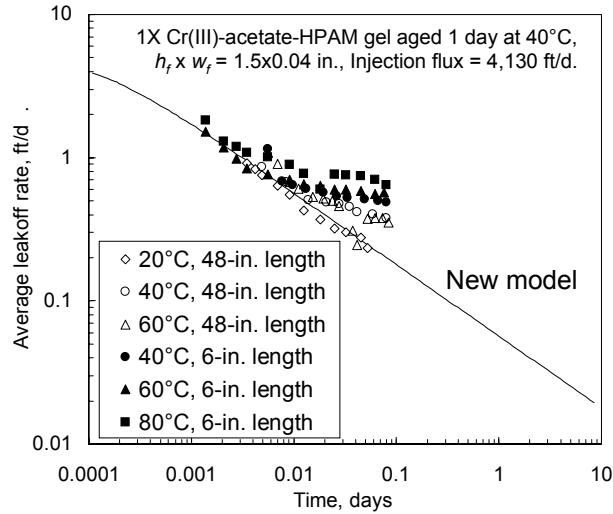
Fig. 17—Effect of temperature on leakoff results for a Cr(III)-acetate-HPAM gel.

For times shorter than 0.01 days (15 minutes), the leakoff data were very consistent with the predictions from our new leakoff model (solid curve in Fig. 17). For times longer than 0.01 days, the leakoff results exceeded the predictions associated with the new model, especially for the shorter cores. We suspect that this deviation was an artifact associated with the use of short fractures. In particular, some of the concentrated gel may be dislodged and produced from short fractures—thus, permitting greater wormhole-fracture surface areas and higher leakoff rates for longer time periods. In longer fractures, the effect was less noticeable, although some deviation was noted at 40°C and 60°C (see Fig. 17).

The pressure gradients during gel extrusion were insensitive to temperature for these experiments (see Fig. 18). The elastic modulus (G') of this gel was also independent of temperature.[16] In contrast, the viscosity of water decreased by a factor of approximately 3 as temperature increased from 20°C to 80°C.
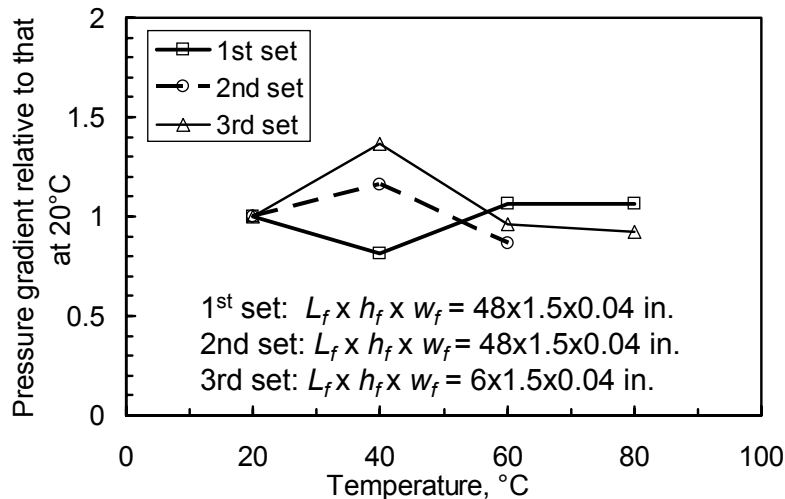
Fig. 18—Effect of temperature on pressure gradients for a Cr(III)-acetate-HPAM gel.

17

Effect Of Gel Composition. Experiments were performed to investigate how gel extrusion and dehydration vary with gel composition. Most of our previous work used our "1X" gel that contained 0.5% HPAM, 0.0417% Cr(III) acetate, 1% NaCl, and 0.1% $CaCl_2$. However, we also tested a series of five compositions, including 1X, 1.5X, 2X, 2.5X, and 3X Cr(III)-acetate-HPAM gels. The multiplier refers to the HPAM and chromium concentrations relative to those in our standard 1X gel. In all cases, the HPAM/Cr(III)-acetate ratio was fixed at 12/1, and the gels were aged for one day at 40°C before injection at 4,130 ft/d (2,000 cm^3/hr) into 6-in. long, 1.5-in. diameter Berea sandstone cores that each contained a 0.04-in. wide fracture. Because high-pressure gradients were anticipated during extrusion of the concentrated gels, we used 6-in. long cores that were cast in a metal alloy. Our 48-in. long cores (that were cast in epoxy) would not withstand the required pressures.

Leakoff results from these five experiments are plotted in Fig. 19. Interestingly, the gels showed similar leakoff behavior. Predictions from the new model matched the leakoff results quite well for times less than 0.01 days. However, for longer times, the leakoff results exceeded the predictions. As mentioned earlier, this deviation may be an artifact associated with the use of short fractures.
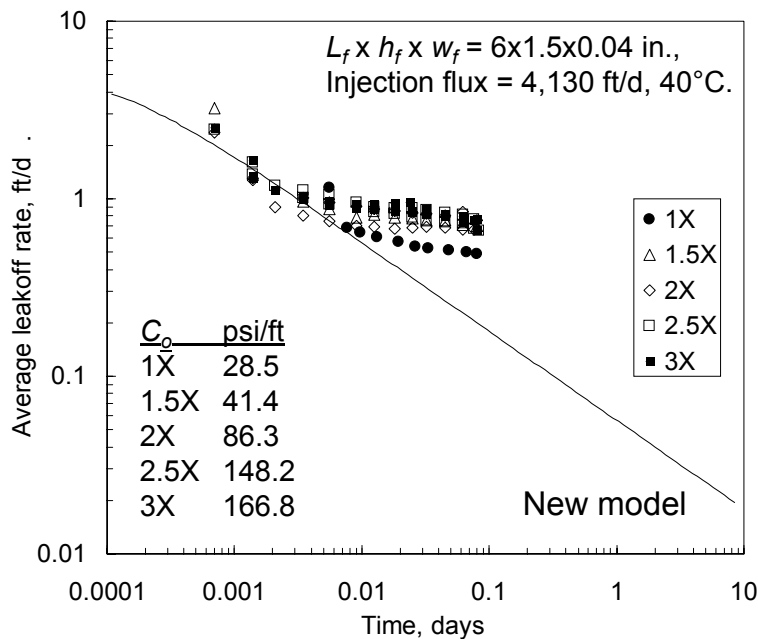
Fig. 19—Effect of composition on leakoff results for a Cr(III)-acetate-HPAM gel.

Pressure gradients during gel extrusion for the five experiments are plotted using solid circles in Fig. 20. This figure also plots the quantity, $2G'/w_f$, using open circles. The elastic modulus, G', was measured over a range of gel compositions using a Paar-Physica Model UDS 200 Dynamic Spectrometer.[16] Based on a force balance, the quantity, $2G'/w_f$, should predict the pressure gradient required to extrude a gel through a fracture of a given width.[16] Fig. 20 reveals that this force-balance approach typically under-predicts the pressure gradient by a factor of 87. Thus, more work is needed to relate rheological measurements to our extrusion results. However, the

G' measurements paralleled the extrusion pressure gradients when plotted versus gel composition. In Fig. 20, $2G'/w_f$ increased with $e^{2.27\%HPAM}$ (where %HPAM indicates the HPAM concentration in the gel). Also, for the lower four gel compositions (1X to 2.5X), the pressure gradient for gel extrusion also varied with $e^{2.27\%HPAM}$.
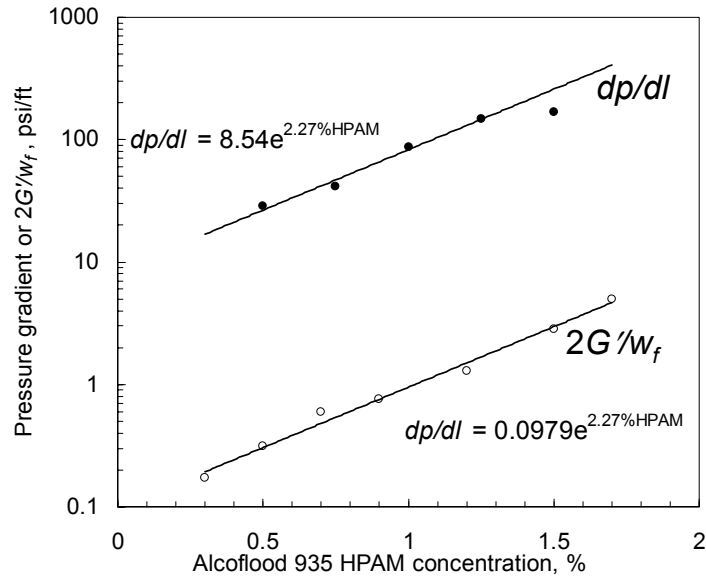
Fig. 20—Effect of composition on pressure gradients for a Cr(III)-acetate-HPAM gel.

Gel Washout From Fractures

In many field applications, gel treatments were less effective than expected in reducing water production from fractured wells. Concern exists about the ability of gels to resist washout after placement. During brine flow after gel placement in a fracture, what pressure gradient is needed to re-mobilize the gel? To address this question, several experiments were performed where brine was injected at various rates after gel placement. In all cases, the core material was 650-md Berea sandstone, with a fracture placed lengthwise down the middle of each core. In each fractured core, 3.7 liters of one-day-old Cr(III)-acetate-HPAM gel were injected using a rate of 2,000 cm³/hr (4,130 ft/d). After gel placement, the core was shut in for one day. (These experiments were performed at 41°C.) Next, brine was injected at a low rate (e.g., 206 ft/d or 100 cm³/hr). A steady state was quickly established, and the pressure gradient was recorded. Then the brine injection rate was doubled, and the measurements were repeated. This process was repeated in stages up to a final brine injection rate of 16,000 cm³/hr (33,000 ft/d). Then the brine injection rate was decreased in stages.

Representative results were obtained using our standard 1X gel in a fracture with a width of 0.04 in. To a first approximation, the pressure gradient for gel failure was the pressure gradient for gel extrusion through the fracture. The solid circles in Fig. 21 show that during gel injection (at 4,130 ft/d effective velocity in the fracture or 2,000 cm³/hr), the pressure gradient rapidly rose to 17 psi/ft during the first 0.7 fracture volumes of gel injected. Thereafter, the pressure gradient was fairly stable during the course of injecting another 80 fracture volumes of gel. When brine

was subsequently injected (at 206 ft/d or 100 cm³/hr), the pressure gradient rapidly increased to 16 psi/ft within 0.6 fracture volumes. Thereafter, the pressure gradient dropped sharply, ending at 1.8 psi/ft after injecting 3 fracture volumes of brine.
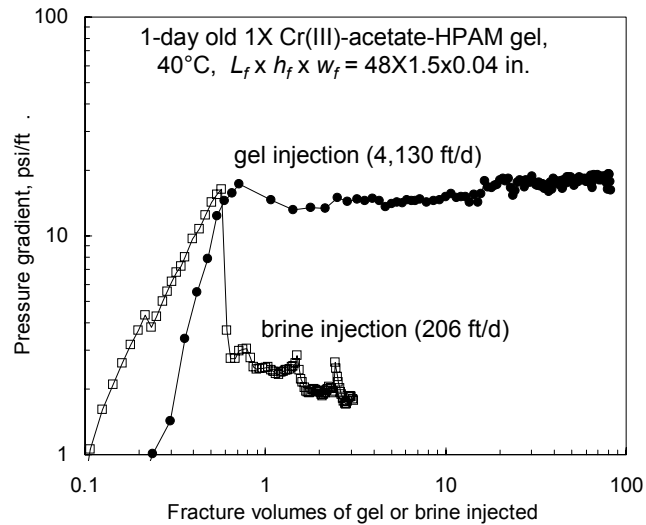
Fig. 21—Pressure gradients during gel versus brine injection.

Presumably, the gel in the wormholes provided the point of failure during brine injection. This presumption was qualitatively consistent with the pressure gradients noted near the end of brine injection. Standard calculations for laminar flow of brine in tubes or slits[23] (coupled with the brine pressure gradients and flow rates) suggested that only about 10% of the gel washed out during brine injection. In contrast, if the entire gel mass had washed out, the brine pressure gradients should have been lower by a factor of 7,000. Also, at the end of the experiment (i.e., after the rate studies described below), the fracture was opened—revealing that most of the fracture was filled with concentrated gel.

The pressure gradients during brine injection at other rates are shown in Fig. 22. The open circles show the maximum pressure gradients (at a given rate), when the rates were increased in stages. Note that the maximum pressure gradient decreased for the first three rates in the sequence, and then the pressure gradients consistently rose for the higher rates. Presumably, brine displaced gel in the wormholes during brine injection at the lowest rate (Fig. 21). For the next two rate increases, significant additional erosion of the gel occurred. For subsequent rate increases, gel erosion was less significant, although some probably occurred. During brine injection at 4,130 ft/d (2,000 cm³/hr), the maximum pressure gradient was 26% less than the average pressure gradient during gel injection at the same rate (solid square in Fig. 22).

The solid circles in Fig. 22 show the maximum pressure gradients when the rates were decreased in stages. At the final rate of 413 ft/d, the maximum pressure gradient was 1.7 psi/ft—much lower than the 9.0 psi/ft value noted at the same rate for the increasing rate part of the sequence.

The open diamonds in Fig. 22 show the average pressure gradients when the rates were increased in stages. The solid diamonds show the average pressure gradients when the rates were decreased

in stages. As expected, for both curves, the pressure gradients increased monotonically with increased rate. Exposure to the increasing/decreasing rate cycle caused the average pressure gradient at 413 ft/d (200 cm^3/hr) to decrease by 50% (from 2.4 to 1.2 psi/ft).
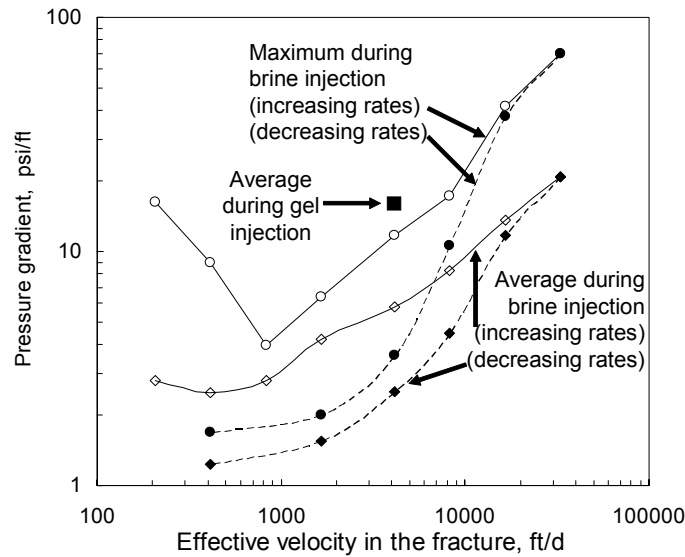
Fig. 22—Pressure gradients during brine flow at various rates.

Of course, the objective of this kind of gel treatment is to dramatically reduce the flow capacity of the fracture so that fluid will flow instead through the porous rock. During brine injection after gel placement, Fig. 23 plots the percent of the brine flow through the fracture versus through the matrix. At the first (and lowest) rate (206 ft/d or 100 cm^3/hr), 100% of the flow occurred in the matrix, so the fracture was effectively plugged. Unfortunately, at higher rates (i.e., after the gel plug experienced some washout), most flow occurred through the fracture. The gel substantially reduced the flow capacity of the fracture throughout the various brine injection stages—by a factor greater than 500 even at the highest flow rate. However, this fact may seem of minor consolation since the fracture still dominated the flow capacity of the system.
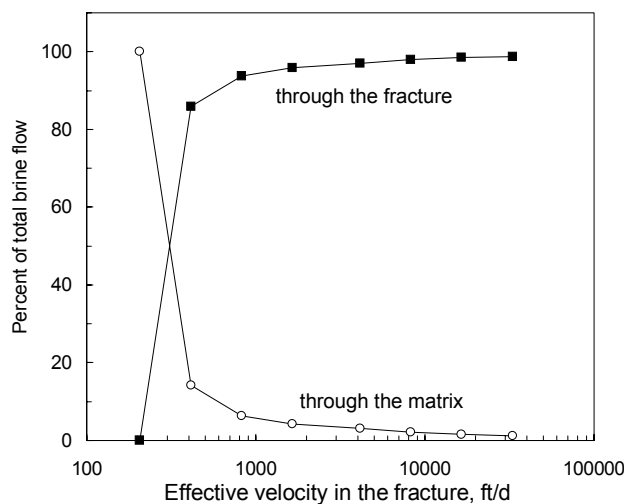
Fig. 23—Brine flow through fracture versus matrix.

Figs. 21-23 indicate that the greatest damage to the gel occurred during the first exposure to a pressure gradient similar to that during gel injection. Certainly, exposure to larger pressure gradients caused additional damage to the gel. However, the incremental damage was less severe than that after the first large pressure pulse (Fig. 21). This behavior is consistent with gel of the original composition being washed out from wormholes. Presumably, larger pressure gradients were required to erode the more concentrated gel.

Guar-Borate Gel. A similar washout experiment was performed after placing the guar-borate gel in the core that was described earlier. During gel injection (Fig. 24), the pressure gradient rose to a value of 51 psi/ft (at 12 fracture volumes), followed by a gradual decline to 30 psi/ft after 100 fracture volumes of gel. During brine injection, the peak pressure gradient of 1.2 psi/ft was reached at 0.8 fracture volumes, and a dramatic decrease in pressure gradient occurred at 16 fracture volumes of brine. Thus, the guar-borate gel washed out of the fracture much easier than the 1X Cr(III)-acetate-HPAM gel. This behavior may be desirable for hydraulic fracturing since "fracture clean-up" is important in these applications. In contrast, the greater resistance to washout exhibited by the Cr(III)-acetate-HPAM gel is more desirable for water shutoff applications. Nonetheless, increased resistance to washout is needed for these gels.
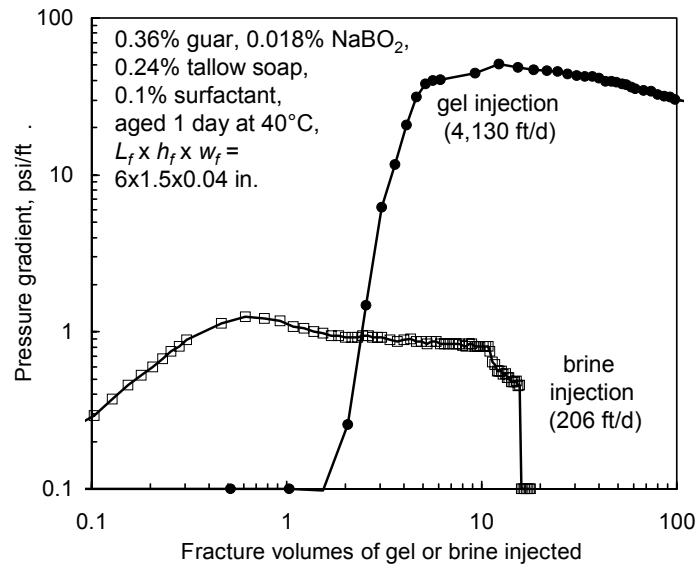
Fig. 24—Gel placement and washout for a guar-borate gel.

Phenol-Formaldehyde-HPAM Gel. Washout experiments were also performed for the phenol-formaldehyde-HPAM gels that were associated with Fig. 16. After gel placement for each of these experiments, brine was injected to determine the washout behavior. Figs. 25 and 26 show the results for the 0.04-in. (1-mm) wide fractures—for the 413-ft/d and 4,130-ft/d gel placement rates, respectively. Consistent with the behavior for the Cr(III)-acetate-HPAM gels, washout for the phenol-formaldehyde-HPAM gels occurred at pressure gradients that were at or below the pressure gradient exhibited during gel placement. We noted that the peak pressure gradient during brine injection was higher when the gel was placed at 413 ft/d (Fig. 25) than when placed at 4,130 ft/d (Fig. 26).

22
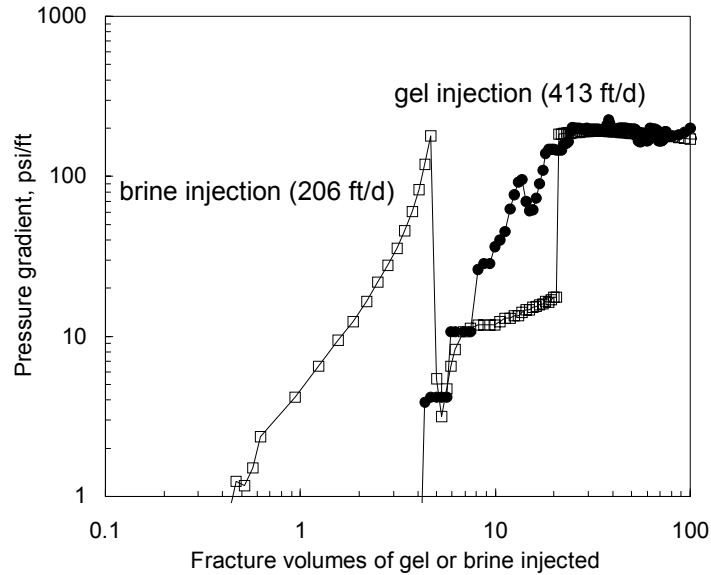
Fig. 25—Washout for phenol-formaldehyde-HPAM gels, 413 ft/d.
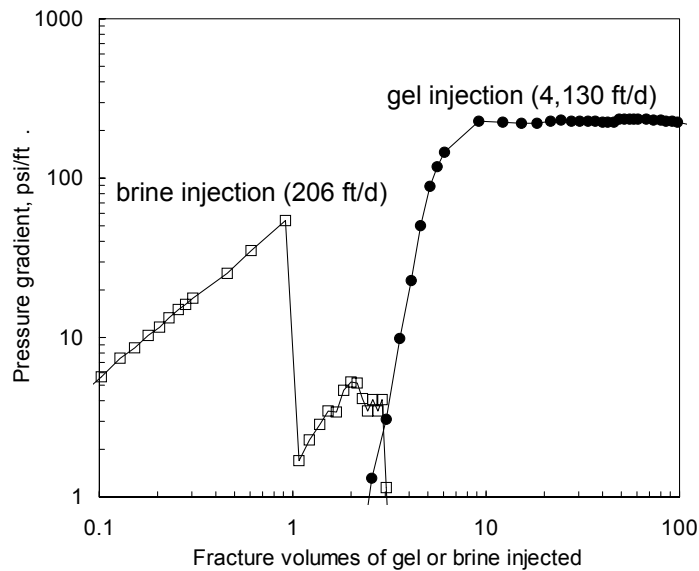
Fig. 26—Washout for phenol-formaldehyde-HPAM gels, 4,130 ft/d.

Effect Of Fracture Width. Experiments were performed (using Cr(III)-acetate-HPAM gels) to examine how gel washout was affected by fracture width. The effects of fracture width are show in Fig. 27 for 0.5- and 1-mm wide fractures in 122-cm (4-ft) long cores and in Fig. 28 for 1-, 2- and 4-mm wide fractures in 15-cm (6-in) long cores. In these figures, the *y*-axis plots the final core permeability relative to the permeability of an unfractured core. A *y*-value of unity or less means that the fracture was basically "healed." As the *y*-value increased above unity, the fracture became more open or conductive—indicating a greater degree of gel washout. The *x*-axis plots the maximum pressure gradient observed during brine injection at a particular rate (i.e., using the

brine injection sequence described in Fig. 22). The pressure gradients where dramatic increases in permeability occurred (i.e., washout) were generally similar to or less than the pressure gradients observed during gel placement.[20] As expected, the gel's resistance to washout increased with decreased fracture width.
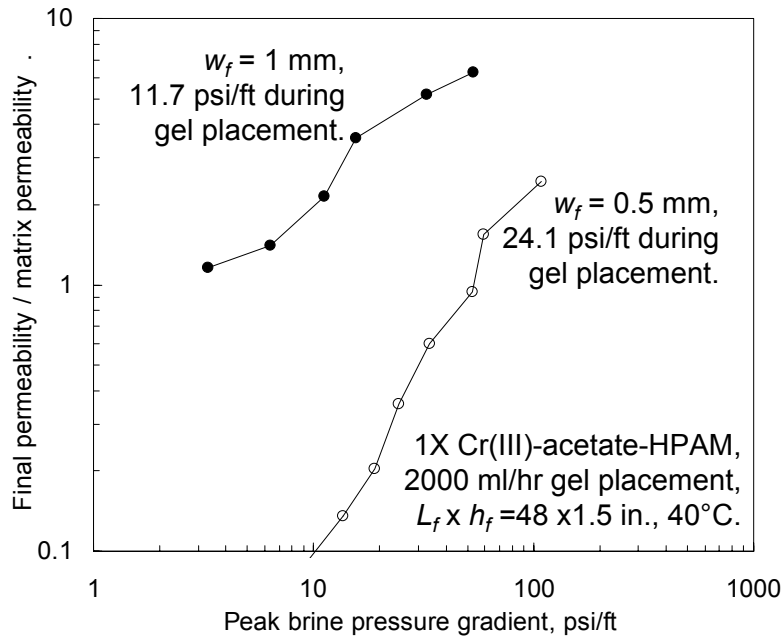
Fig. 27—Effect of fracture width on washout: 0.5- and 1-mm wide fractures.
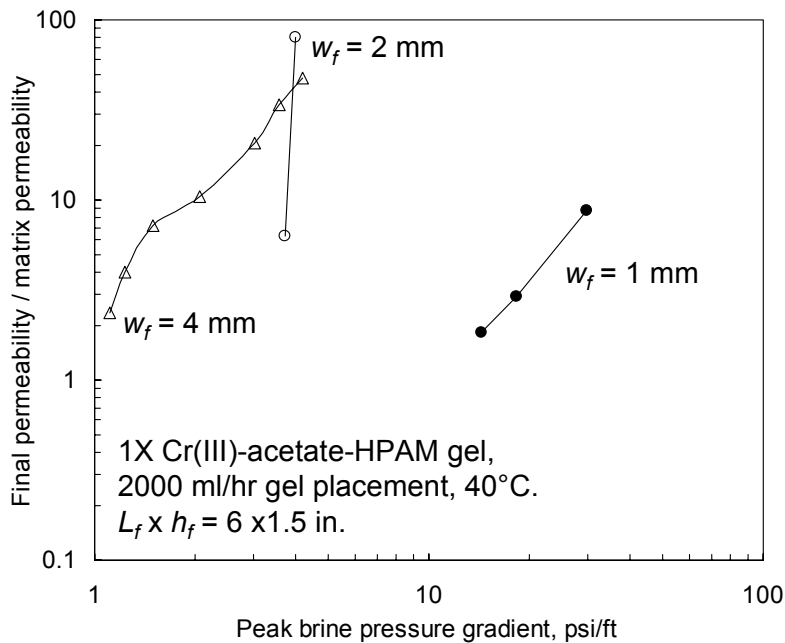
Fig. 28—Effect of fracture width on washout: 1-, 2-, and 4-mm wide fractures.

Effect Of Gel Concentration. Gel washout was less severe for a 2X Cr(III)-acetate-HPAM gel (i.e., a gel with twice the Cr and twice the HPAM) than for a 1X gel (see Fig. 29). However, the pressure gradient required for placement was significantly greater for the 2X gel than for the 1X gel. The pressure gradient for gel washout was generally similar to or less than the pressure gradient for gel placement.[20]
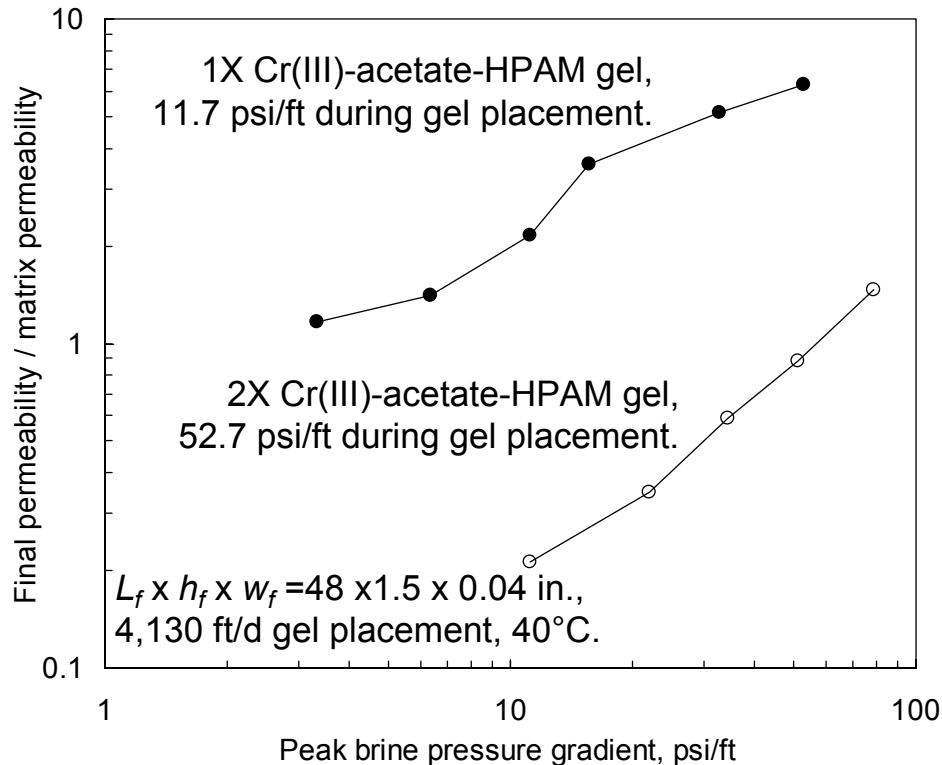
Fig. 29—Effect of gel concentration on washout.

Effect Of A Constriction In The Fracture. In the experiments described to this point, the fractures had relatively uniform widths throughout their lengths. We wondered whether gel washout would be less severe if a significant constriction occurred within the fracture. To explore this possibility, an experiment was performed using a 48-in. long fracture where the fracture width was 0.08 in. (2 mm) in the first 16-in. (41-cm) long section, 0.02 in. (0.5 mm) in the second 16-in. long section, and 0.08 in. in the final 16-in. long section. The cross-sectional area of the Berea sandstone core that contained the fracture was about 1.5 in. x 1.5 in.

We injected 3.7 liters of our standard one-day-old 1X Cr(III)-acetate-HPAM gel using a rate of 2,000 cm^3/hr. After gel placement, the core was shut in for one day. (These experiments were performed at 41°C.) Next, brine (1% NaCl, 0.1% $CaCl_2$) was injected at a low rate (i.e., 100 cm^3/hr). After recording the pressure gradient, the brine injection rate was doubled, and the measurements were repeated. This process was repeated in stages up to a final brine injection rate of 16,000 cm^3/hr. Then the brine injection rate was decreased in stages.

Table 2 and Figs. 30 and 31 summarize some of the results. During gel injection, the pressure gradient quickly stabilized at values of 5.0 psi/ft in the first fracture section and 4.9 psi/ft in the third fracture section. (See Fig. 30 and the first data column of Table 2.) Thus, the pressure gradients during gel extrusion were similar in the two 0.08-in. wide sections, even though they were separated by a 0.02-in. wide fracture section. This result was consistent with an earlier experiment.[22] In the 0.02-in. wide section of the fracture, the pressure gradient stabilized at 19.5 psi/ft. Consistent with our earlier work,[22] the pressure gradient for gel extrusion increased with decreasing fracture width.

Table 2—Pressure gradients during gel and brine injection
into a 48-in. long fracture with variable width.

$L_f x w_f$ in. x in.	Gel average, psi/ft	Brine peak, psi/ft	Final brine, psi/ft
16 x 0.08 (1st section)	5.0	9.6	0.6
16 x 0.02 (2nd section)	19.5	6.9	2.6
16 x 0.08 (3rd section)	4.9	3.2	0.9
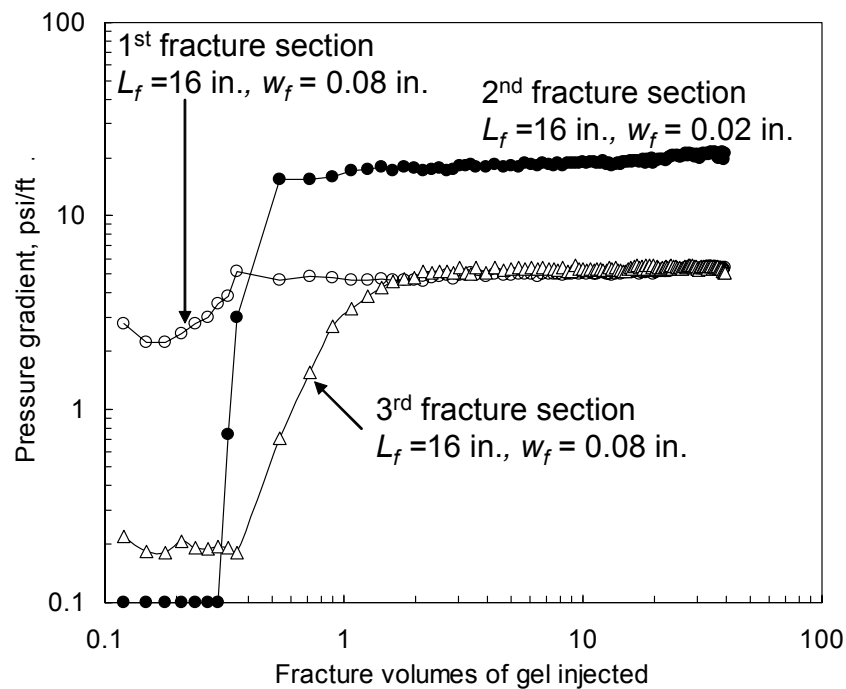
Fig. 30—Pressure gradients during injection of a Cr(III)-acetate-HPAM gel (2,000 cm^3/hr).

The second data column of Table 2 lists the peak pressure gradients observed during the first brine injection (at 100 cm^3/hr) after gel placement. In the first fracture section, the pressure gradient rose rapidly to 9.6 psi/ft (within 0.15 fracture volumes of brine injection), followed by a rapid decrease to 0.6 psi/ft. A spurious secondary peak was observed at 1 fracture volume— suggesting additional gel mobilization and dislodging (Fig. 31). The peak pressure gradients were 6.9 psi/ft in the second fracture section and 3.2 psi/ft in the third section. It is interesting

that the primary pressure peaks diminished in magnitude by about 3 psi/ft sequentially through the three sections. One might have expected the largest pressure peak to be observed in the second (and most narrow) section. For the three sections, the primary pressure peaks were observed at about the same time (i.e., 0.15 to 0.18 fracture volumes of brine injection—see Fig. 31). This result indicates that gel failure occurred simultaneously in all three fracture sections.
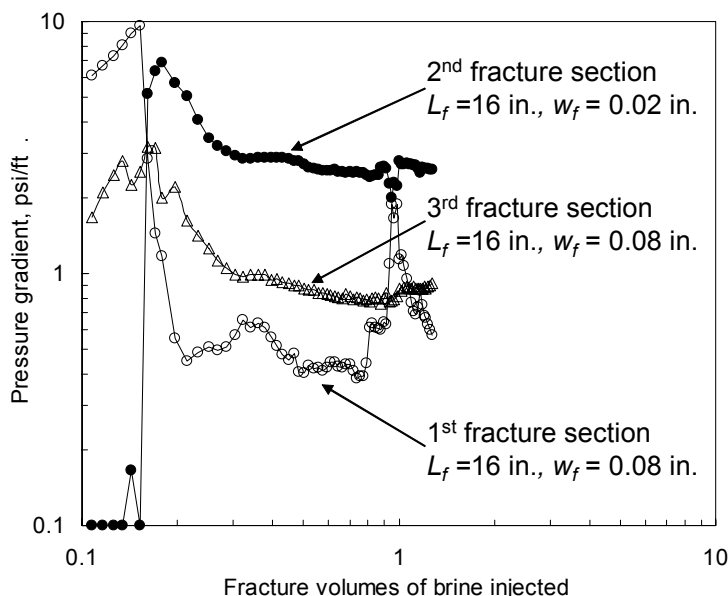
Fig. 31—Pressure gradients during brine injection after gel placement (100 cm^3/hr).

For the first fracture section, the peak pressure gradient during brine injection (9.6 psi/ft from Table 2) was almost twice the average pressure gradient during gel injection (5 psi/ft). We expected that the pressure gradient for gel mobilization during brine injection would be about the same as that during gel injection. Thus, the constriction associated with the middle fracture section may have inhibited gel washout during the first phase of brine injection. Interestingly, however, in the second fracture section, the peak brine pressure gradient was only about one-third of the average pressure gradient during gel injection (6.9 versus 19.5 psi/ft, from Table 2).

During gel placement, mobile gel (with the same composition as the injected gel) forms wormholes through a much more concentrated immobile (dehydrated) gel in the fracture.[20] Presumably, during brine injection after gel placement, the gel in these wormholes provided the point of failure. This presumption was qualitatively consistent with the pressure gradients noted near the end of brine injection. Standard calculations for laminar flow of brine in tubes or slits[23] (coupled with the brine pressure gradients and flow rates) suggested that less than 2% of the gel washed out during brine injection. In contrast, if the entire gel mass had washed out, the brine pressure gradients should have been lower by at least a factor of 300 in the 0.02-in. (0.5-mm) wide section of the fracture and at least a factor of 10,000 in the 0.08-in. (2-mm) wide sections of the fracture. Also, at the end of the experiment (i.e., after the rate studies described below), the fracture was opened—revealing that most of the fracture was filled with concentrated gel.

The average pressure gradients during brine injection at other rates are shown in Fig. 32. The behavior in the third fracture section closely tracked that in the first section—indicating that the degree of gel washout was similar in both 0.08-in. wide fracture sections. In the above discussion of Table 2, we suggested that the constriction associated with the middle fracture section may have inhibited gel washout during the first phase of brine injection. Evidently, during the subsequent phases of brine injection (at higher rates), the constriction did not inhibit washout in the upstream fracture section any more than in the downstream section.
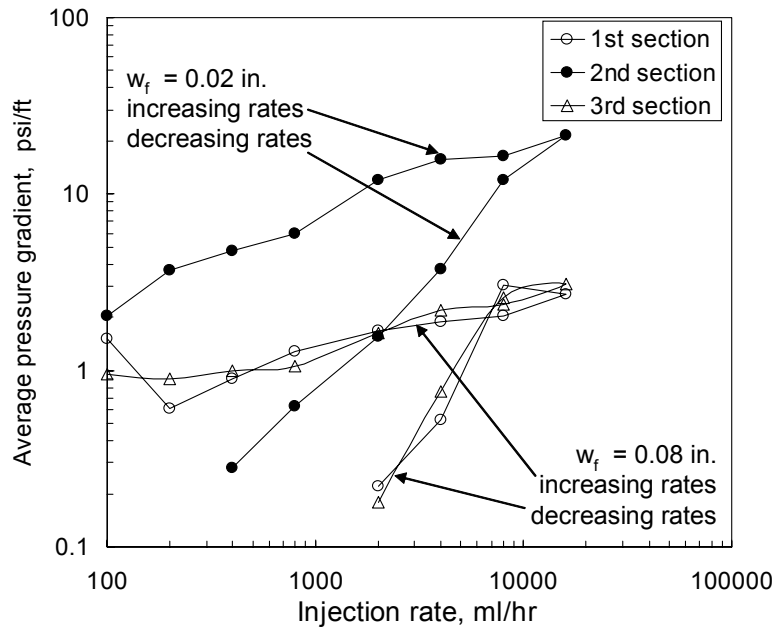
Fig. 32—Pressure gradients versus brine injection rate after gel placement.

In all fracture sections, the pressure gradients consistently increased with increased brine injection rate. If the brine flow paths (i.e., the open wormholes) were of fixed size, the pressure gradient should be directly proportional to the brine injection rate. For the increasing rate sequence in the middle fracture (solid symbols in Fig. 32), the pressure gradient varied with rate raised to the 0.5 power. Since the rate exponent was less than unity, the flow paths became progressively more open with increased rate. For comparison, in the first and third fracture sections (open symbols in Fig. 32), pressure gradients varied with rate raised to the 0.25 power. These results revealed that increased brine rates widened the flow openings to a proportionately greater extent in the 0.08-in. wide fractures then in the 0.02-in. wide fracture.

For all fracture sections, when the rates were decreased in stages, pressure gradients varied with rate raised approximately to the first power. This result indicated no further erosion of the wormhole pathways when subjected to diminishing brine injection rates.

During brine injection after gel placement, if we assume that all flow occurs through a single cylindrical wormhole, the diameter of that flow path can be estimated using the pressure drop and rate information.[23] Fig. 33 shows these calculated diameters for the three fracture sections during the increasing sequence of brine injection rates. For the middle fracture section, the

28

calculated wormhole diameter rose from 0.007 in. (0.18 mm) at the lowest rate to 0.014 in. (0.36 mm) at the highest rate. Thus, the effective wormhole width remained less than the fracture width (0.02 in. or 0.5 mm). For comparison, in the 0.08-in. (2-mm) wide fracture sections, the calculated wormhole diameters were about the same at the lowest rate (100 cm^3/hr) as that in the 0.02-in. wide section (i.e., 0.008 in. versus 0.007 in.). However, as the brine injection rate increased in the 0.08-in. wide sections, the wormhole diameters increased proportionately more—from 0.008 in. (0.2 mm) at the lowest rate to 0.023 in. (0.58 mm) at the highest rate.
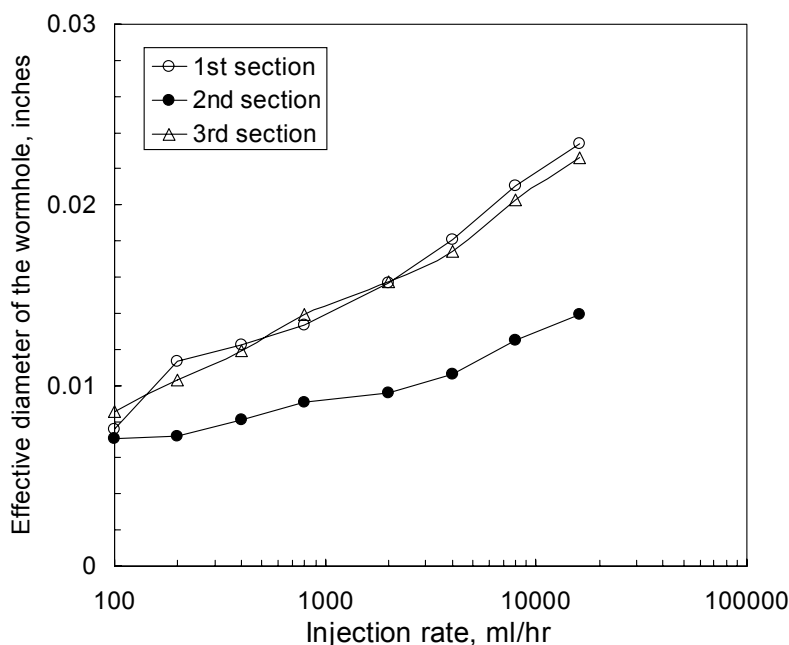
Fig. 33—Calculated wormhole diameters versus brine injection rate after gel placement.

In summary, the pressure gradients during gel extrusion were similar in two 0.08-in. wide fracture sections, even though they were separated by a 0.02-in. wide fracture section. The constriction associated with the middle fracture section may have inhibited gel washout during the first pulse of brine injection after gel placement. However, during subsequent phases of brine injection, the constriction did not inhibit washout in the upstream fracture section any more than in the downstream section.

Use Of Particulates To Reduce Washout. Of course, we seek methods to maximize the pressure gradient at which gel washout occurs. Thus, we are exploring how incorporation of particulate matter into the gel affects mobilization. Preliminary studies were performed in beakers to examine properties of gels that incorporated one of six particulates, including fine mica (supplied by MI), fine nut plug (MI), diatomaceous earth (Drilling Specialties Diaseal M), celloflakes, shredded polypropylene, and fiberglass insulation. For each particulate, suspensions were prepared in our 1X gelant, and we noted the qualitative strength and appearance of the final gel. The mica, nut plug, and diatomaceous earth were significantly denser than the gelant. High stir rates were required to suspend the particulates (1%, 3%, and 5% concentrations) in the gelant. Once the agitation rate decreased, the particulates immediately separated from the gelant.

Also, although the mica and nut plug did not inhibit gelation, we were unable to form a gel with uniformly suspended particles. The diatomaceous earth changed the pH to high values (i.e., 12), so the gel never formed. The celloflakes (1% concentration) did not interfere with gelation. However, except at very high agitation rates, they were too light (low density) and did not suspend effectively in the gelant or gel. In contrast, the fiberglass insulation (0.1% to 0.2% concentrations) and the shredded polypropylene (0.2% to 2% concentration) formed uniform suspensions even at very low stir rates, and they did not appear to interfere with gelation. Even after agitation ceased, these particulates remained suspended quite well.

Gel extrusion and washout experiments were performed using our 1X gel that was prepared with and without 0.1%-0.2% suspended fiberglass insulation. These experiments used the same procedures described above. The open symbols in Fig. 34 plot washout results for gel with no fiberglass, while the solid symbols show results for gel with fiberglass. Gel with 0.1-0.2% fiberglass significantly increased the pressure gradient for washout in 1-mm and 2-mm wide fractures. However, the pressure gradients for gel placement were quite high (e.g., 220 psi/ft in a 1-mm wide fracture). In both cases, the pressure gradient for washout was less than or equal to the pressure gradient during gel placement. Also, in 4-mm wide fractures, the washout behavior of Cr(III)-acetate-HPAM gel was no better with fiberglass than without fiberglass. For gels containing 0.2 to 0.5% shredded polypropylene, the pressure gradients during washout were significantly lower than during gel placement.[24]
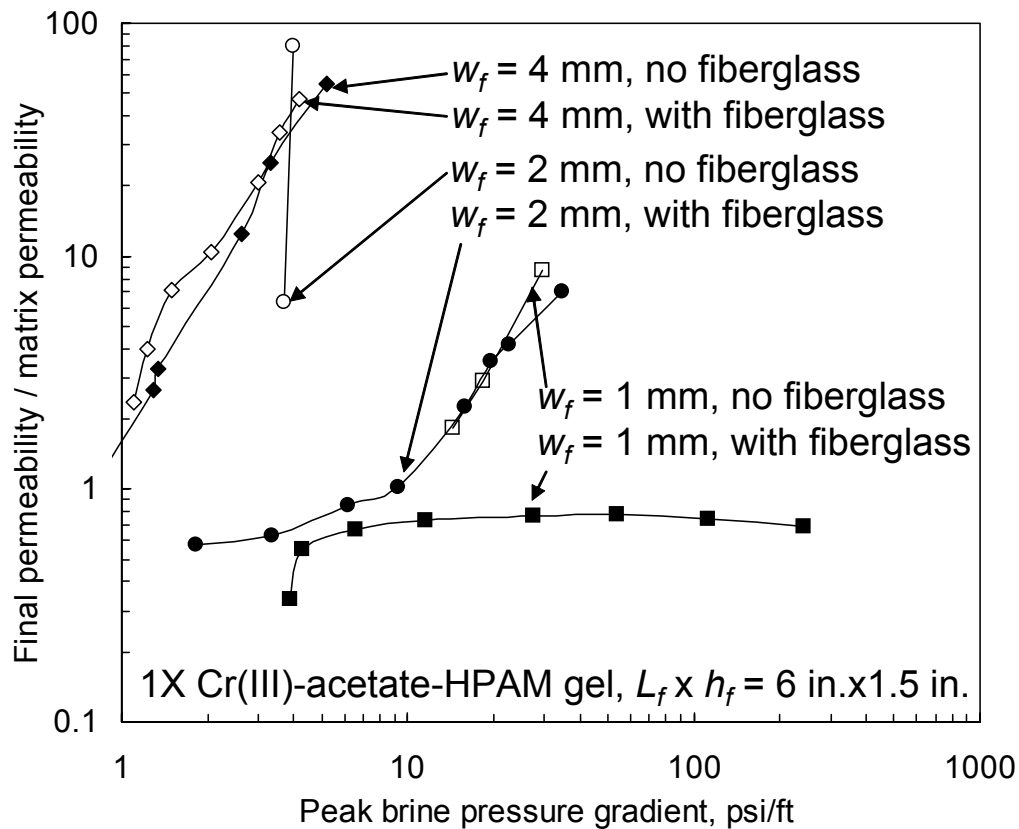
Fig. 34—Effect of fiberglass on gel washout.

Rate Control. For the above work, the pressure gradient for washout was less than or equal to the pressure gradient during gel placement. Ideally, we would like the pressure gradient for washout to be much higher than the pressure gradient required to place the gel. We investigated whether washout could be reduced by controlling gel injection rate to form concentrated gels during placement. Gels are known to concentrate or dehydrate as they extrude through fractures.[20] If the gel is injected as rapidly as possible, it will propagate the maximum distance along the fracture with minimum water loss. In contrast, as the injection rate decreases, the concentration increases for the gel deposited in the fracture. Presumably, this gel will be increasingly resistant to washout as it becomes more concentrated.

A key difference exists between this idea and the concept described earlier where a concentrated gel was placed by injecting a 2X gel. The pressure gradient for gel extrusion increased significantly with increased concentration of the injected gel (see Fig. 20). Thus, pressure gradients can be very high when injecting a 2X gel. In the new concept, the injected gel would have a relatively low polymer concentration (e.g., a 1X gel). For a given fracture width and composition of the injected gel, the pressure gradient is insensitive to injection rate (see Table 1). Therefore, by lowering the injection rate, we can place a concentrated gel in the fracture without resorting to high pressure gradients.

To test this idea, we performed three corefloods that were identical except for the gel placement rate. In all cases, the core material was 700-md Berea sandstone, with a fracture placed lengthwise down the middle of each core. The core dimensions were 122-cm long and 3.8x3.8-cm in cross section. The fracture dimensions were 122x3.8x0.1 cm (48x1.5x0.04 in.). In each fractured core, 3.7 liters (80 fracture volumes) of one-day-old 1X Cr(III)-acetate-HPAM gel were injected using rates of 400, 2,000, or 16,000 cm^3/hr (effective velocities of 826, 4,130, or 33,070 ft/d). After gel placement, the core was shut in for one day. (These experiments were performed at 40°C.) Next, brine was injected at a low rate (i.e., 100 cm^3/hr). A steady state was quickly established, and the pressure gradient was recorded. Then the brine injection rate was doubled, and the measurements were repeated. This process was repeated in stages up to a final brine injection rate of 16,000 cm^3/hr. Then the brine injection rate was decreased in stages.

Two measures of washout were used at each brine injection rate. The first method used the final measured brine permeability for the core (with the fracture and gel in place) divided by the matrix permeability (i.e., 700 md—the core permeability before the fracture and gel were placed in the core), k_{final}/k_m. For the three experiments, Fig. 35 plots this parameter versus the peak (highest) pressure gradient experienced during brine injection at a given rate.

If the ratio, k_{final}/k_m, was greater than unity, gel washout must have occurred to some extent. As the value of k_{final}/k_m increases, greater degrees of gel washout are indicated. In Fig. 35, the curve associated with gel placement at the lowest rate (826 ft/d) showed the greatest resistance to washout during brine injection. The pressure gradients during gel placement (9.2 to 15.3 psi/ft) did not vary greatly, considering the 40-fold difference in placement rates.

The second measure of washout was the fraction of brine that flowed through the matrix. During these experiments, we collected the effluent from the fracture separate from that produced from the matrix. If the gel effectively plugged the fracture, 100% of the brine should have been

produced from the matrix. As more and more gel is washed from the fracture, the fraction of fluid produced from the matrix should diminish. Fig. 36 shows the results from the three experiments—plotting fraction of matrix flow versus peak pressure gradient during brine injection at a given rate. This figure confirms that the greatest resistance to gel washout was exhibited during the experiment where gel was placed at the slowest rate (826 ft/d).
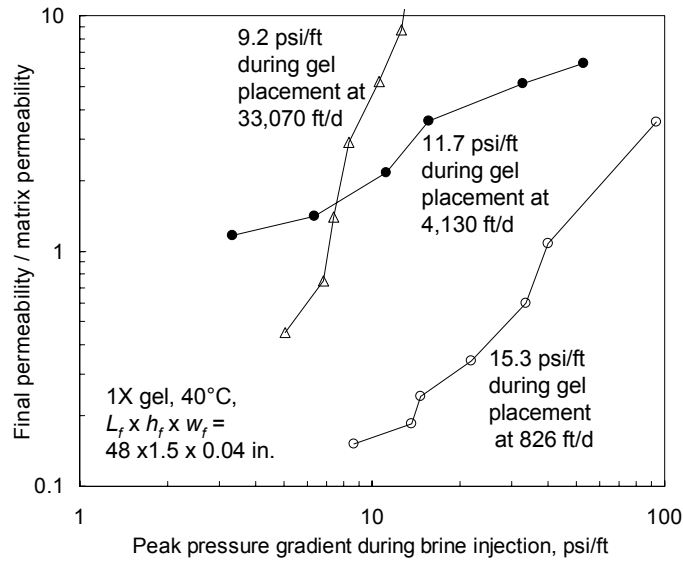
Fig. 35—Final permeability as a measure of gel washout.

Consequently, adjustment of gel placement rates is a promising method to control gel washout. Depending on the gel and fracture width, one may wish to first inject gel at a high rate to maximize penetration into the fracture. Near the end of the treatment, gel injection at low rates should form concentrated gels to better resist washout for the high pressure gradients experienced near the wellbore.
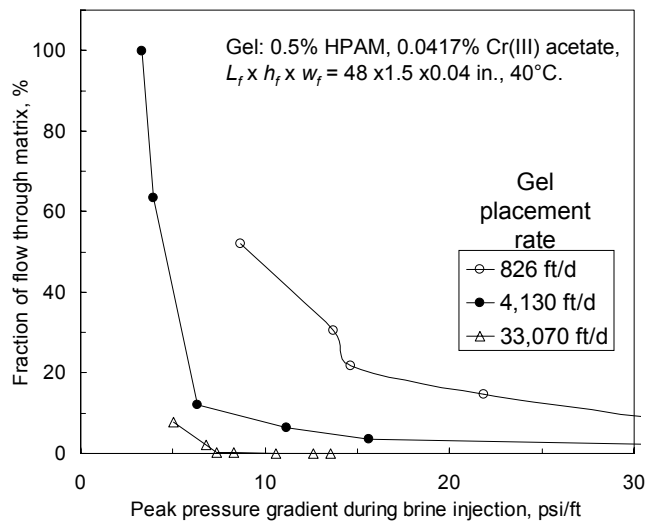
Fig. 36—Fraction of flow through the matrix as a measure of gel washout.

Use Of Secondary Reactions. Another method that we examined to control gel washout involved use of secondary gelation reactions. The concept is to inject a gel that undergoes two separate crosslinking reactions. The first (primary) reaction is timed to take place before entry into the fracture. The second crosslinking reaction occurs after the gel has been placed. The first reaction forms a crosslinked polymer that will not enter the porous rock but will be sufficiently fluid to exhibit relatively low pressure gradients during the extrusion process. The second reaction strengthens the gel and significantly increases the gel's resistance to washout. The crosslinker for the second reaction should not gel with any component that leaks off into the porous rock. In this way, damage to the porous rock is minimized.

In our first test of this concept, the primary reaction involved 0.5% Alcoflood 935 HPAM crosslinked with 0.5% formaldehyde and 0.5% resorcinol. (The gel also contained 1% NaCl and 0.1% $CaCl_2$. Gel injection occurred at 2,000 cm^3/hr or 4,130 ft/d.) During two baseline experiments, 80 fracture volumes (3.7 liters) of this formed gel showed pressure gradients of 4.1 and 20.9 psi/ft during extrusion through 122-cm (4-ft) long, 1-mm (0.04-mm) wide fractures. We are uncertain why the first experiment provided significantly lower extrusion pressure gradients than the second.

The same volume of the same gel was injected into a third 1-mm wide fracture. An additional 5 fracture volumes of the same formed gel was injected that included 0.0417% Cr(III) acetate. The Cr(III) acetate crosslinker was mixed with the formed resorcinol-formaldehyde-HPAM gel and injected into the fracture before the secondary crosslinker had time to react. The pressure gradient during gel injection averaged 20.9 psi/ft. Figs. 37 and 38 show that the secondary reaction with 0.0417% Cr(III) acetate significantly increased the gel's resistance to washout. Thus, the use of secondary reactions deserves further investigation.
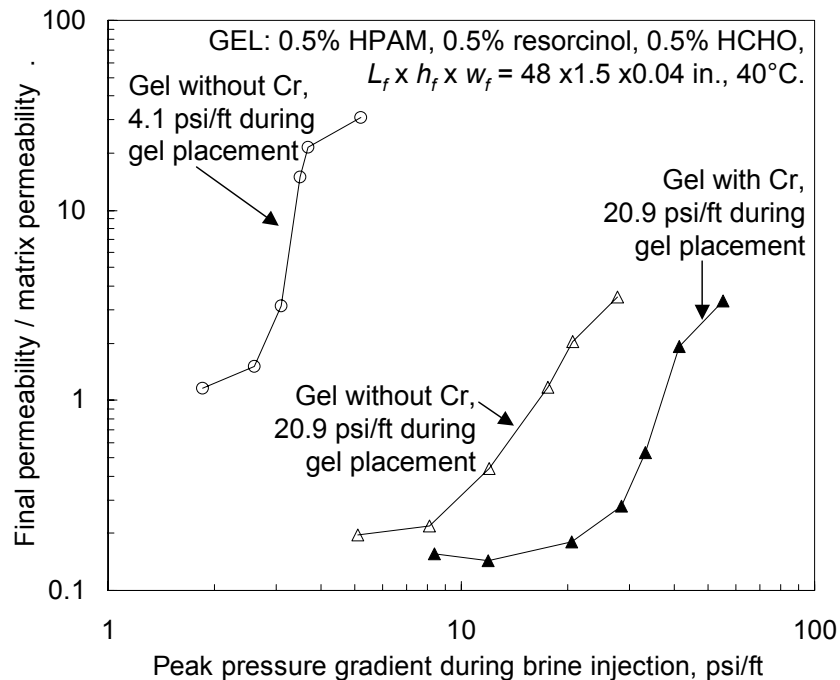
Fig. 37—Final permeability: Influence of a secondary reaction.

33
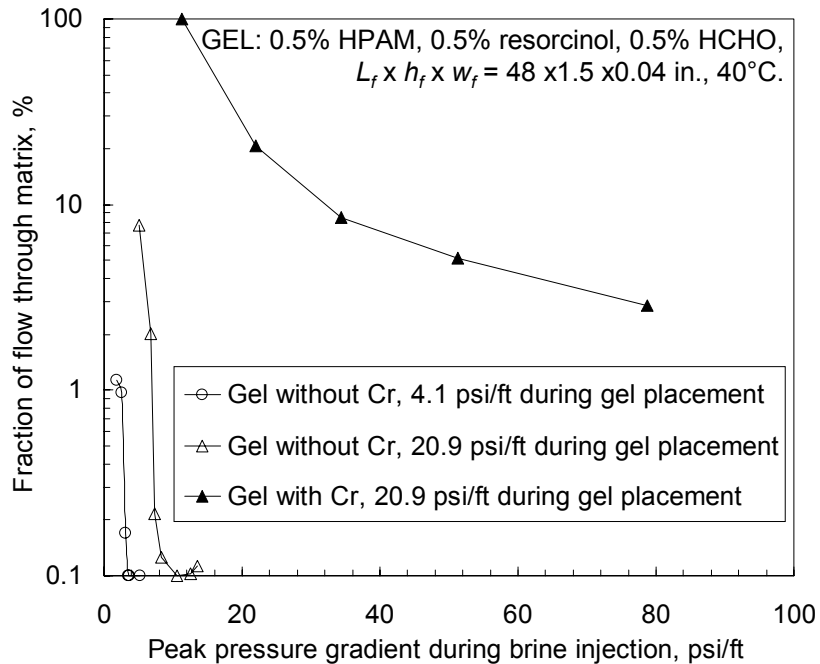
Fig. 38—Fraction of flow through the matrix: Influence of a secondary reaction.

Effect Of Rock Surface. In earlier work, we demonstrated that the pressure gradient and the degree of gel dehydration during gel extrusion were not sensitive to the permeability of the rock that contained the fracture.[11-14] We also showed that when the rock was Berea sandstone, the extrusion behavior was the same if the fracture faces were smooth surfaces that were generated by cutting the cores with a diamond saw or were jagged surfaces that were generated by cracking the core open. We were asked whether the extrusion and washout behavior depends on the wetting character of the fracture surface. Some speculated that gel slippage on a strongly oil-wet plastic surface might be different than on a water-wet sandstone surface. To address this issue, we prepared two fractured cores from 10-darcy polyethylene cores. These cores were 31-in. (78-cm) long and 1.5-in (3.9-cm) in diameter. The fractures were created by cutting the cores in half lengthwise. One fracture was 0.02-in. (0.5-mm) wide while the other was 0.04-in. (1-mm) wide. Our standard 1X Cr(III)-acetate-HPAM gel (3.7 l) was injected using a rate of 2,000 cm^3/hr (40°C). During gel extrusion, the pressure gradients were 7.7 psi/ft in the 1-mm wide fracture and 10.7 psi/ft in the 0.5-mm wide fracture. These values (solid circles in Fig. 5) are consistent with those observed during extrusion of the same gel through fractures in Berea sandstone and Indiana limestone. Fig. 39 shows that the leakoff rates during extrusion through the fractured polyethylene cores were consistent with predictions from our new leakoff model—which in turn were consistent with leakoff results in the fractured Berea cores. Recall that the permeability of the matrix was about 10 darcys for the polyethylene versus about 0.75 darcys for Berea.

After gel placement, brine was injected at various rates to assess washout. Figs. 40 and 41 compare the washout results in the fractured polyethylene cores versus in the fractured Berea sandstone cores. Both figures indicated that the polyethylene data follow the Berea trends, although the polyethylene results generally were associated with lower pressure gradients. The lower pressure gradients for polyethylene were not surprising since those cores were much more

34

permeable than the Berea cores. In other words, for a given total brine injection rate, the polyethylene matrix had a greater flow capacity than the Berea matrix.

The main conclusion from this study was that the extrusion and washout behavior in fractures contained by strongly oil-wet polyethylene cores were not significantly different than those in strongly water-wet Berea sandstone.
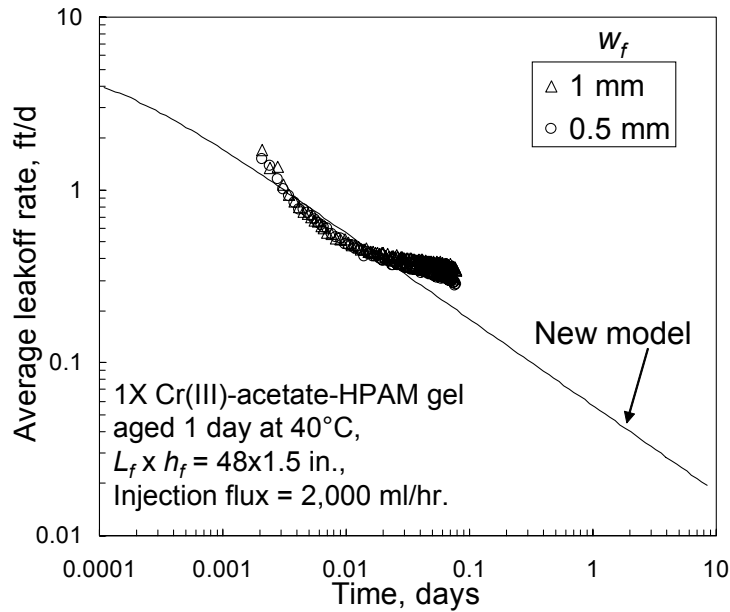
Fig. 39—Leakoff rates during gel extrusion through fractures in polyethylene cores.
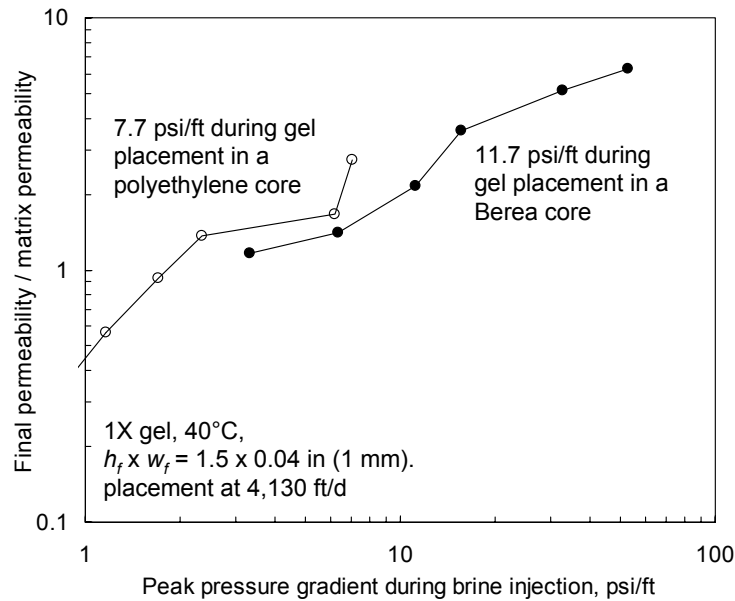
Fig. 40—Washout in Berea versus polyethylene: w_f = 1 mm.
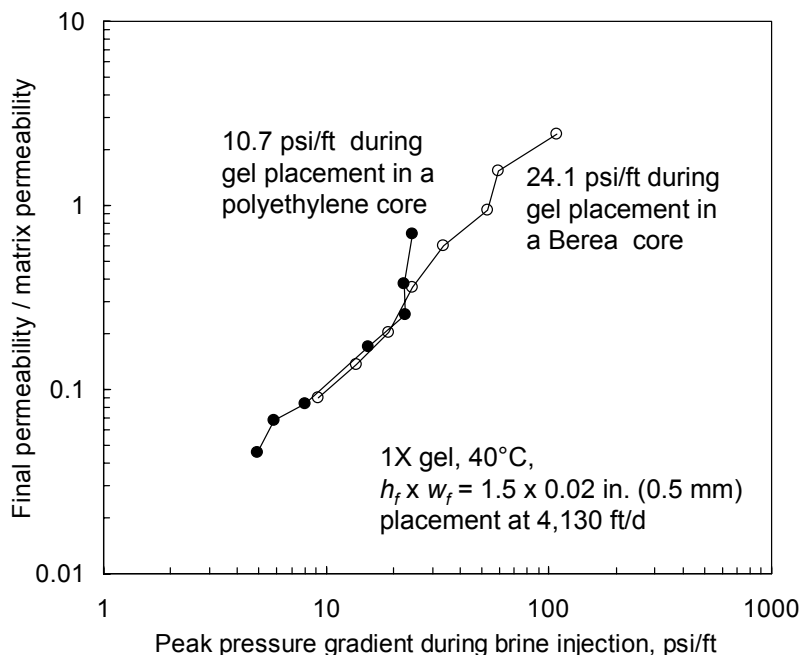
Fig. 41—Washout in Berea versus polyethylene: $w_f = 0.5$ mm.

Effect Of Oil Flow. The washout experiments described to this point involved brine injection. Would the washout behavior be different if oil was used instead of brine? This question is especially relevant to gel treatments in production wells. Ideally, we would like gel in the fracture to washout more easily during oil flow than during brine flow.

To address this issue, we performed two extrusion experiments in 4-ft (122-cm) long Berea cores—with a fracture width of 1 mm (0.04-in.) for one and 0.5 mm (0.02-in.) for the other. During injection of our standard 1X Cr(III)-acetate-HPAM gel at 2,000 cm^3/hr (40°C), the pressure gradient was 10.2 psi/ft in the 1-mm wide fracture versus 26.6 psi/ft in the 0.5-mm wide fracture. These pressure gradients were similar to those from extrusion experiments using fractures of comparable widths (see Fig. 27).

After gel placement Soltrol 130™ oil (1.05 cp at 40°C) was injected using the same sequence of rates described earlier for brine. Figs. 42 and 43 compare these results with analogous results from brine injection experiments. In both fractures, the final permeability to oil was much higher than that for brine. Interestingly, as the applied pressure gradient increased, the relative permeability to oil remained fairly constant at 5 times the matrix permeability in the 0.5-mm wide fracture and at 33 times the matrix permeability in the 1-mm wide fracture. In contrast, the relative permeability to brine increased dramatically as the applied pressure gradient increased.

These results are plotted in a different form in Fig. 44. For a given fracture width, the pressure gradients during oil injection at low rates were 10 to 20 times less than those during water injection. At high rates, the differences between water and oil pressure gradients became less pronounced—especially in the 0.5-mm wide fracture.
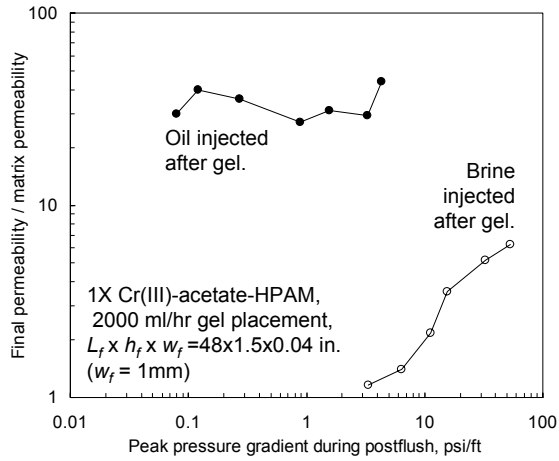
Fig. 42—Washout using oil versus water: w_f = 1 mm.
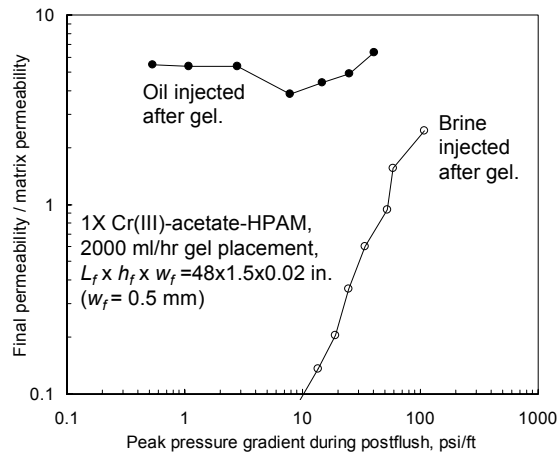
Fig. 43—Washout using oil versus water: w_f = 0.5 mm.
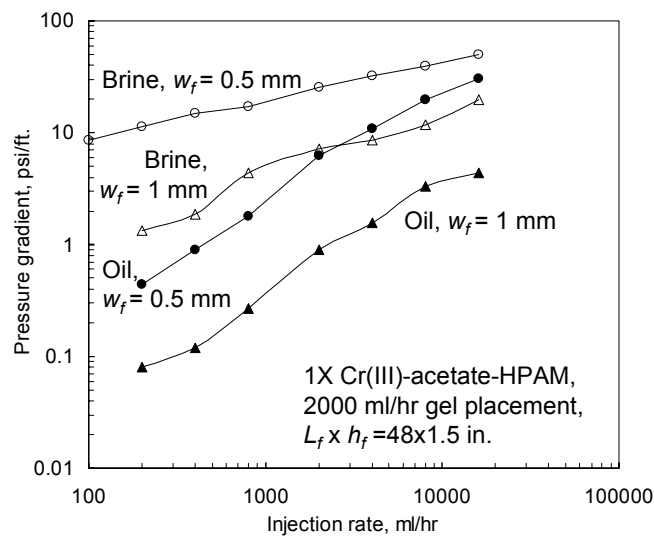
Fig. 44—Pressure gradients during washout: oil versus water.

The important implication from these results is that gels in fractures could provide a significant disproportionate permeability reduction—i.e., reducing permeability to water much more than that to hydrocarbon. This result was unexpected, since based on limited earlier work, we believed that attaining disproportionate permeability reduction required that the gel reside in a porous medium. Consequently, these new findings will receive close examination and further testing in our future work.

Conclusions
This chapter described the placement and washout properties of gels in fractures. During the placement process, two key parameters that affect the distance of gel penetration along a fracture are the pressure gradient and the degree of water loss exhibited by the gel. We characterized these properties as a function of fracture width, injection rate, gel composition, temperature, and rock properties. The pressure gradient for gel extrusion was insensitive to injection rate, temperature, and rock lithology, permeability, and character of the rock face. It varied with the square of polymer content and inversely with the square of fracture width. We now have a fairly clear understanding of the mechanism for gel propagation through fractures. Gel that dehydrates basically becomes immobile in the fracture. The only mobile gel has the same composition as the injected gel. This mobile gel forms wormholes through the concentrated gel.

After formed gels are extruded into fractures, we wish to minimize gel washout when the well is returned to service. In fractures that were 1-mm wide or less, the pressure gradient for gel washout during brine injection was about the same as the pressure gradient observed during gel placement. However, in fractures wider than 2 mm, the pressure gradient for washout can be significantly less that the pressure gradient during gel placement. The mechanism of gel failure appears to involve the displacement of relatively mobile gel from wormholes. Generally, only a small fraction of the gel was displaced during the washout process. Resistance to washout can be increased by injection of more concentrated gels or by incorporation of particulate matter into the gel. However, these approaches are accompanied by significantly higher pressure gradients during the gel placement process. Also, with these approaches, the pressure gradients for washout were less than or equal to the pressure gradients during gel placement.

We examined two promising new ideas to reduce gel washout from fractures. The first concept involved controlling gel injection rate during placement. Gels placed at lower rates experienced greater dehydration and were more resistant to washout. The second method to control gel washout involved use of secondary gelation reactions. The concept is to inject a gel that undergoes two separate crosslinking reactions. The first reaction is timed to take place before entry into the fracture—to prevent gel from entering the porous rock and yet provide low pressure gradients during extrusion. The second reaction occurs after gel placement—to strengthen the gel. Both concepts showed considerable promise during our experiments.

We found that the extrusion and washout behavior in fractures contained by strongly oil-wet polyethylene cores were not significantly different than those in strongly water-wet Berea sandstone. We also found that gels in fractures could provide a significant disproportionate permeability reduction—i.e., reducing permeability to water much more than that to hydrocarbon.

3. PLUGGING PINHOLE LEAKS USING GELS

Many old wells exist where corrosion leads to casing leaks. For medium to large leaks, cement squeezes are commonly used for remedial treatment.[10,25] However, when the leaks are very small (i.e., "pinhole leaks"), difficulty may exist in finding the holes. Also, even when the leaks are located, cement may be ineffective as a plugging agent because of difficulty in penetrating into small holes. In these cases, gelants may provide a viable alternative to cement.[10,26-28]

Cements exhibit much greater (~1 million times greater[25]) mechanical strength than gels. Consequently, concern exists about the ability of gels to withstand high pressure gradients when plugging casing leaks. In this chapter, we consider the plugging abilities of a Cr(III)-acetate-HPAM gel.

Experimental Work
The gel contained 5% Alcoflood 254S™ HPAM (nominally 500,000 MW and 5% hydrolyzed), 0.417% Cr(III) acetate, 1% NaCl, and 0.1% $CaCl_2$. (Commercially, this gel is known as "MARA-SEAL^{SM}".) This gelant was placed in two sandpacks. Both sandpacks were 30.48 cm (1ft) in length and 11.25 cm^2 in cross-sectional area. The permeability was 20 darcys for the first pack and 9.7 darcys for the second pack. The first pack was flooded with 2.6 PV (400 cm^3) of gelant, while the second pack was flooded with 5.6 PV (860 cm^3) of gelant. The gelant viscosity (at 41°C) was 93 cp, and the resistance factor was 135 during gelant injection. After gelant placement, both packs were shut in for one day at 41°C.

After shut-in, brine was injected into the first pack using a pressure drop of 1,000 psi (at 41°C). Over a one-week period, the brine flow rate was constant, yielding a final permeability for the sandpack of 1.5 μd and a residual resistance factor (F_{rrw}) of 13,500,000. (See Table 3.)

Table 3—Sandpack plugging using a Cr(III)-acetate-HPAM gel.

	Initial permeability, darcys	Δp, psi	Injection flux, ft/d	Final permeability, μd	F_{rrw}
Sandpack 1	20	1,000	0.014	1.5	13,500,000
Sandpack 2	9.7	1,000	0.011	1.2	8,400,000
		2,000	0.030	1.6	6,200,000
		3,000	0.066	2.3	4,200,000
		2,000	0.033	1.7	5,600,000
		1,000	0.012	1.3	7,600,000

The second sandpack was also subjected to a pressure drop (using brine) of 1,000 psi after gel placement and shut-in. Over a two-day period, the pack exhibited a brine permeability of 1.2 μd and a residual resistance factor of 8,400,000. Then the pressure drop was increased to 2,000 psi for two days, and the permeability and residual resistance factor measurements were repeated. Next, the pressure drop was increased to 3,000 psi for two days. Finally, the pressure drop was lowered to 2,000 and 1,000 psi (again, for two days at each pressure). Brine permeabilities and

residual resistance factors are listed in Table 3. The final permeabilities ranged from 1.2 to 2.3 µd. Thus, the gel very effectively reduced the sandpack permeability for pressure gradients up to 3,000 psi/ft. A reversible, apparent shear thinning behavior was noted—i.e., residual resistance factors decreased with increased pressure gradient or injection rate. Least squares fits to the data yielded the following equivalent relations:

$$F_{rrw} = 2 \times 10^6 \, u^{-0.36} \dotfill (10)$$

$$k = 6 \, u^{0.36} \dotfill (11)$$

$$F_{rrw} = 4 \times 10^8 \, (dp/dl)^{-0.55} \dotfill (12)$$

$$k = 0.0266 \, (dp/dl)^{0.55} \dotfill (13)$$

In these equations, brine injection flux (u) has units of ft/d; pressure gradient (dp/dl) has units of psi/ft; and final permeability (k) has units of µd. The correlation coefficients were 0.97 for Eqs. 10 and 11 and 0.93 for Eqs. 12 and 13. An apparent shear thinning behavior during brine injection was noted for other gels in previous experiments.[29-33]

How Much Gelant Should Be Injected?
The experimental data can be used to estimate how much gelant should be injected to allow a particular well to pass a casing or mechanical integrity test. Commonly, the test requires that the annulus of a well be pressured to a certain value, p_1, and the pressure should not drop below a second pressure, p_2, within a specified period of time, Δt. The annulus volume is V_a and the annulus is filled with a fluid of compressibility, c_a. The maximum acceptable flow rate through the leak, q_{max}, is given by Eq. 14.

$$q_{max} = c_a V_a (p_1 - p_2) / \Delta t \dotfill (14)$$

Assume that once fluid has penetrated through the casing leak, it has free access along the wellbore for some distance, h, and thereafter, flow is forced to proceed radially away from the wellbore. Let r_1 be the inner radius of the gelant bank (i.e., the wellbore radius) and r_2 the outer radius of the gelant bank. The reservoir pressure is p_r, the viscosity of the fluid in the annulus is μ, and the gel reduces permeability to k. Also assume that the gel bank will experience the entire pressure drop from the wellbore to the formation. In that case, the required radius of gelant penetration is given by Eq. 15 (i.e., the Darcy equation for radial flow).

$$r_2 = r_1 \, exp \, [(p_1 - p_r) \, k \, h \, / (\, q_{max} \mu)] \dotfill (15)$$

The minimum volume of gelant required is then given by Eq. 16.

$$V_{gelant} = \pi \, h \, [(r_2)^2 - (r_1)^2] \phi (1 - S_{or}) \dotfill (16)$$

We now consider typical values for the above parameters. The pressure difference is generally around 500 psi. From Table 3, k is from 1 to 2 µd. Water viscosity ranges from 1 cp at room temperature to 0.28 cp at 100°C. Assume that the annular volume is about 1.5 bbl/100 ft. For

4,000 ft of casing length, the annular volume would be about 60 bbl. If the annular volume was filled with only water, with a compressibility of 3×10^{-6} psi^{-1} (actual units are volume change per total volume per psi), a 1 psi pressure drop would result in a volume increase of 1.8×10^{-4} bbl (i.e., 3×10^{-6} x 1 x 60). If 1 psi were the maximum allowable pressure drop over 30 minutes to pass the casing integrity test, the value for q_{max} would be only 0.00864 BPD. Of course, if the annulus contained free gas, the compressibility and the value for q_{max} would be greater.

With these values, we can estimate the minimum required distances of gelant penetration and the minimum volumes of gelant that must be injected to pass the casing integrity test. For the most conservative case, q_{max}=0.00864 BPD (i.e., no gas in the annulus), μ=0.28 cp (high-temperature, low-viscosity water), k=2 μd, and ($p_1 - p_r$)=500 psi. Assume that the wellbore radius is 4 inches. Also assume that h is one foot. (The latter assumption may not seem conservative, but we make it just so that we can normalize the amount of gelant injection on a per ft basis.) Plugging these numbers into Eq. 15 yields a minimum required radius of gelant penetration (r_2) of 6.4 inches. In other words, the gelant only needs to penetrate 2.5 inches from the wellbore face. From Eq. 16 (assuming ϕ=0.2 and S_{or}=0), this radius translates to a minimum gelant volume requirement of 0.02 bbl/ft of interval treated. Of course, in any practical field application, the injected gelant volume will be significantly higher than this value. Consequently, these calculations suggest optimism that gelant treatments can be effective for treating small casing leaks.

Diffusion
Diffusion must be considered when injecting very small gelant banks.[34] The gelant bank must maintain some minimum concentration of the reactants for gelation to occur. To be conservative, assume that the gelation reaction will be stopped by only a 10% dilution. Also being conservative, assume that the gelation time is 24 hours. The size of the mixing zone (L_m in cm) is estimated using Eq. 17.

$$L_m = 3.62\,(Dt)^{0.5} \dotfill (17)$$

In this equation, t is time (in seconds) and D is the diffusion coefficient (in cm^2/s). The diffusion coefficient is typically 10^{-8} cm^2/s for polymers in solution and 10^{-5} cm^2/s for small molecules in solution.[34] Again, to be conservative, we will assume that the diffusion coefficient is 10^{-5} cm^2/s. Using this value in Eq. 17 along with a gelation time of 24 hours (86,400 seconds), we estimate the length of the mixing zone to be 3.4 cm or 1.3 inches. To insure that a large enough gel bank forms, half of this mixing zone distance must be added to the minimum distance of gelant penetration.[34] Thus, in our conservative example above, the minimum distance of gelant penetration should be 3.7 inches instead of 2.5 inches, and the minimum gelant volume should be at least 0.034 bbl/ft of interval treated. Again, this value is much smaller than the volumes used in most field applications.

Other Considerations
Two notes of caution should be mentioned here. First, the gel withstood high pressure gradients (up to 3,000 psi/ft during this study) because it formed in a porous medium (i.e., a sandpack of 20 darcys or less). The mechanical integrity of the gel is expected to be less for the case of an open flow channel.

Second, we make no judgment about potential toxicity and environmental issues that might be associated with the Cr(III)-acetate-HPAM gel. If a Cr(III)-acetate-HPAM gelant treatment is applied near a fresh water aquifer, some may be concerned about contaminating the water, even though Cr(III) is known to be much less toxic than Cr(VI). We leave this issue for others to address. However, presumably, the small volume of the gelant treatment and the retention characteristics of Cr(III) on clays and reservoir rocks should minimize chromium movement away from the wellbore.[31,35]

4. ADSORPTION-BASED DISPROPORTIONATE PERMEABILITY REDUCTION

The ability of polymers and gels to reduce permeability to water much more than that to oil or gas is often critical to the success of water shutoff treatments in production wells. The values for the oil and water residual resistance factors determine how much polymer or gelant should be injected.[36] For a given volume of polymer or gelant injected, the treatment will not reduce water production sufficiently if the water residual resistance factor is too low. On the other hand, the treatment may seriously damage hydrocarbon production if the oil residual resistance factor is too high. One of the key challenges to the successful application of this technology is that it has not been predictable or controllable from one application to the next. A treatment may be very successful in one well, but fail in the next application because the residual resistance factors were not the same for the two treatments.

Zaitoun *et al.*[37] advocated using adsorbed polymers to produce a disproportionate permeability reduction. In concept, this method could provide more reproducible residual resistance factors if all water wet surfaces became coated with a uniform layer of adsorbed polymer. With this in mind, we began an investigation of a polymeric product.

AquaCon
BJ provided the product, AquaCon™, as a liquid concentrate containing 3% of the polymer. We don't know its exact composition, but from discussions with others, indications are that it is dominantly an acrylamide/acrylate type of copolymer with a low fraction of vinyl phosphonate, and possibly sulfonate-type monomers, incorporated into the polymer backbone. The concentrate had a viscosity of about 600 cp at 25°C—exhibiting near Newtonian behavior. When diluted in 2% KCl, the viscosities (at 25°C) were 1.6 cp for a 0.09% polymer solution and 2.5 cp for a 0.18% polymer solution. These viscosities suggest an intermediate molecular weight for an HPAM type of polymer—perhaps roughly 10^6 daltons.

Core Properties and Flooding Sequences. Eight floods were performed using nominally 800-md Berea sandstone cores that were ~15 cm in length and 3.8 cm in diameter. These cores had two internal pressure taps, located about 2.3 cm from the inlet and outlet core faces. The permeabilities and residual resistance factors that are reported here were measured over the middle 10 cm of the core. The brine and polymer solutions all contained 2% KCl; the oil was a mixture of 85% hexadecane and 15% 1-bromohexadecane; and the floods occurred at room temperature. All flooding steps (before, during, and after polymer placement) were performed using a pressure gradient of 30 psi/ft. The cores were initially saturated with brine and followed by 20 PV of oil to drive the cores to connate water saturation (S_{wr}). Next, 20 PV of brine were injected to drive the cores to a residual oil saturation (S_{or}). Table 4 lists properties of the cores. Core properties were reasonably uniform (possibly excepting Cores 359 and 360, which had somewhat lower permeabilities).

After establishing S_{or}, about 10 PV of polymer solution were injected. To this point, the flooding procedures and materials were identical for the eight cores listed in Table 4. Two polymer concentrations were investigated: 900 and 1,800 ppm. For each polymer concentration, one set of experiments followed polymer injection with the sequence: oil injection, water injection, oil injection. A second set of experiments followed polymer injection with the sequence: water

injection, oil injection, water injection. One set of experiments involved small volumes (e.g., 1 to 5 PV) of the oil and water banks after polymer placement. In another set of experiments, the oil and water banks were about 100 PV.

Table 4—Summary of Berea core properties.

polymer, ppm	Core	k_w, md	k_{ocw}, md	k_{wro}, md	S_{wr}	S_{or}
900	355	853	732	293	0.264	0.253
	359	469	430	124	0.292	0.295
	353	778	715	266	0.289	0.283
	354	754	704	298	0.256	0.268
1,800	356	913	793	310	0.245	0.258
	360	498	582	126	0.289	0.283
	342	847	768	238	0.267	0.267
	343	825	701	222	0.246	0.275

Resistance Factors

Resistance factors during polymer injection are shown in Figs. 45 and 46 for Cores 355, 356, 359, and 360. Fig. 45 shows resistance factors for the middle 10 cm of the cores. For all four cores, the resistance factors were fairly low after 10 PV of polymer injection—ranging from 1.7 to 3.3. These values are not greatly different from the solution viscosities—1.6 and 2.5 cp. For all four cores, the resistance factors increased gradually with increased polymer throughput. This behavior was expected for a polymer with strong adsorption properties. Three of the resistance factors curves tracked fairly closely. Surprisingly, one of the 900 ppm curves showed higher resistance factors than the two 1,800 ppm curves. With their higher viscosities (2.5 cp), we expected that the 1,800 ppm polymer solutions to show higher resistance factors than the 900 ppm polymer solutions (1.6 cp).
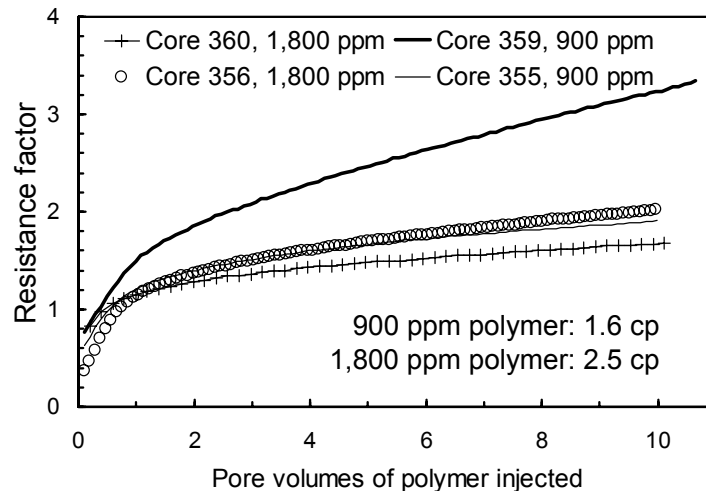
Fig. 45—Resistance factors in the middle (10-cm) section during polymer injection.

Resistance factors for the first sections of the cores are shown in Fig. 46. The maximum resistance factor was 3.5 after 10 PV. The resistance factors for three of the curves in Fig. 46 are not greatly different from those in Fig. 45—suggesting that the polymer did not significantly plug the inlet core faces. For Core 360, the resistance factors were less than one. This result is presumed to be an artifact associated with pressure measurements over the short inlet section of the core. In reality, the resistance factor should not have values below one.
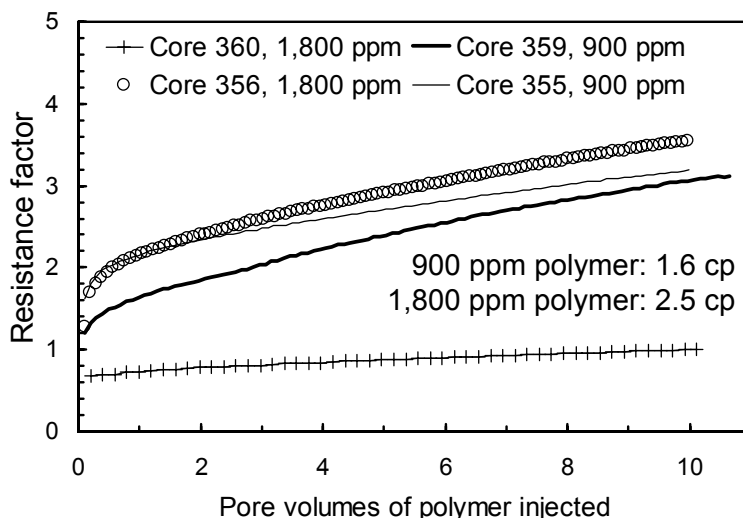
Fig. 46—Resistance factors in the first (2.3-cm) section during polymer injection.

Residual Resistance Factors
Large Oil and Water Banks. For Cores 355, 356, 359, and 360, 100 PV banks of oil and brine were injected after polymer placement. Figs. 47-50 plot oil and water residual resistance factors (F_{rr}) versus throughput for the various injection steps. These figures use a log scale for the *x*-axis. In the comments and comparisons that follow, we will generally focus on the behavior after injection of 1 PV of a given phase. Behavior before 1 PV may be complicated by rapid changes in fluid saturations.

In Fig. 47, the F_{rro1} curve shows the oil residual resistance factors during injection of 100 PV of oil after placement of 900 ppm polymer in Core 355. The F_{rrw} curve plots water residual resistance factors during the subsequent injection of 100 PV of brine. The F_{rro2} curve plots oil residual resistance factors during the final injection of 100 PV of oil. Both the oil and water residual resistance factors were fairly low, and the F_{rrw} values were never much greater than the F_{rro} values. For all three curves, the residual resistance factors decreased with increased throughput. At first, one might interpret this decrease to indicate polymer washout. However, the close similarity of the F_{rro1} and F_{rro2} curves introduce some doubt for this interpretation.

When a production well is returned to production after a polymer treatment, the polymer in the oil zone(s) will experience a high fractional oil flow. Thus, the F_{rro1} curve in Fig. 47 would be relevant to this situation. One could argue that the F_{rrw} and F_{rro2} curves in Fig. 47 would not be relevant to most field applications. In particular, polymer in any given zone should not see cycles

of water and oil production—the fractional fluid flow should remain fairly constant unless water breakthrough is imminent.
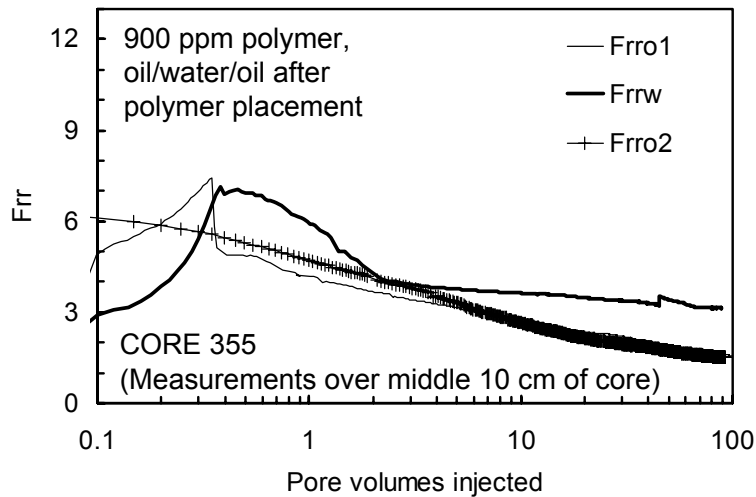
Fig. 47—Residual resistance factors in Core 355.

Similarly, when a production well is returned to production after a polymer treatment, the polymer in the water zone(s) will experience a high fractional water flow. Thus, the F_{rrw1} curve in Fig. 48 would be relevant to this situation. As shown in Fig. 48, Core 359 was treated the same as Core 355 (i.e., with 900 ppm polymer), except that after polymer placement, the injection cycle was water/oil/water instead of oil/water/oil. Consistent with the behavior of Core 355, the F_{rrw1} and F_{rro} curves decreased with increased throughput. After one PV, F_{rrw1} was about twice F_{rro} (at any given throughput value). Interestingly, the F_{rrw2} curve was fairly constant at a value of 3.3. The F_{rrw1} curve approached this value after injection of 100 PV. This result suggests that washout was important for the water residual resistance factors.
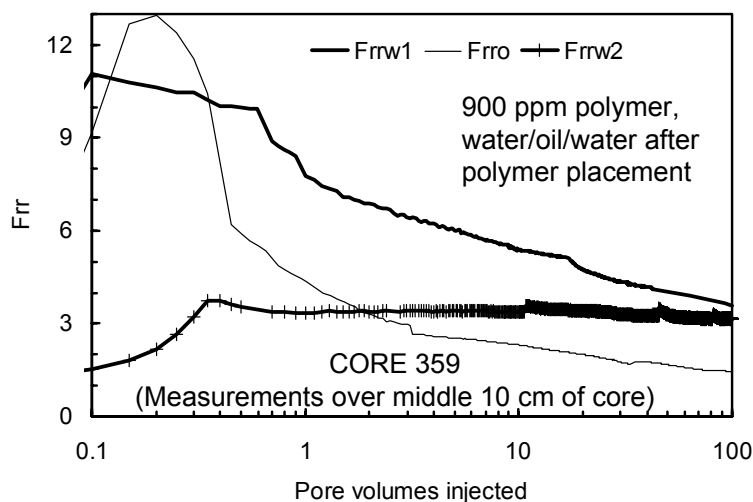
Fig. 48—Residual resistance factors in Core 359.

46

Cores 356 and 360 were treated analogously to Cores 355 and 359, except that 1,800 ppm polymer was used instead of 900 ppm polymer. Fig. 49 shows residual resistance factors associated with Core 356, while Fig. 50 shows values for Core 360. Note that the F_{rro1} and F_{rro2} curves (after 1 PV) closely tracked each other for both Cores 355 and 356. These results suggest that washout may be less of an issue for the oil residual resistance factors than for the water residual resistance factors (see previous paragraph). Of course, this statement does not explain the reason why the F_{rro} values decreased with increased throughput.

For a given throughput value (after 1 PV) in Fig. 49, F_{rrw} was about twice F_{rro}. This behavior was consistent with that for Core 359 (Fig. 48) but not with the behavior of Core 355 (Fig. 47). To further complicate the picture, the behavior of Core 360 (Fig. 50) appeared closer to that for Core 355 (Fig. 47)—i.e., low F_{rrw} values and little distinction between F_{rrw} and F_{rro}–even though the flooding treatment of Cores 355 and 360 had the least in common for the four cores.
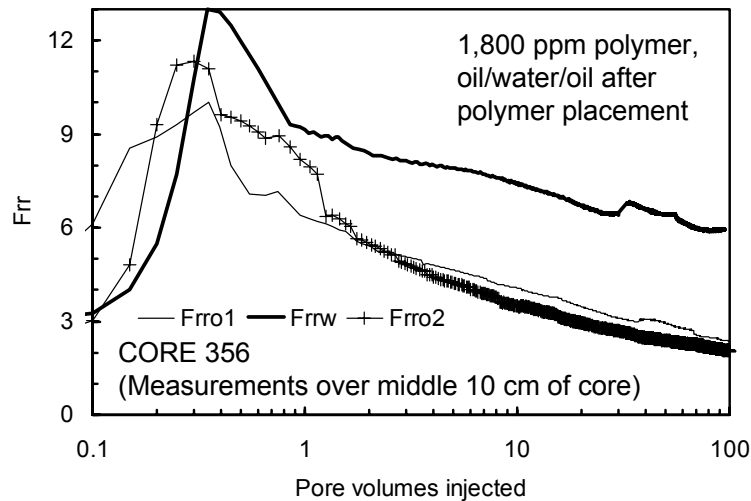
Fig. 49—Residual resistance factors in Core 356.
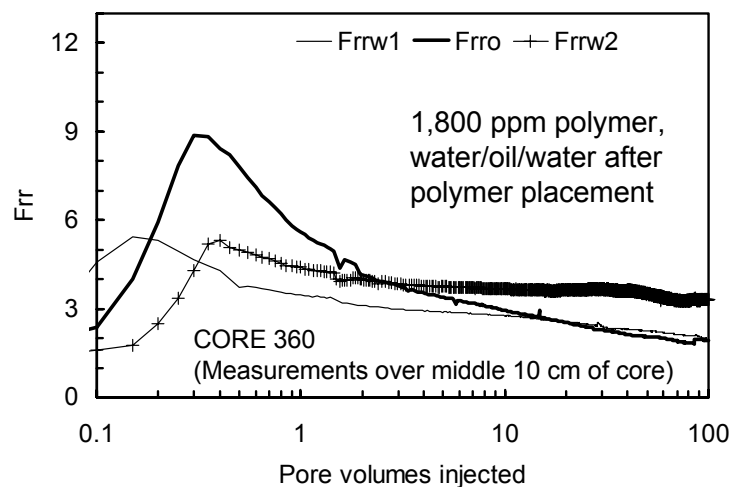
Fig. 50—Residual resistance factors in Core 360.

Small Oil and Water Banks. For Cores 353, 354, 342, and 343, much smaller banks (1-5 PV) of oil and brine were injected after polymer placement. Figs. 51-54 plot oil and water residual resistance factors (F_{rr}) versus throughput for the various injection steps. Except for the smaller oil and water bank sizes, the experiments associated with Figs. 51-54 were analogous to those associated with Figs. 47-50. In all cases, oil and water residual resistance factors were significantly greater for Cores 342-354 than for Cores 355-360. For those cores where two cycles of oil were injected after polymer placement, the F_{rro1} and F_{rro2} curves tracked each other fairly closely. In contrast, for those cores where two cycles of water were injected after polymer placement, the F_{rrw1} and F_{rrw2} behavior could not be explained readily—especially when F_{rrw2} was significantly greater than F_{rrw1}.
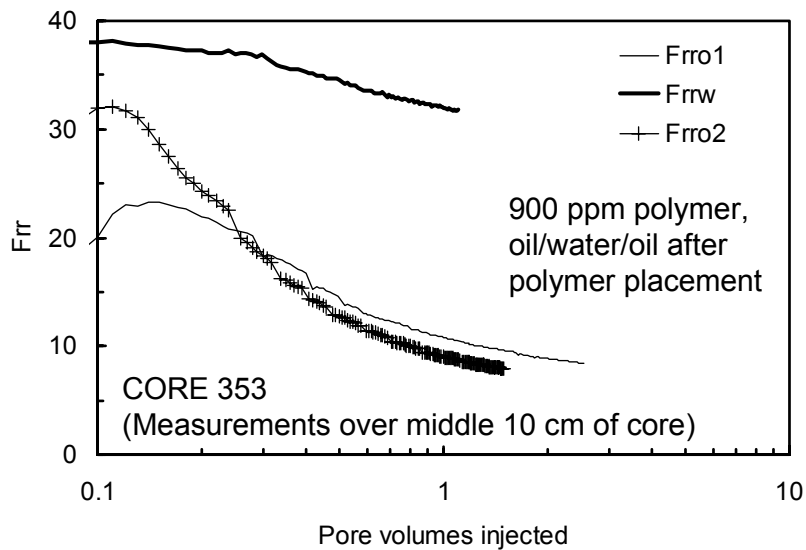
Fig. 51—Residual resistance factors in Core 353.
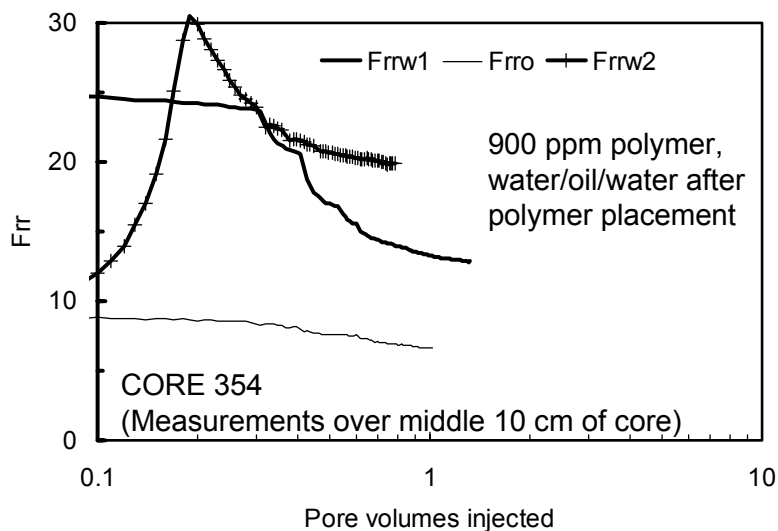
Fig. 52—Residual resistance factors in Core 354.
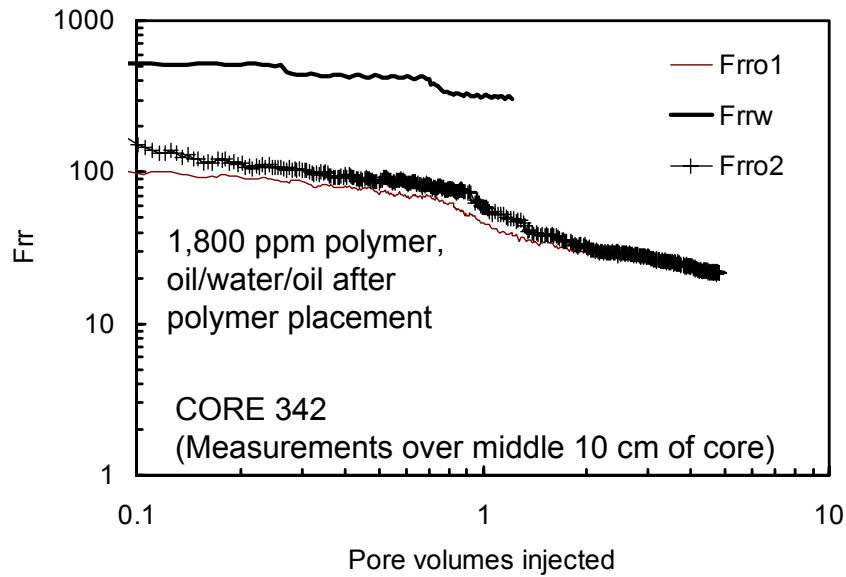
Fig. 53—Residual resistance factors in Core 342.
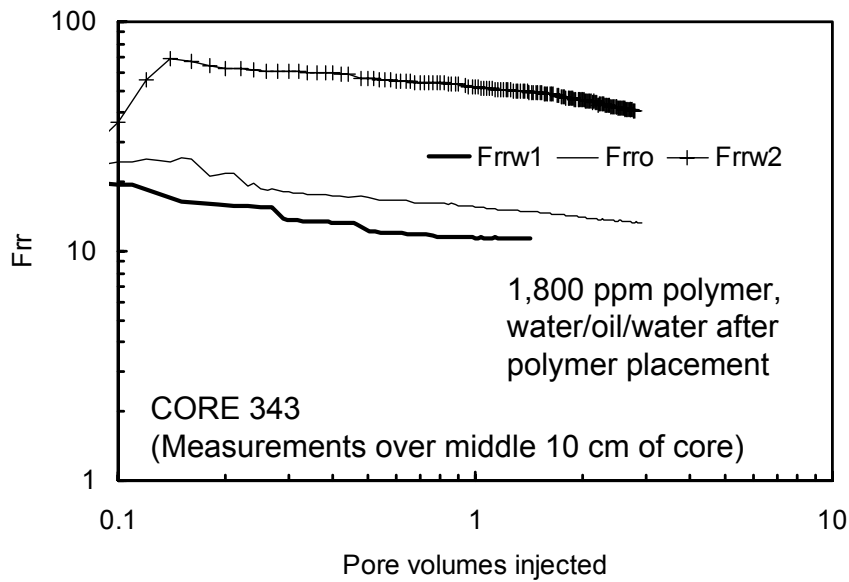
Fig. 54—Residual resistance factors in Core 343.

Performance Variability

Residual resistance factors from these experiments are compared in another way in Figs. 55 through 58. In these figures, curves labeled "oil 1st" or "water 1st" indicate the phase that was first injected after polymer placement, while curves labeled "oil 2nd" or "water 2nd" indicate data collected during injection of the second phase after polymer placement.
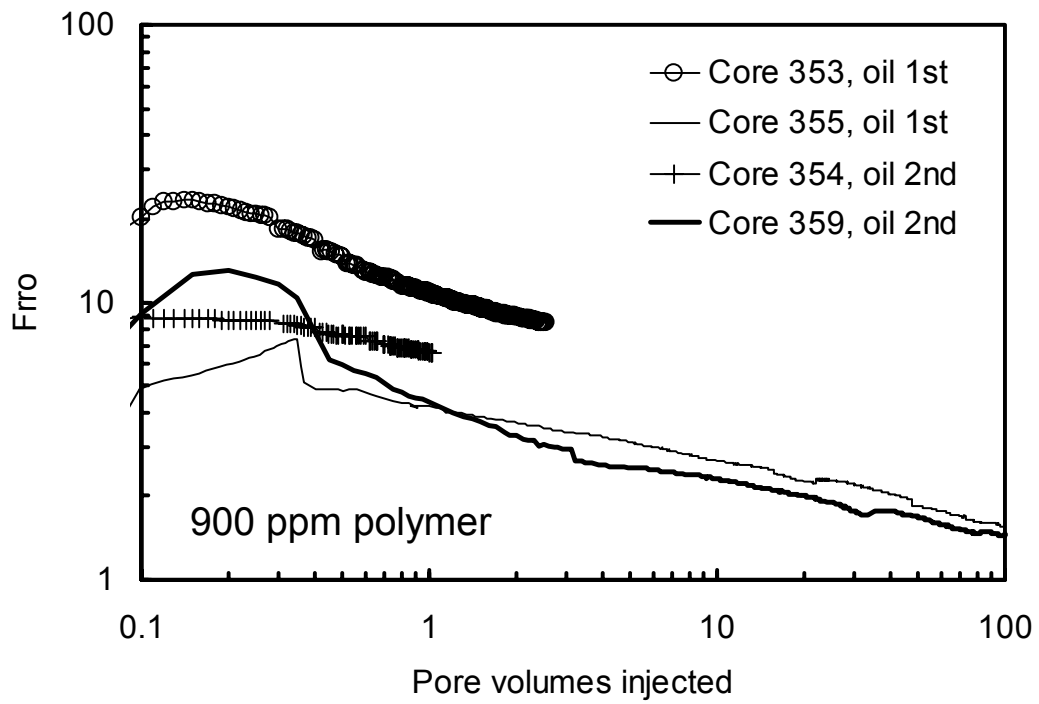
Fig. 55—Oil residual resistance factors (F_{rro}) for 900 ppm polymer.
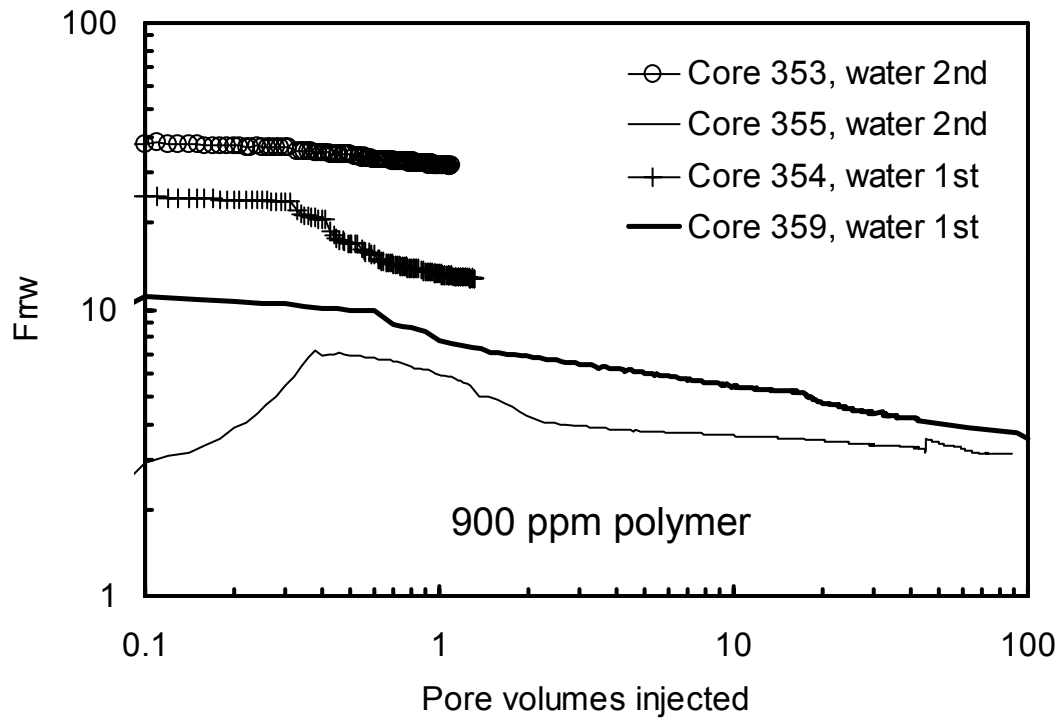
Fig. 56—Water residual resistance factors (F_{rrw}) for 900 ppm polymer.
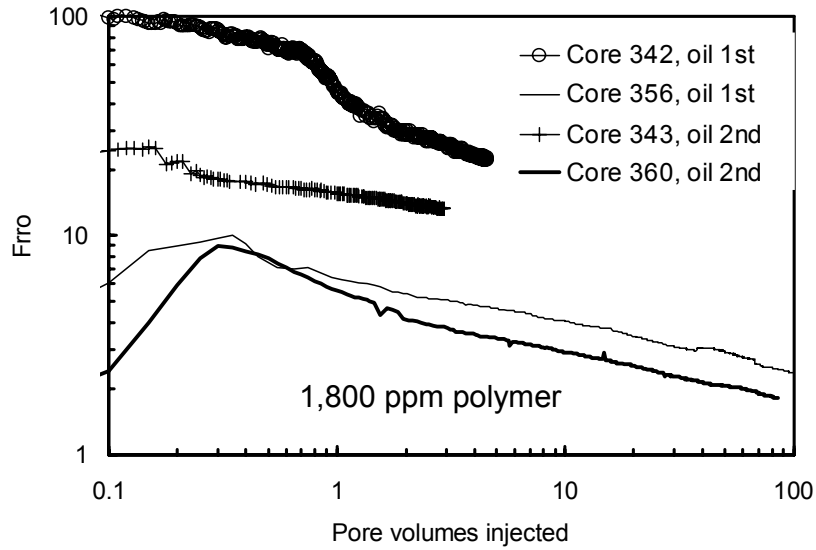
Fig. 57—Oil residual resistance factors (F_{rro}) for 1,800 ppm polymer.
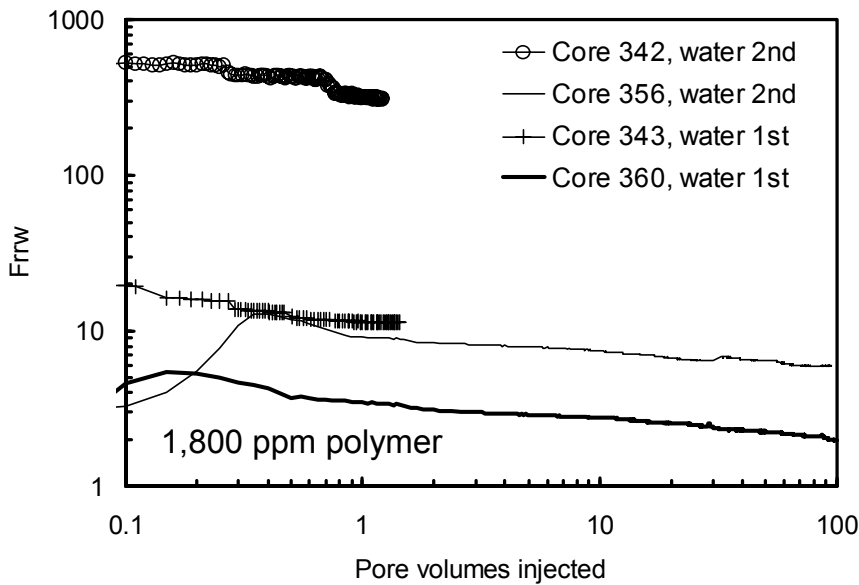
Fig. 58—Water residual resistance factors (F_{rrw}) for 1,800 ppm polymer.

A key point from these figures is that a significant degree of variability exists for the AquaCon results. For 900 ppm polymer, Fig. 55 plots oil residual resistance factors versus pore volumes of oil injected. Up to 2.5 PV of oil injection (after polymer placement), Cores 353 and 355 were treated identically. Nevertheless, the oil residual resistance factors differed by a factor of 2.5 for the two cores. Similarly for 1,800 ppm polymer, the oil resistance factors differed by a factor of 6 for two cores that were treated identically up to 4.5 PV (Cores 342 and 356 in Fig. 57). Similar observations were made for the water residual resistance factors (Figs. 56 and 58). Why does this variability exist? A single batch of polymer was used, so compositional variations should not be significant. Corefloods 342 and 343 were performed in January/February of 2002, while Corefloods 353 to 360 were performed within a three-week period in April. One might suspect

51

that degradation of the polymer between February and April resulted in lower residual resistance factors for the later floods. However, this suggestion does not explain the variations observed for Corefloods 353 to 360 or the differences noted for Corefloods 342 and 343.

The core properties before polymer placement (Table 4) do not reveal an obvious explanation for the performance differences. The core properties were quite similar, and only one batch of Berea sandstone was used. Of course, variations in mineralogy within this Berea batch can occur. Whether these variations were sufficient to account for the observed differences is unknown.

One could argue that Cores 359 and 360 had a significantly lower permeability than the other cores (Table 4). However, lower permeability for Berea usually implies higher clay content and higher polymer adsorption levels. In that case, residual resistance factors should have been highest for these two cores. Instead, their residual resistance factors were among the lowest values (see Figs. 55-58).

Comparison of Figs. 55-58 reveals that water residual resistance factors (F_{rrw}) were generally greater than oil residual resistance factors (F_{rro}). However, for any given core at a specified PV throughput, the ratio, F_{rrw}/F_{rro}, typically had a value of two, with a range from one to four. These values were not as high as we would like for field applications. In general, the residual resistance factors decreased with increased PV throughput.

In many field applications, the choice of F_{rrw}/F_{rro} should involve comparing F_{rrw} and F_{rro} values at different throughput values. For example, if a low water production rate is anticipated after a polymer or gelant treatment, the appropriate throughput for comparison may be lower for F_{rrw} than for F_{rro}. On the other hand, the appropriate throughput may be lower for F_{rro} than F_{rrw} for cases where relatively high post-treatment water production rates are expected.

In summary, although the AquaCon polymer consistently reduced permeability to water more than that to oil, the magnitude of the disproportionate permeability reduction varied significantly. Thus, as with most materials tested to date, the issue of reproducibility and control of the disproportionate permeability reduction remains to be resolved. Of course, an important premise of our research project is that the disproportionate permeability reduction could be made more reproducible and controllable if we understood the mechanism behind the phenomenon.

Polyethylene Cores
We performed two studies of the polymer in strongly oil-wet polyethylene cores. The core dimensions and flooding procedures were the same as for the Berea cores described above, except that the polyethylene cores were first saturated with oil instead of brine, and an extra waterflood was performed before polymer injection. The polyethylene cores were an order of magnitude more permeable than the Berea cores and had twice the porosity (i.e., 40% versus 21%). The S_{or} values for the polyethylene and Berea cores were similar (~0.3), but the polyethylene S_{wr} values were about half those for Berea sandstone (compare Tables 4 and 5). As was the case with Berea, little hysteresis of the endpoint permeabilities and saturations occurred when flooding from S_{or1} to S_{wr} to S_{or2} before polymer injection.

Table 5—Summary of polyethylene core properties.

polymer, ppm	Core	$k_o,$ md	$k_{wro1},$ md	$k_{ocw},$ md	$k_{wro2},$ md	S_{or1}	S_{wr}	S_{or2}
	341	6,400	4,000	3,100	4,000	0.295	0.155	0.293
1,800	344	10,100	3,600	3,000	3,800	0.319	0.160	0.327

The polymer concentration was 1,800 ppm for both corefloods. In Core 341 (Fig. 59), the flooding sequence was oil/water/oil after polymer placement, while in Core 344 (Fig. 60), the flooding sequence was water/oil/water. In Core 341, interestingly, the F_{rro} value was 95 for the first 0.45 PV of oil injection and experienced a significant drop to 1.5 during the next 3 PV of oil injection. This behavior suggests washout of much of the polymer slug between 0.45 and 3.5 PV. Ironically, one would not expect high resistance factors and adsorption levels for this hydrophilic polymer in an oil-wet porous media. During injection of 6.4 PV of brine, the F_{rrw} values declined but were still more than 2.5 times the F_{rro} values. Thus, somewhat surprisingly, the disproportionate permeability reduction factor in strongly oil-wet polyethylene was as great as that in strongly water-wet Berea sandstone. Consistent with the results in Berea, after 1 PV, the F_{rro} values during the second cycle of oil injection were similar to those during the first cycle.
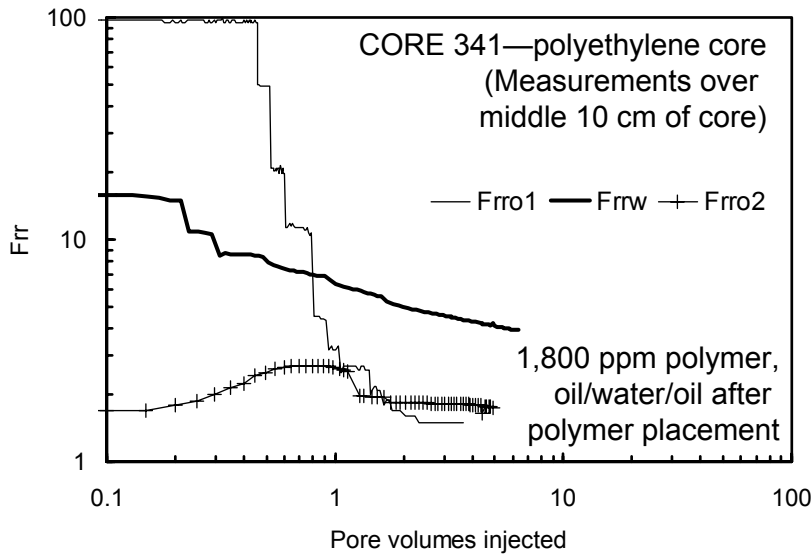
Fig. 59—Residual resistance factors in Polyethylene Core 341.

In Core 344 (Fig. 60), the flooding sequence was water/oil/water. Again, the F_{rrw} values were fairly high considering that the polymer was hydrophilic and the porous media was oil wet. During injection of 6.6 PV of brine, F_{rrw1} declined to a value of 5—similar to the value noted for Core 341. During the subsequent oil injection, the F_{rro} values were about 1.5—again, similar to the values noted for Core 341. Thus, the same level of disproportionate permeability reduction (~2.5) was observed for Cores 341 and 344. Finally, after 1 PV, the F_{rrw} values during the second cycle of water injection were similar to those during the first cycle. Thus, the residual resistance factors showed more reproducible behavior in polyethylene than in Berea sandstone.

53
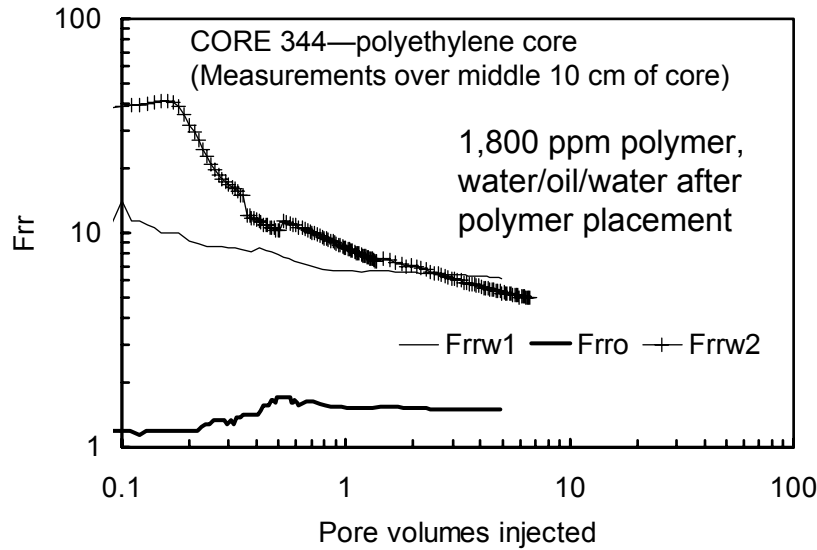
Fig. 60—Residual resistance factors in Polyethylene Core 344.

Small Berea Cores

Two sets of experiments (Cores 345 and 346) were performed in small Berea cores that were ~7 mm in diameter and 3-cm long. Cores of this dimension were required for our studies using X-ray computed microtomography. These cores had one internal pressure tap located 4 mm from the inlet sandface. Properties of these cores and floods are summarized in Table 6. These two cores had similar permeabilities to oil and water before polymer placement, but their k_{wro} values were one-half to one-sixth the values seen in the larger cores (see Table 4). In these cores, the flooding pressure gradient was 200 psi/ft, compared with 30 psi/ft for the larger cores described above. Again, all experiments were performed at room temperature.

Table 6—Floods in small Berea sandstone cores.

Core	k, md	k_{ocw}, md	k_{wro}, md	F_{rro1}	F_{rrw1}	F_{rro2}	F_{rrw2}
345	584	400	56		246	8.7	127
346	747	448	48	4.2	52.0	3.2	29.5

In both cores, 1,800 ppm polymer was injected. For Core 345, 5.3 PV of polymer solution were injected, while 7.5 PV were injected into Core 346. For Core 345 after polymer placement, water was injected first, followed by cycles of oil and water injection. For this case, F_{rrw1} was 246 after 1.1 PV of water; F_{rro2} was 8.7 after 3.6 PV of oil; and F_{rrw2} was 127 after 1.0 PV of water (Table 6). For Core 346, oil was injected first after polymer placement, followed by cycles of oil and water injection. In this core, F_{rro1} was 4.2 after 6.3 PV of oil; F_{rrw1} was 52 after 1.3 PV of water; F_{rro2} was 3.2 after 7.2 PV of oil; and F_{rrw2} was 29.5 after 0.7 PV of water (Table 6). Qualitatively, these results were consistent with those of the other cores—the polymer reduced permeability to water more than that to oil, and F_{rro1} was similar to F_{rro2}. The F_{rrw} values were significantly greater than the F_{rro} values—by factors up to 28, compared with factors less than 4

54

for the experiments in the larger cores. We do not know why greater disproportionate permeability reduction was observed in the smaller cores.

Incidentally, Core 346 was used to study the polymer during X-ray computed microtomography experiments. Unfortunately, technical difficulties compromised these microtomography images, so they were lost.

Ether And Alcohol Preflushes And Postflushes
The polymer vendor (BJ) recommended (1) preflushing the core with 2% KCl, 0.2% NE-940, 10% US-40, (2) injecting the polymer bank containing 2% KCl, 0.2% NE-940, 1,800 ppm polymer, and (3) postflushing with 2% KCl, 0.2% NE-940. US-40 is a BJ product that contains ethylene glycol monobutyl ether. NE-940 is a BJ product that contains 40-70% methanol, 5-10% 2-ethylhexanol, 5-10% isopropanol, 1-5% ethoxylated alcohol, and 5-10% heavy aromatic naptha. We performed six corefloods (Cores 349, 350, 351, 352, 357, 358) using the BJ-recommended procedure. These Berea sandstone cores were about 15-cm long and 3.8 cm in diameter. Properties of the cores before polymer placement are listed in Table 7. The core properties were fairly uniform and consistent with those in Table 4.

Table 7—Berea cores for preflush/postflush experiments.

Core	k_w, md	k_{ocw}, md	k_{wro}, md	S_{wr}	S_{or}	Preflush, PV	Polymer, PV	Postflush, PV
349	810	700	306	0.276	0.251	1	8	1
350	883	791	314	0.272	0.243	1	9	1
351	915	821	319	0.259	0.261	1	10	1
352	817	767	267	0.255	0.263	1	10	1
357	931	835	343	0.243	0.251	1	10	20
358	794	714	363	0.273	0.263	1	10	20

In all six cores, a 1 PV preflush was used, and the polymer bank was 8-10 PV. In four cores (Cores 349, 350, 351, and 352), a 1 PV postflush was applied—before the usual oil or water banks were injected. In two cases (Cores 357 and 358), the postflush was 20 PV. Residual resistance factors recorded during injection of the subsequent oil and water injection cycles are shown in Figs. 61-66. These floods were compromised to some extent because oil was mobilized during gelant injection—even at low pressure gradients. We suspect that the alcohols and ether present in US-40 and NE-940 were responsible for oil mobilization.

Even with the complications associated with mobilized oil, the results shown in Figs. 61-66 showed the same general behavior that was reported earlier in this chapter. Both water and oil residual resistance factors generally decrease with throughput. Both F_{rrw} and F_{rro} values exhibited significant variability from core to core. In Cores 349 and 350, F_{rrw} values were 2 to 6 times greater than F_{rro} values. However, for the other four cores, the residual resistance factors were ultimately about the same for water and oil—or in some cases, F_{rro} was actually greater than F_{rrw}.
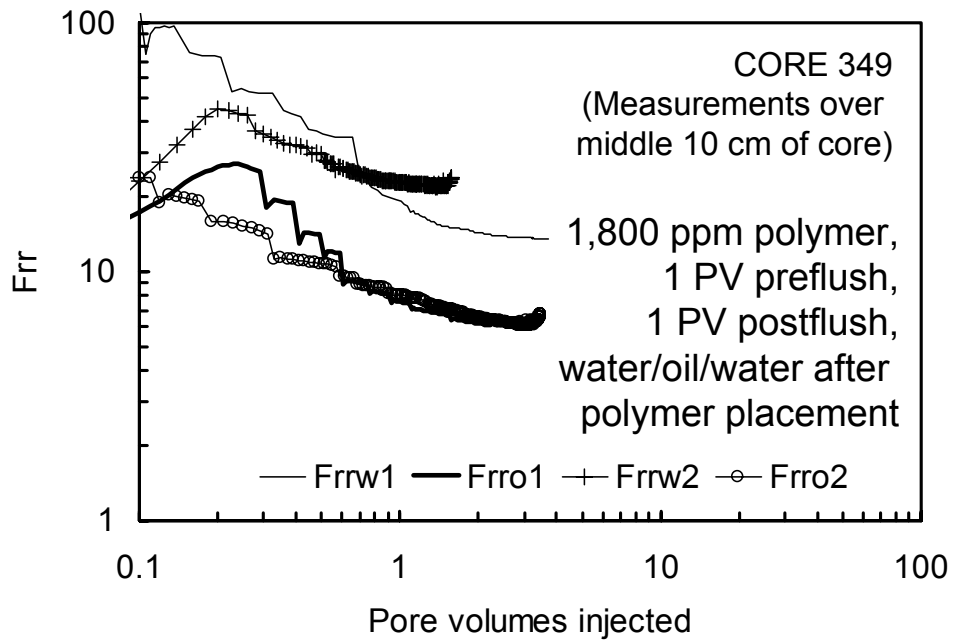
Fig. 61—Residual resistance factors in Berea Core 349.
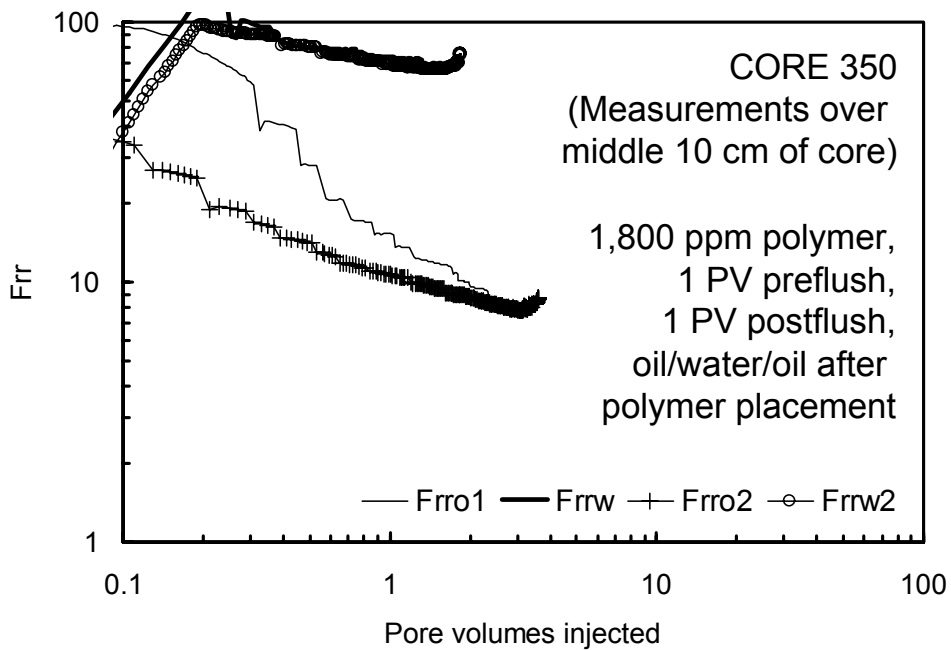
Fig. 62—Residual resistance factors in Berea Core 350.
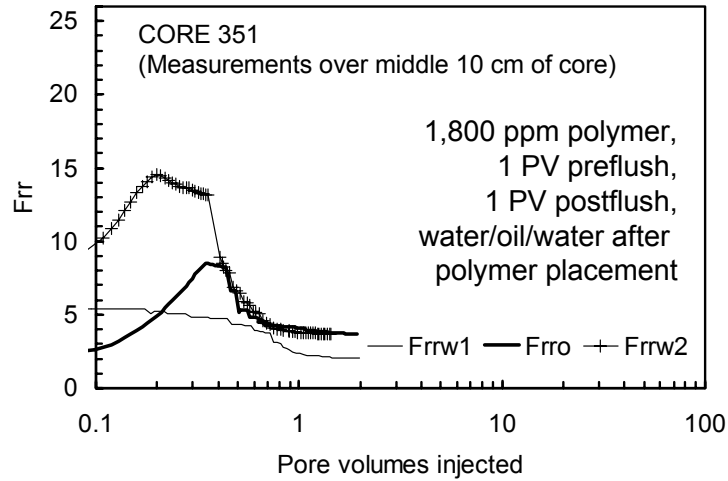
Fig. 63—Residual resistance factors in Berea Core 351.
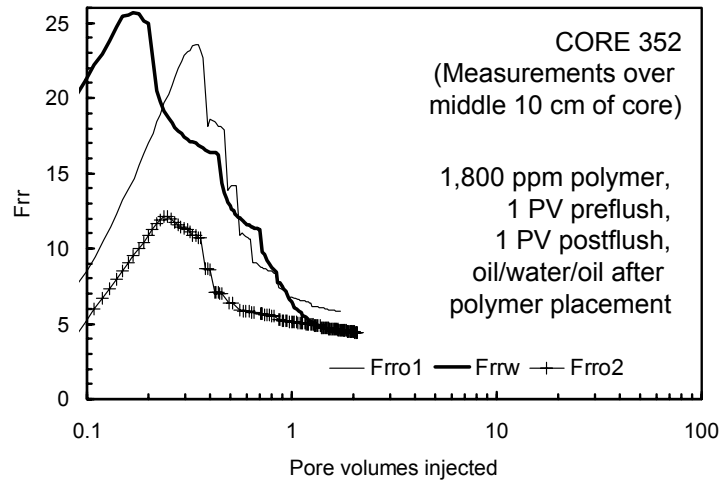
Fig. 64—Residual resistance factors in Berea Core 352.
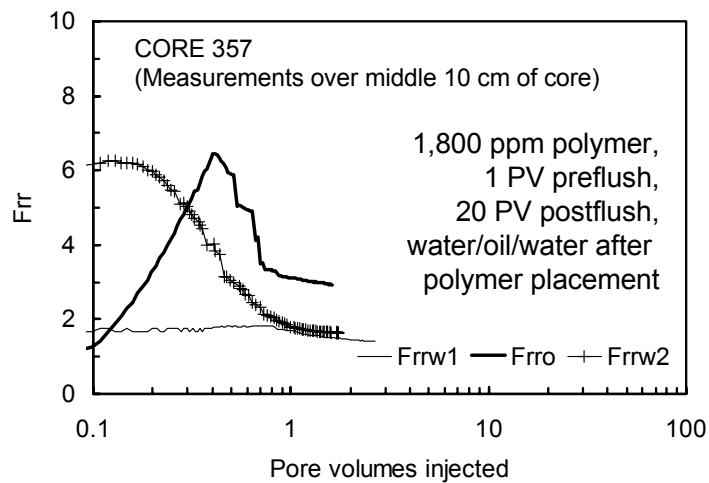
Fig. 65—Residual resistance factors in Berea Core 357.
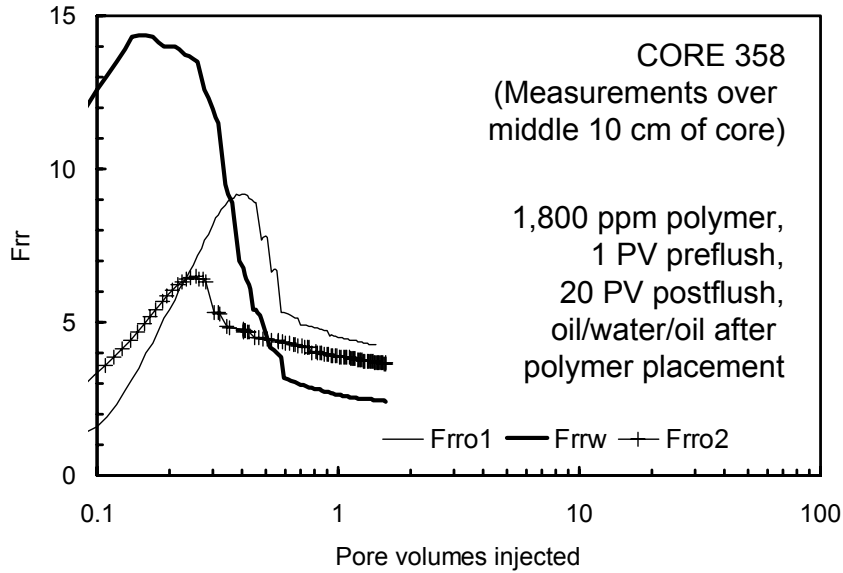
Fig. 66—Residual resistance factors in Berea Core 358.

F_{rr} Values At 1 PV Of Oil Or Water Injection

Another means to compare the experiments for the polymer is using the residual resistance factors after injection of 1 PV of oil or water. These values are listed in Table 8.

Table 8—Summary of F_{rro} and F_{rrw} values at 1 PV oil or water injection.

Porous media	Polymer ppm	Core	Preflush/ postflush?	Oil/water bank size	F_{rro1}	F_{rrw1}	F_{rro2}	F_{rrw2}	F_{rro3}
Berea sandstone	900	353	no	small	10.8	32.0	9.0		
		354				13.3	6.6	19.9	
		355		large	4.2	6.0	4.7		
		359				6.7	4.3	3.3	
	1,800	342		small	46.0	317	59.0		
		343				11.4	13.3	52.0	
		356		large	6.3	9.1	8.1		
		360			3.5	5.6	4.4		
		349	yes	small		19.3	7.6	22.8	8.0
		350			15.4	73.4	10.7	68.5	
		351				2.3	4.1	3.8	
		352			6.8	6.5	5.1		
		357				1.7	3.1	1.8	
		358			4.5	2.6	3.9		
polyethylene		341	no	small	3.2	6.3	2.7		
		344				6.6	1.5	8.5	
				Average	11.2	32.5	9.3	22.6	
				Standard deviation	13.6	77.9	13.6	24.9	

58

The average and standard deviation values for the oil and water residual resistance factors are listed at the bottom of the table. This table emphasizes the large variations for the F_{rro} and F_{rrw} values. In all cases listed in Table 8, the standard deviations were larger than the averages. The variations did not correlate with (1) whether the core was Berea sandstone or polyethylene, (2) whether the polymer concentration was 900 or 1,800 ppm, (3) whether preflushes and postflushes were used, or (4) whether the first fluid injected after polymer placement was oil or water.

The F_{rrw} values were noticeably greater than the F_{rro} values for at least half of the cores. The F_{rro1} and F_{rro2} values were generally similar. In contrast, the F_{rrw1} and F_{rrw2} values were similar for only half of the cores. The 1-PV residual resistance factors tended to be somewhat larger when small oil or water banks were injected.

For most cores, the disproportionate permeability reduction was not large—F_{rrw} /F_{rro} was less than 3 for more than 80% of the cores. This level of disproportionate permeability reduction would be unacceptably low for most field applications—either in unfractured or fractured production wells. In unfractured wells, F_{rro} should usually be less than two, while F_{rrw} should be at least 20.[10] In fractured production wells, F_{rrw} should be at least 200, and F_{rrw} /F_{rro} should be at least 10.[36,38] The polymer did provide acceptable ratios for F_{rrw} /F_{rro} in a few cases—leaving hope that the polymer may be valuable if a controlled disproportionate permeability reduction can be attained.

Conclusions
The following conclusions were noted during studies of disproportionate permeability reduction by the AquaCon polymer.

1. A significant degree of variability exists for the oil and water residual resistance factors. The variations did not correlate with (a) whether the core was Berea sandstone or polyethylene, (b) whether the polymer concentration was 900 or 1,800 ppm, (c) whether preflushes and postflushes were used, or (d) whether the first fluid injected after polymer placement was oil or water. As with any material used for disproportionate permeability reduction, understanding and controlling this performance variability will be key to the successful application of this polymer in production wells.
2. For most cores, the disproportionate permeability reduction was not large—F_{rrw} /F_{rro} was less than 3 for more than 80% of the cores. This level of disproportionate permeability reduction would be unacceptably low for most field applications—either in unfractured or fractured production wells. The polymer did provide acceptable ratios for F_{rrw} /F_{rro} in a few cases—leaving hope that the polymer may be valuable if a controlled disproportionate permeability reduction can be attained.
3. Oil and water residual resistance factors typically decreased with increased oil or water throughput. For the water residual resistance factors, evidence of washout was noted for some cores. However, washout did not adequately explain the decrease in oil residual resistance factors with increased throughput.
4. For a given throughput value (above 1 PV), oil residual resistance factors were similar through multiple cycles of oil and water injection (i.e., F_{rro1} and F_{rro2} values were generally similar). In contrast, the F_{rrw1} and F_{rrw2} values were similar for only half of the cores.

5. GELANT TREATMENTS IN FRACTURED PRODUCTION WELLS

For most gel treatments applied for conformance improvement and water shutoff, design procedures (especially the methods for treatment sizing) were strictly empirical—a fact that is partly responsible for the erratic success rates of these treatments. Many water shutoff treatments rely on the ability of polymers or gels to reduce permeability to water much more than that to oil. Unfortunately, the magnitude of this disproportionate permeability reduction cannot yet be predicted *a priori* under reservoir conditions. Since laboratory studies are rarely performed before field applications, widely varying field results are not surprising.

In some cases, individuals have suggested that field results with gelant treatments were at odds with laboratory data or with basic petroleum engineering principles. Depending on their background, operators, service companies, and researchers naturally place more credence in some observations than others. For example, a service company may prefer to emphasize certain field observations to rationalize an explanation that researchers find in contradiction with laboratory findings or in violation of established petroleum engineering principles. Consequently, all data (field, laboratory, and theoretical) should be considered when applying and evaluating field applications of gelant treatments. Of course, observations can be misinterpreted. Laboratory experiments may be botched or performed in misleading ways; theoretical or numerical studies may suffer from incorrect assumptions (e.g., garbage in/garbage out); and field results may be interpreted incorrectly. However, by combining sound laboratory, theoretical, and field observations, a consistent picture should emerge that can be used to improve the success rate for future field applications.

This chapter describes an engineering-based approach to design and interpret gelant treatments in naturally fractured production wells. First, properties of the Motatan field are summarized, and laboratory and field results associated with the gelant treatments are reviewed. A mechanism of action is proposed for the gelant treatments. Field data are utilized to judge the heights and permeabilities of oil and water zones and the role of fractures in the excess water production problem. Analyses using gelant injection data provide valuable insight into the fracture area open to flow and the distance of gelant penetration from the fracture face. Post-treatment production results are used to estimate in situ oil and water residual resistance factors, which are compared with laboratory values. Finally, the results are examined with regard to optimizing gelant volumes for future applications.

The Motatan Field

A detailed description of the Motatan field is provided in Ref. 39. The field is located in western Venezuela, southeast of Lake Maracaibo. The South Dome area of the field is an anticline with north-south elongation and is cut by numerous faults. The South Dome consists of four areas—two of which (P-35 and P-39) had high water cut wells that were treated with gelants. Each area produced from two reservoirs: the Pauji and Misoa formations, which are Eocene sandstones. Within these formations, the gelant treatments were targeted at three specific flow units, designated A9, A10, and B0. Depending on the well treated, the targeted sands existed at depths ranging from 7,930 to 9,000 ft and formation temperatures ranged from 210°F to 240°F. Water viscosity at these temperatures was about 0.25 cp. Gross pays ranged from 184 to 920 ft.

Formation porosities were typically around 10%, while permeabilites were typically from 20 to 50 md. PVT analysis indicated an oil viscosity of 3.7 cp at reservoir conditions.

Exploitation of these naturally fractured, undersaturated reservoirs began in 1975. They were produced by water drive and rock-fluid expansion. Until the mid-1990s, the wells drilled in the P-35 and P-39 areas typically produced from 1,500 to 4,000 BOPD (per well) with very little water production. Subsequently, the water cuts rose steadily. At the time of the gelant treatments (1998-1999), the total production was 8,100 BOPD and 15,050 BWPD, yielding an average water cut of 65%. However, some of the wells had water cuts above 80%. (Production histories for the treated wells can be found in Ref. 39.)

The Gelant And Treatment Results
The gelant system was a high molecular weight, partially hydrolyzed polyacrylamide (HPAM) crosslinked with phenol and formaldehyde. Details of this gelant can be found in Refs. 40-42. In Berea sandstone at reservoir conditions, this gel provided a water residual resistance factor (F_{rrw}) around 200 and an oil residual resistance factor (F_{rro}) around 20.[39,42]

Gelant treatments were applied in four wells: P-43, P-47, P-48, and P-50. Descriptions of the treatments and the production performance are available in Ref. 39. Table 9 summarizes the results. Significant reductions in water cut were observed in all treated wells. The mechanism of action that we envision for these treatments involves: (1) gelant injection with subsequent flow through the fracture system, accompanied by gelant leakoff through the fracture faces into both the oil and water zones, (2) shut-in to allow gel to form, and (3) return to production, with the gel substantially retarding water flow from the matrix into the fracture system but inhibiting oil flow to a significantly lesser degree.[36] The success of these treatments depends on the distance of gelant leakoff and the residual resistance factors in the oil and water zones.

Table 9—Results from four gelant treatments.

Well	Gelant volume, bbls	Water cut before gel, %	Water cut just after gel, %	Water cut a few months after gel, %
P-43	1,100	98	28	64
P-47	1,000	97	42	64
P-48	3,600	75	40	64
P-50	2,000	80	20	60

This chapter focuses on the results from Well P-47. The primary reason for this choice was that pressure data was recorded during critical parts of the treatment in this well. This pressure data is crucial for the proper interpretation of any gel treatment.

In Well P-47, the A9 and A10 flow units were treated with gelant. These sands were located at depths from 7,930 to 8,357 ft, with a net pay of 90 ft (distributed through six perforated intervals). The average rock matrix permeability and porosity of the net pay were 22 md and 9.8%, respectively. Shortly before the gel treatment, these sands produced 1,460 BWPD and 53 BOPD. The reservoir pressure was 2,600 psi and the pressure drawdown was 350 psi (i.e.,

between the reservoir and the well). The gelant treatment was applied during December 1999, when 1,000 bbl of gelant were injected at a rate of 1 barrel per minute (BPM). During gelant injection, the wellhead pressure ultimately rose to 3,500 psi. After gelant placement, the well was shut in for one week. Upon return to production, the intervals produced 63 BWPD and 87 BOPD, yielding a 42% water cut and a 64% increase in oil production rate. Four months later, the intervals produced 128 BWPD and 72 BOPD with a 1,300 psi drawdown, resulting in a 64% water cut. One year after the treatment, the production rates were 81 BWPD and 141 BOPD with a 465 psi drawdown.

Using Field Data To Estimate Flow Properties

Heights Of Oil And Water Zones. Production data can be used to estimate some of the in situ flow properties within the reservoir. These parameters will ultimately be used in our assessment of the gelant treatment. The first parameters to be estimated are the heights of the oil and water zones, h_{oil} and h_{water}. In early 1994, Well P-47 produced 1,335 BOPD with a 2% water cut—the open zones experienced 98% fractional oil flow and were near the connate water saturation. In contrast, just before the gelant treatment in 1999, the well produced 1,460 BWPD and 53 BOPD. At this time, at least two possibilities existed. First, the entire open interval could have exhibited a uniform fractional water flow of 97%. If this case applied, a gelant treatment would not be effective because near wellbore treatments cannot alter the pseudo-steady state fractional flow of a single producing zone.[43] Alternatively, a small fraction of the original net pay may have continued to produce nearly 100% fractional oil flow, while most of the net pay was watered out. This scenario could be amenable to successful treatment using gelants.

Since the gelant treatments were ultimately found to reduce the water/oil ratio, distinct water and oil zones must exist within the net pay.[43] Assume that the total height (90 ft), completion, pressure drawdown, and degree of stimulation remained relatively unchanged between 1994 and 1999. Also, in examining the production data from the various wells, the total fluid production rates held reasonably constant over this same time period. With these assumptions, Eqs. 18 and 19 may be used to estimate the heights of the oil and water zones within the net pay at the time of the gelant treatment.

$$h_{oil1999} = h_{oil1994} [q_{oil1999} /q_{oil1994}]=90[53/1,335] = 3.6 \text{ ft} \dotfill (18)$$

$$h_{water1999} = h_{total} - h_{oil1999} = 90 - 3.6 = 86.4 \text{ ft} \dotfill (19)$$

Thus, given a net pay of 90 ft, the heights associated with the oil and water zones before the gelant treatment were 3.6 ft and 86.4 ft, respectively. This determination allows for the possibility that multiple oil and water zones may exist (i.e., it does not assume that there is only one oil zone and one water zone). Also, the location of the oil zone(s) could be anywhere within the total pay.

k_w/k_o. With the above assumptions, the ratio of in situ endpoint permeabilities can be estimated from fluid production rates, viscosities (μ_o and μ_w), zone heights, and formation volume factors (B_o and B_w).[44]

$$k_w/k_o \approx [q_{water1999} \mu_w B_w h_{oil1994}]/[q_{oil1994} \mu_o B_o h_{water1999}] \dotfill (20)$$

Given that $q_{water1999}$=1,460 BWPD, $q_{oil1994}$=1,335 BOPD, μ_w=0.25 cp, μ_o=3.7 cp, B_w=1.0 reservoir bbl/stock tank bbl, B_o=1.2 reservoir bbl/stock tank bbl, $h_{oil1994}$=90 ft, and $h_{water1999}$=86.4 ft, the ratio of endpoint permeabilities, k_w/k_o, was calculated to be 0.064.

$$k_w/k_o \approx [1,460\text{x}0.25\text{x}1\text{x}90]/[1,335\text{x}3.7\text{x}1.2\text{x}86.4]=0.064 \dots\dots\dots(21)$$

For comparison, laboratory measurements on three field cores yielded k_{rw}/k_{ro} values of 0.167, 0.235, and 0.394. Also, for comparison, a k_{rw} value of 0.69 was assumed for a "unified simulation reservoir model" of the Motatan field. These comparisons suggest that caution is needed when selecting the relative permeability values. The field value of 0.064 seems to be the most appropriate for our purposes.

Was The Well Fractured? The calculations associated with Eqs. 18-21 do not depend on whether fractures intersected the well. The geological description for the Motatan field indicated that faults and natural fractures were present.[39] Productivity data can be used to confirm the presence of fractures. For Well P-47 before gelant injection, 1,513 BPD of total fluid were produced with a pressure drawdown of 350 psi. Thus, the productivity index, $q/\Delta p$, was 4.32 BPD/psi. Individual productivity indexes can be calculated for oil and water—i.e., 53 BOPD/350 psi = 0.151 BOPD/psi for oil and 1,460 BWPD/350 psi = 4.17 BWPD/psi for water. If flow were radial around the well (i.e., the well was not fractured), the measured productivity index should be less than or equal to that calculated using the Darcy equation for radial flow.[4]

$$q/\Delta p \leq kh/[141.2\ \mu\ ln(r_e/r_w)] \dots\dots\dots(22)$$

On the other hand, if the actual productivity index is significantly greater than the value calculated from the right side of Eq. 22, a fracture is probably present.[4]

For Well P-47, the wellbore radius, r_w, was 7 inches, and the external drainage radius, r_e, was assigned a value of 2,000 ft, based on the "unified simulation reservoir model" that was developed by PDVSA for this field. For oil production, the effective permeability to oil k_o, was assumed equal to the absolute permeability of the rock matrix—a value of 22 md. Given that h_{oil} was 3.6 ft and μ_o was 3.7 cp, the right side of Eq. 22 yields a value of 0.0186 BOPD/psi. This value was about one-eighth the actual productivity index for oil (0.151 BOPD/psi) and supports the supposition that a fracture intersects the wellbore. For water production, the effective permeability to water, k_w, was assumed equal to 0.064 k_o or 1.4 md (from Eq. 21). Given that h_{water} was 86.4 ft and μ_w was 0.25 cp, the right side of Eq. 22 yields a value of 0.42 BWPD/psi. This value was about one-tenth the actual productivity index for water (4.17 BWPD/psi) and confirmed the presence of a fracture.

Analyses During Gelant Injection
Lpw/Lpo. During the process of gelant injection, the gelant flowed rapidly through the fracture system while leaking off some distance from the fracture faces in all permeable zones that were cut by the fracture. How much different was the distance of gelant leakoff in the water zone (L_{pw}) from that in the oil zone (L_{po})? The methods of Refs. 43 and 45 were applied to determine that the ratio, L_{pw}/L_{po}, was close to unity. Although the detailed calculations are not included here, the

findings can be appreciated with the following arguments. First, the aqueous gelant experienced about the same residual oil saturation in the oil zone as in the water zone. The water zone originally had a high oil saturation but has become watered out. In contrast, the oil zone, of course, had a high oil saturation ahead of the gelant front. However, behind the viscous gelant front, the oil saturation was efficiently flooded to its residual level. Since the gelant experienced nearly the same oil saturation (i.e., S_{or}) in both the water and oil zones, the permeability to water was about the same in both zones (i.e., k_w=0.064k_o=1.4 md). Finally, the viscous gelant exhibited a very efficient (piston-like) displacement in both zones. Specifically, the mobility ratio was about 0.003 in both zones [i.e., (0.064/75 cp)/(1/3.7 cp) for gelant displacing oil in the oil zone and (0.064/75 cp)/(0.064/0.25 cp) for gelant displacing water in the water zone]. Thus, the gelant penetrated to nearly the same distance in the water zone as in the oil zone.

This analysis assumed that the rock permeability was the same in the water and oil zones. The outcome from the analysis would be unchanged if fluids could freely crossflow between the water and oil zones and if the ratio of the permeabilities of the water and oil zones was less than the mobility ratio (a factor of about 300 in this case).[46] If fluids cannot crossflow between the oil and water zones, the distance of gelant leakoff into the water zone relative to that in the oil zone would be approximately the square root of the permeability of the water zone relative to that of the oil zone.[45,46]

Estimation Of Fracture Area. Additional useful information about the fracture system can be obtained during injection of the viscous gelant. During injection of 1,000 bbl of gelant[39] (HPAM crosslinked with phenol and formaldehyde) at a rate of 1 BPM, the wellhead pressure reached 3,500 psi. The hydrostatic head associated with the 8,000-ft fluid column was about 3,465 psi. Using standard methods, the pressure drop associated with friction down the pipe was judged to be small compared to the total pressure drop. Therefore, it was neglected in our analysis, and the estimated downhole pressure was about 6,965 psi. Nonetheless, downhole measurements would increase confidence in the parameters that will be calculated based on the downhole pressure.

Given that the reservoir pressure was 2,600 psi, the downhole pressure difference between the well and the formation was about 4,350 psi. The viscosity of the gelant was 75 cp at reservoir temperature (230°F) and 300 cp at room temperature. Some uncertainty exists about the downhole temperature during gelant injection; however, considering the depth and the volume of gelant injected, it was believed to be much closer to the reservoir temperature than to the wellhead temperature. This uncertainty points out the value of downhole measurements during gelant treatments. Consequently, wherever practical, we recommend that temperatures and pressure be measured downhole before, during, and after gelant placement.

In a naturally fractured reservoir, the fracture system is generally more complicated than in a two-wing hydraulic fracture. Instead of a planar fracture that is symmetric about the well, the fracture system may be branched, nonplanar, and asymmetric. Nevertheless, there is a certain fracture area, A_f, associated with the fracture system, regardless of its nature. (Of course, the open fracture area in a given system can change with conditions, such as with a change in wellbore pressure.)

As mentioned earlier, the actual productivity of Well P-47 was about eight times greater than that expected for radial flow through rock matrix in an unfractured well. Therefore, the flow capacity

of the fracture system was substantially greater than that of the porous rock (at least, in the vicinity of the wellbore). Consequently, we assumed that the pressure drop through the fracture was negligible compared to that through the porous rock. For a short distance of gelant penetration from the fracture face in the water zone, the pressure drop across the gelant bank was approximately equal to the downhole pressure drop during gelant injection minus the downhole pressure drop during brine flow at the same rate. The downhole pressure drop during gelant injection (at 1 BPM or 1,440 BPD) was estimated at 4,350 psi. For a productivity index of 4.17 BPD/psi in the water zone, the pressure drop during brine flow at the same flow rate was about 350 psi (1,440 BPD ÷ 4.17 BPD/psi). Thus, the pressure drop across the gelant bank was approximately 4,000 psi (i.e., 4,350 psi minus 350 psi).

With the information provided above, the Darcy equation can be applied to estimate A_f/L_p, the ratio of fracture area to the average distance of gelant penetration from the fracture face.

$$A_f/L_p = (q/\Delta p)\, \mu_{gelant}/k_m \quad\text{..(23)}$$

Given that q was 1,440 BPD, Δp was 4,000 psi, $\mu_{gelant} = 75$ cp, and $k_m = 1.4$ md at S_{or}, A_f/L_p was 17,000 ft.

To solve for A_f and L_p, another relation is needed—i.e., that between the volume of gelant injected, V_{gelant}, and the distance of gelant penetration from the fracture face.

$$V_{gelant} = L_p\, A_f\, \phi\, (1\text{-}S_{or}) \quad\text{..(24)}$$

Combining Eqs. 23 and 24 leads to Eq. 25, which can be used to estimate the fracture area during gelant injection.

$$A_f = \{V_{gelant}\, q\, \mu_{gelant} / [\Delta p\, k_m\, \phi\, (1\text{-}S_{or})]\}^{0.5} \quad\text{...(25)}$$

Given a gelant volume of 1,000 bbl, a porosity of 0.098, k_m of 1.4 md, and S_{or} of 0.249, the fracture area, A_f, was about 36,000 ft^2 and the distance of gelant penetration from the fracture face, L_p, was 2.1 ft.

On first consideration, one might have expected a much larger fracture area than the calculated value of 36,000 ft^2. Given a fracture height of 90 ft and assuming that the fracture system consisted simply of two planar wings, the fracture length would be only 100 ft. In contrast, naturally fractured reservoirs are often envisioned as massive networks of interconnecting fractures, with a tremendous area associated with the fracture surfaces. However, our observation of a relatively low fracture area for Well P-47 is not inconsistent with a natural fracture system. The network of natural fractures near Well P-47 may have limited or no physical connection with other fractures or fracture systems in the reservoir. This idea is consistent with the production performance of the well. In particular, the water cut increased gradually over the course of six years from 1994 through 1999.[39] This result would not have been expected if the fractures were extensively connected throughout the reservoir. Instead, water would have channeled quickly and abruptly from the aquifer through the most conductive fractures into the production wells.

Sensitivity Studies. Sensitivity calculations were performed to examine the estimated fracture area and the distance of gelant leakoff. Of course, errors could enter the calculations for many of the input parameters, including pressure drops, flow rates, gelant viscosity, permeability, and porosity. Fig. 67 examines the impact of errors: considering combined parameter errors ranging from -50% to +50% of the base values (i.e., that led to A_f=36,000 ft^2 and L_p=2.1 ft). For example, a combined parameter error of –50% would result if Δp was assumed to be 2,000 psi instead of 4,000 psi, and all other parameters in Eq. 25 remained unchanged (i.e., V_{gelant}=1,000 bbl, q=1,440 BPD, μ_{gelant}=75 cp, ϕ=0.098, k_m=1.4 md, and S_{or}=0.249). Over the range considered in Fig. 67, the calculated fracture area varied from 29,000 to 51,000 ft^2 and the distance of gelant penetration (leakoff) varied from 1.5 to 2.6 ft. The calculated values appear to be reasonably tolerant of errors because the fracture area varies with the square root of the assorted input parameters (see Eq. 25).
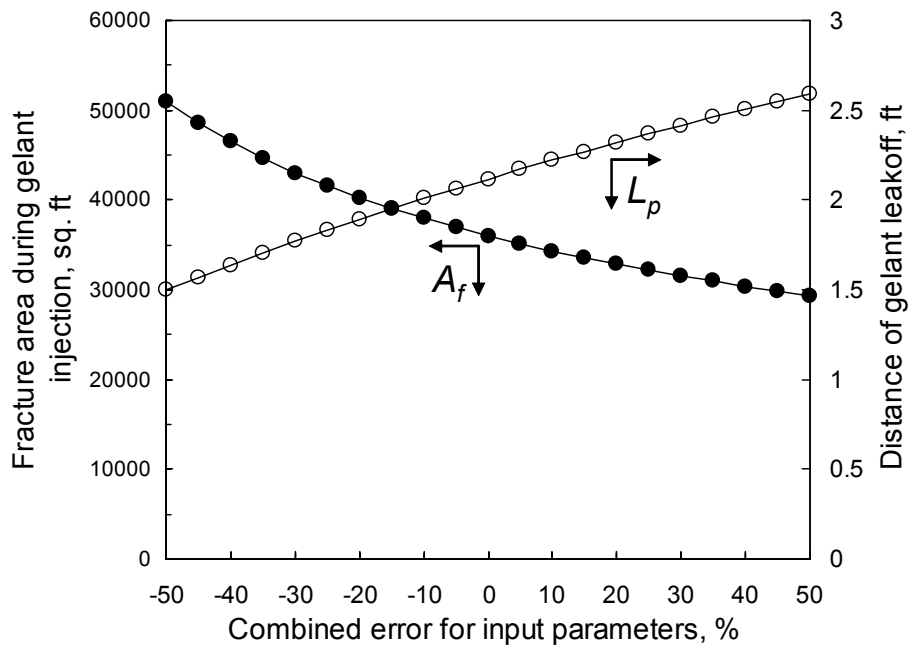
Fig. 67—Effect of errors on fracture area and gelant penetration calculations.

After Gelant Placement

In Situ Oil and Water Residual Resistance Factors. Field results can be used to estimate the oil and water residual resistance factors that were exhibited by the gel after placement in the well. Equations relating in situ residual resistance factors to productivity indexes can be found in Refs. 36, 43, and 45. Eqs. 26 and 27 provide these relations for oil and water, respectively.

$$(q/\Delta p)_{oilafter}/(q/\Delta p)_{oilbefore} = 1/[1+(L_{po}/L_e)(F_{rro}-1)] \dotfill (26)$$

$$(q/\Delta p)_{waterafter}/(q/\Delta p)_{waterbefore} = 1/[1+(L_{pw}/L_e)(F_{rrw}-1)] \dotfill (27)$$

66

Here, the before and after subscripts refer to oil or water productivity indexes before and after application of the gelant treatment. These equations are based on linear Darcy flow, and simply reflect how the productivity index in a given oil or water zone relates to the distance of gel penetration from the fracture face (L_{po} or L_{pw}) and the residual resistance factor (F_{rro} or F_{rrw}). The parameter, L_e, is provided from the Darcy equation for linear flow before the gelant treatment.

$$L_e = [k_w \, A_f / \mu_w] / [(q / \Delta p)_{waterbefore}] \dots\dots\dots\dots\dots\dots\dots\dots\dots\dots\dots\dots\dots\dots\dots\dots\dots\dots\dots(28)$$

In Eq. 28, given that k_w was 1.4 md, A_f was 36,000 ft^2, μ_w was 0.25 cp, q was 1,460 BWPD, and Δp was 350 psi, L_e was calculated to be 55 ft.

As mentioned earlier, before the gelant treatment, the oil productivity, $(q/\Delta p)_{oilbefore}$, was 0.151 BOPD/psi, and the water productivity, $(q/\Delta p)_{waterbefore}$, was 4.17 BWPD/psi. Four months after the treatment, the oil productivity, $(q/\Delta p)_{oilafter}$, was 0.0554 BOPD/psi, and the water productivity, $(q/\Delta p)_{waterafter}$, was 0.0985 BWPD/psi. Given that $L_{po}=L_{pw}=2.1$ ft, and $L_e=55$ ft, Eqs. 26 and 27 indicate that F_{rro} was 46 while F_{rrw} was 1,080. The ratio, F_{rrw}/F_{rro}, was 23.5. These values were greater than those measured in the laboratory in Berea sandstone ($F_{rro} = 20$, $F_{rrw} =200$, and $F_{rrw}/F_{rro}, =10$).

Effect Of Assumed Fracture Area. In the above calculations, the assumed fracture area (36,000 ft^2) was determined during gelant injection. One could argue that the fracture area open to flow during gelant injection was greater than that during production (either before or after gelant placement) because the downhole pressure was roughly 5,000 psi higher during gelant injection than during oil/water production. Fig. 68 examines the effects of assumed fracture area for the calculations associated with Eqs. 26-28. F_{rro}, F_{rrw}, and F_{rrw}/F_{rro} were determined for fracture areas ranging from 1,000 to 100,000 ft^2. Over much of the range investigated, F_{rrw}/F_{rro} was about 23. Thus, regardless of assumed fracture area, the in situ residual resistance factors differ to some extent from the laboratory values, where F_{rrw}/F_{rro} was about 10. This result is not surprising since the extent of the disproportionate permeability reduction varies with the character of the porous medium.[47]

We can adjust the assumed fracture area to achieve an in situ residual resistance factor that matched the value of either F_{rro} or F_{rrw} that was measured in the laboratory. For a fracture area of 15,200 ft^2, the in situ F_{rro} matched the laboratory value of 20, but the in situ F_{rrw} (457) was more than twice the lab value (200). On the other hand, for a fracture area of 6,640 ft^2, the in situ F_{rrw} matched the laboratory F_{rrw} (200), but the in situ F_{rro} (9.3) was less than half the laboratory F_{rro}.

The above residual resistance factors were relevant four months after the gelant treatment was applied in Well P-47. Another set of calculations can be performed based on data collected one year after the treatment. In November 2000, the well produced 81 BWPD and 141 BOPD with a 465 psi drawdown. Therefore, productivity values were 0.174 BWPD/psi for water and 0.303 BOPD/psi for oil. The productivity for oil (coupled with Eqs. 26 and 28) suggests that F_{rro} at this time was near unity—indicating that the gel provided no significant resistance to flow in the oil zone. In contrast, the water productivity indicates that the gel continued to restrict water entry into the fracture—although somewhat less effectively than at four months after the treatment. For assumed fracture areas of 6,640, 15,200, and 36,000 ft^2, the calculated F_{rrw} values were 141, 322,

and 761, respectively. These values were about 30% less than at four months after the treatment. Thus, the gel experienced relatively little wash out from the water zone during the first year.

In summary, these calculations indicate the range of fracture areas and residual resistance factors that may be applicable. As discussed in the next section, the calculations are needed to optimize the volume of gelant treatments.
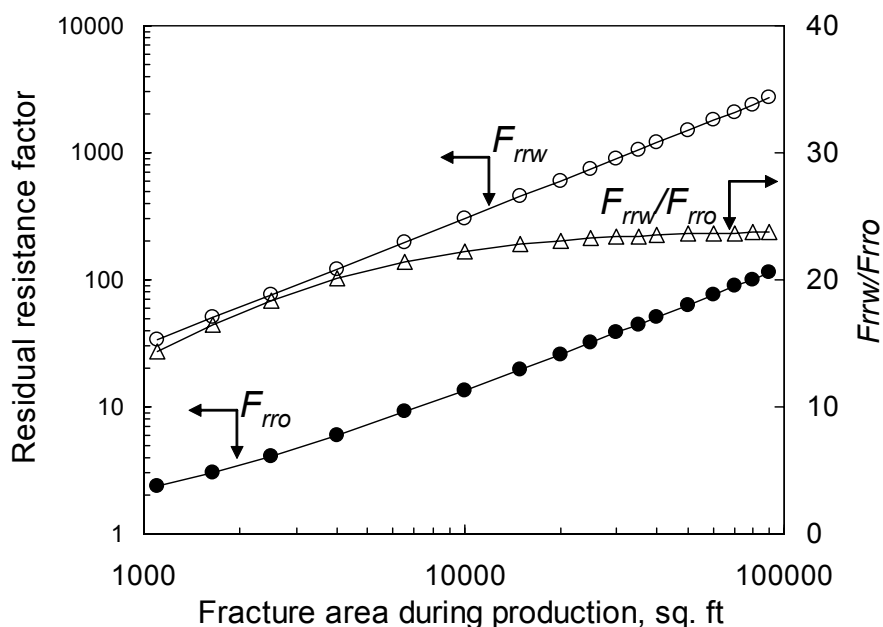

Fig. 68—Sensitivities for calculated *in situ* residual resistance factors.

Optimizing Gelant Volume

Would the gelant treatment in Well P-47 have been more effective if a different volume of gelant was injected? Eqs. 24, 26, and 27 can be used to address this question. When using Eq. 24 to determine the distance of gelant penetration, A_f, must be assigned the value determined during gelant injection—36,000 ft^2 in this case. This assignment is mandatory in order for the predictions to match the actual water and oil productivity values associated with 1,000 bbl of gelant. The L_p values can then be calculated and used in Eqs. 26 and 27 to estimate post-treatment oil and water productivities as a function of gelant volume. Fig. 69 shows the results for the base case input parameters of 46 for F_{rro}, 1,080 for F_{rrw}, and 55 ft for L_e. This plot confirms the observed field result—i.e., the use of 1,000 bbl of gelant caused a 63% loss of oil productivity—from 0.151 to 0.0554 BOPD/psi.

The reader should note that a loss of oil productivity does not necessarily mean a loss of oil production rate. If the pressure drawdown is increased sufficiently, the oil production rate increases even though oil productivity decreases. This point may be better appreciated by considering Figs. 70 and 71. These figures translate Fig. 68 for the specific drawdowns of 1,300 psi (Fig. 70) and 500 psi (Fig. 71). As observed in the actual field application, a 1,000-bbl gelant treatment, coupled with a 1,300 psi post-treatment drawdown, resulted in a decrease in water

production rate from 1,460 to 128 BWPD and an increase in oil production rate from 53 to 72 BOPD (Fig. 70), even though the oil productivity decreased by 63% (Fig. 69). In contrast, with a 500 psi post-treatment drawdown, the final oil production rate was 27 BOPD (Fig. 71) for the same 1,000-bbl gelant treatment.
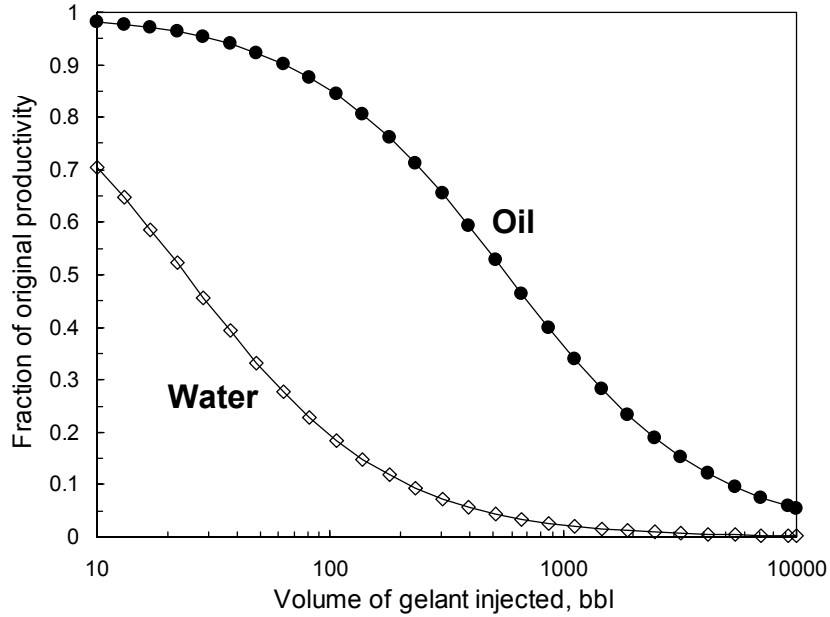

Fig. 69—Effect of gelant volume on fluid productivities.
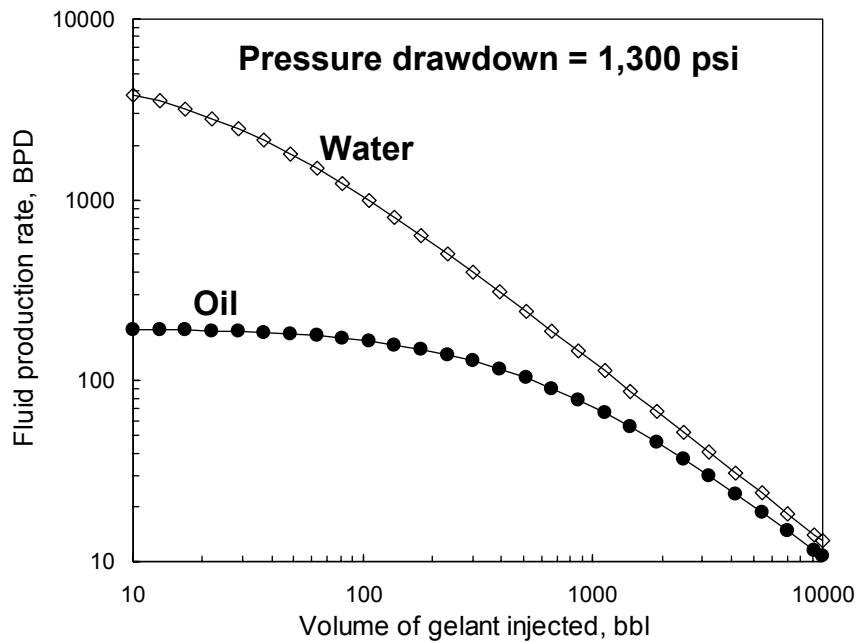
Fig. 70—Production rates versus gelant volume: Δp=1,300 psi.
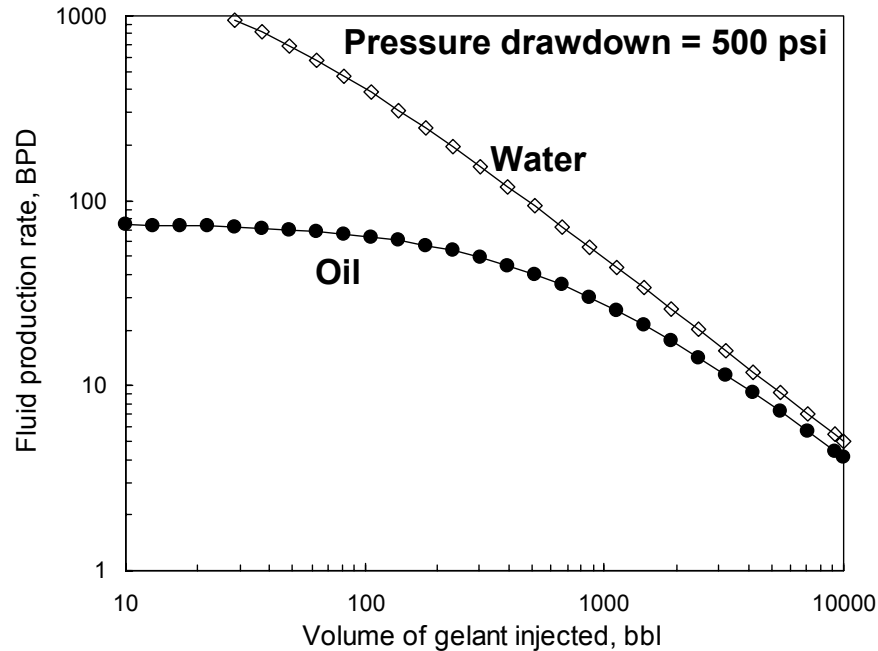
Fig. 71—Production rates versus gelant volume: Δp=500 psi.

Careful examination of Figs. 69 and 70 suggests that a more positive outcome may have resulted from using a smaller gelant volume in Well P-47. For example, Fig. 70 predicts that a 500-bbl gelant treatment would have resulted in the oil rate increasing to 105 BOPD while the water rate decreased from 1,460 to 248 BWPD. Compared to the results from the 1,000-bbl gelant treatment, the value of the extra 33 BOPD (i.e., 105 minus 72 BOPD) would easily offset the additional disposal cost for the extra 120 BWPD (i.e., 248 minus 128 BWPD).

Figs. 69-71 were generated using the set of input parameters where F_{rro}=46, F_{rrw}=1,080, and L_e=55 ft. This set of parameters assumed that the open fracture area was 36,000 ft^2. In the previous section, we investigated cases where the fracture areas during production were either 6,640 or 15,200 ft^2. For the case of 6,640 ft^2, Eqs. 26-28 yielded the set of parameters: F_{rro}=9.3, F_{rrw}=200, and L_e=10.1 ft. For the case of 15,200 ft^2, Eqs. 26-28 yielded the set of parameters: F_{rro}=20, F_{rrw}=457, and L_e=23.1 ft. If either of these sets of F_{rro}, F_{rrw}, and L_e values are entered into Eqs. 26 and 27 to generate figures like those in Figs. 69-71, the results will look virtually identical to Figs. 69-71. However, achieving this result requires that the L_p values from Eq. 24 must be calculated using A_f=36,000 ft^2.

As mentioned, consideration of Figs. 69-71 suggests that the treatment in Well P-47 may have shown a more desireable performance (at 4 months after the treatment) if a smaller gelant volume were used. However, this view must be balanced against a concern over washout of the gel. Field results one year after the treatment indicated that gel damage in the oil zone was diminished while residual resistance factors in the water zone decreased by 30%. Depending on the strength and stability of the gel, a smaller gel bank may have experienced more severe washout from the water zone.

In summary, Eqs. 24-28 and figures like those in Figs. 67-71 can be used to optimize the gelant volumes in field applications. These analyses may be especially valuable when utilizing the results from the first gelant treatment in a field to optimize subsequent treatments. PDVSA is also investigating the value of the analysis during sequential applications of gelant in the same well. Specifically, based on an analysis performed after injection of a first batch of gelant, a decision is made whether (and how much) gelant should be injected during a subsequent treatment in the same well.

Conclusions

This chapter demonstrates the value of using basic calculations and relations between laboratory data and field observations for a gelant treatment in Well P-47 at the naturally fractured Motatan field in Venezuela. Some of the important conclusions from this work include the following:

1. Production data were used to estimate the relative permeabilities and heights of the oil and water zones.

2. Before gelant injection, the well productivity was about eight times greater than expected for radial flow—confirming the presence of fractures.

3. Pressure and rate data during gelant injection were instrumental in establishing the fracture area open to flow—estimated at 36,000 ft^2. Sensitivity studies demonstrated the effect of input errors and emphasized the importance of accurate downhole pressure measurements before, during, and after gelant placement.

4. The distance of gelant leakoff from the fracture face was about the same in the water and oil zones—about 2.1 ft.

5. Pressure and rate data collected during production four months after the gelant treatment were used to estimate *in situ* oil and water residual resistance factors—yielding values of 46 and 1,080, respectively. For comparison, laboratory values measured in Berea sandstone were 20 and 200, respectively.

6. Sensitivity analyses suggested that a more desirable oil productivity may have resulted from using a smaller gelant volume—e.g., 500 bbl rather than 1,000 bbl.

7. One year after the treatment, the water and oil productivity indexes indicated that the gel effectively resisted washout in the water zone but was largely destroyed or removed from the oil zone.

6. XMT STUDIES OF DISPROPORTIONATE PERMEABILITY REDUCTION

In our recent work, we used X-ray computed microtomography (XMT) to study why a Cr(III)-acetate-HPAM gel reduces permeability to water much more than that to oil.[47] Studies were performed both in strongly water-wet Berea sandstone cores and in an oil-wet porous polyethylene core. Although the two porous media had very different porosities (22% versus 40%), the distributions of pore sizes and aspect ratios were similar. A Cr(III)-acetate-HPAM gel caused comparable oil and water permeability reductions in both porous media. In both cores, the gel reduced permeability to water by a factor 80 to 90 times more than that to oil. However, the distributions of water and oil saturations (versus pore size) were substantially different before, during, and after gel placement.

When production wells were treated with gelants, some zones had high water saturations and high fractional water flows, while other zones had high hydrocarbon saturations and fractional flows. In water zones in field treatments, water was the first fluid to flow through the gel after gel placement—i.e., no oil flowed through the gel in the water zones. For this circumstance, our previous experience with Cr(III)-acetate-HPAM gels revealed that water residual resistance factors were around 10,000 and the gel occupied virtually all of the aqueous pore space.[49,50] Thus, the mechanism for water permeability reduction in field applications is one of near-total blockage of water flow. Virtually the only means for water flow is through the gel itself (which has a permeability less than 1 md).[24,51]

Of course, for the oil zones, oil was the first fluid to flow through the gel after the treatment. For these zones, our research indicated that oil pathways open after gel placement were largely the same as those open before gel placement. Apparently, oil flooding moved, concentrated, or destroyed much of the gel that formed in the oil pathways.[47] Consequently, after gel placement, the permeability to oil was much higher than that to water.

When water was injected following oil (after gel placement), the permeability to water was still much less than that to oil. This aspect of the disproportionate permeability reduction appeared to occur by different mechanisms in the two porous media. In Berea, gel caused disproportionate permeability reduction by trapping substantial volumes of oil that remained immobile during water flooding. With this high trapped oil saturation, water was forced to flow through narrow films, through the smallest pores, and through the gel itself. In contrast, during oil flooding, oil pathways remained relatively free from constriction by the gel.

In the polyethylene core, oil trapping did not contribute significantly to the disproportionate permeability reduction. Instead, oil films and a relatively small number of pore pathways provided conduits for the oil. For reasons yet to be understood, the small pore pathways appeared largely unavailable for water flow.[47]

Issues Raised
During presentation of our findings at a recent Gordon Conference, three of our observations were surprising to some attendees. All three issues concerned findings before placement of gel. One finding was that the average residual oil saturation was about 40% in the smallest observable pores in Berea sandstone. A second finding that surprised some individuals was that a

wide range of saturations existed for any given pore size. The third surprising observation was that a few large pores had high coordination numbers (up to 70 pore exits). On the one hand, it seems doubtful that resolution of these issues will change our main conclusions about the mechanism for disproportionate permeability reduction in strongly water-wet Berea sandstone. On the other hand, their resolution may lead to a better quantitative understanding of the mechanism. Also, these issues are of basic importance to our understanding of oil and water flow in porous media. Therefore, we plan to pursue these questions to some extent.

High Residual Oil Saturations in Small Pores
One feature of our XMT studies is that we can determine the fluid saturations for individual pores. Fig. 72 plots the water saturations for each of the 1,736 pores of the imaged volume in Berea sandstone at the connate oil saturation (S_{wr}). The pore volume associated with each pore is plotted on the x-axis. The solid line plots the average water saturation for a given pore size. At S_{wr}, the overall average water saturation was 24.7%.
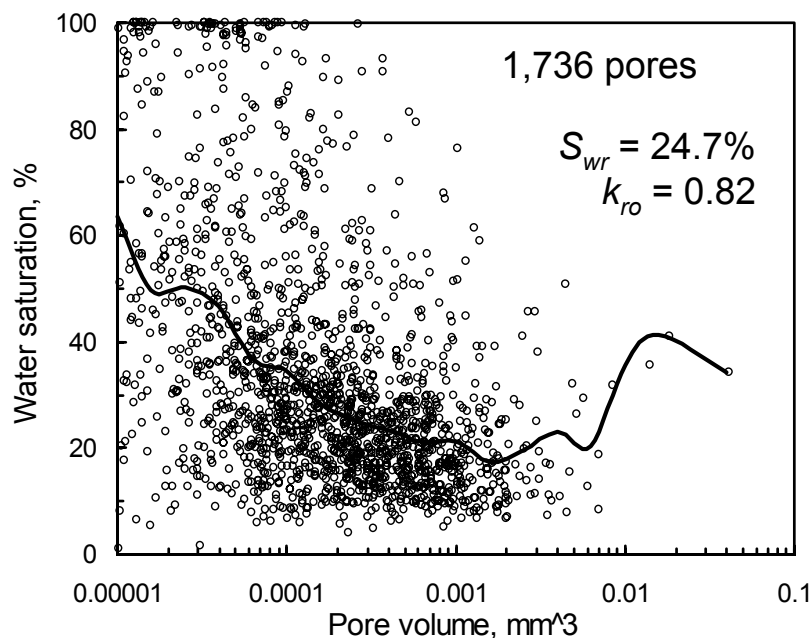
Fig. 72—Water saturations in pores in Berea at S_{wr}.

As expected in a strongly water-wet porous medium, the average water saturation generally increased with decreased pore size (solid line in Fig. 72). However, in the smallest pores shown (10^{-5} mm^3), the water saturation only averaged about 60%. In contrast, one might have expected the water saturation to approach 100% for the smallest pores. A calculation using the Laplace-Young equation confirmed that oil should be able to enter pores with volumes of 10^{-5} mm^3 and throat radii of about 7 μm. Specifically, to enter pore throats with radii of 7 μm, a capillary pressure around 1 psi was needed. This value was much lower than the 17 psi (pressure drop across the core) that was applied during our flooding experiments. The behavior of S_w versus pore size was confirmed during two other imaging experiments in Berea sandstone.[47]

The reader should recognize that pores with volumes of 10^{-5} mm^3 are not necessarily the smallest pores in our rock samples. Much smaller pores exist in clays and other minerals in Berea sandstone that are below the limits of detection for our XMT method. It seems likely that water saturations in these very small pores are nearly 100%. These observations may resolve the apparent discrepancy associated with very high water saturations being expected in the smallest pores. However, we should note that although pores smaller than 10^{-5} mm^3 exist, their contribution to the flow capacity of the rock is insignificant.[47]

Wide Distributions Of Saturations

A second finding that surprised some individuals was that a wide range of saturations existed for any given pore size. This point can be appreciated from Fig. 72. Our first suspicion was that this wide distribution of saturations reflected a wide distribution of pore-body/pore-throat aspect ratios.

The distribution of aspect ratios (effective pore radius/effective throat radius) for two Berea and one polyethylene cores are shown in Figs. 73-75. (The effective pore radius computed is for a sphere with a volume equivalent to that measured for the pore. The effective throat radius computed is for a circle with an area equivalent to that measured for the throat.) The y-axis plots the aspect ratio in pores with a given size (indicated on the x-axis). The solid curves plot average aspect ratios as a function of pore size. The distributions were surprisingly similar for the cores. The average aspect ratio was 4.0 for the first Berea core, 4.2 for the second Berea core, and 4.4 for the polyethylene core. As pore volume increased from 10^{-5} mm^3 (effective pore radius ~13 μm) to 0.002 mm^3 (effective pore radius ~78 μm), the average aspect ratio increased steadily from 2 to 6. Aspect ratios jumped sharply for the few largest pores. For a given pore size, a wide range of aspect ratios were noted. For all cores at a given pore size, the standard deviation (of aspect ratios) was typically 65% of the mean value.

Our examination of the relation between aspect ratios and fluid saturations are in preliminary stages. However, our first studies suggest no significant correlation between fluid saturations and aspect ratios for individual pores.
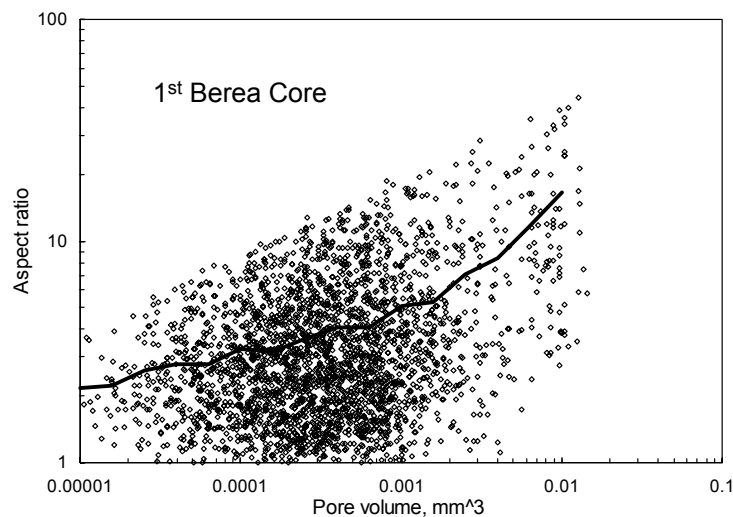

Fig. 73—Aspect ratios in the first Berea core.
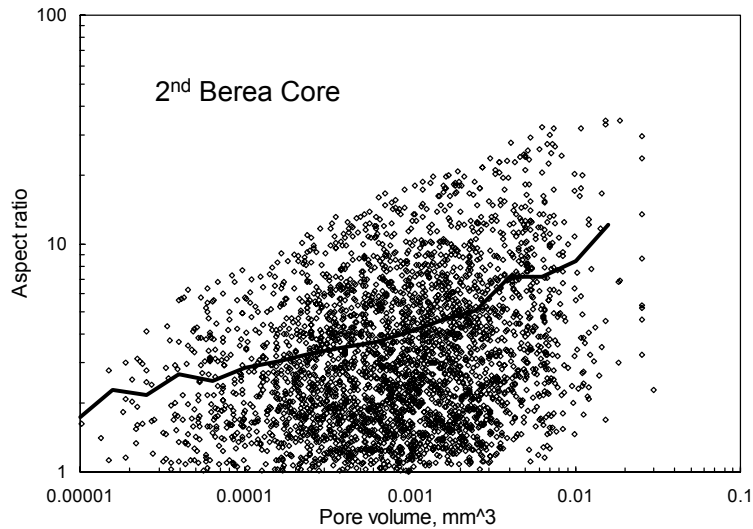
Fig. 74—Aspect ratios in the second Berea core.
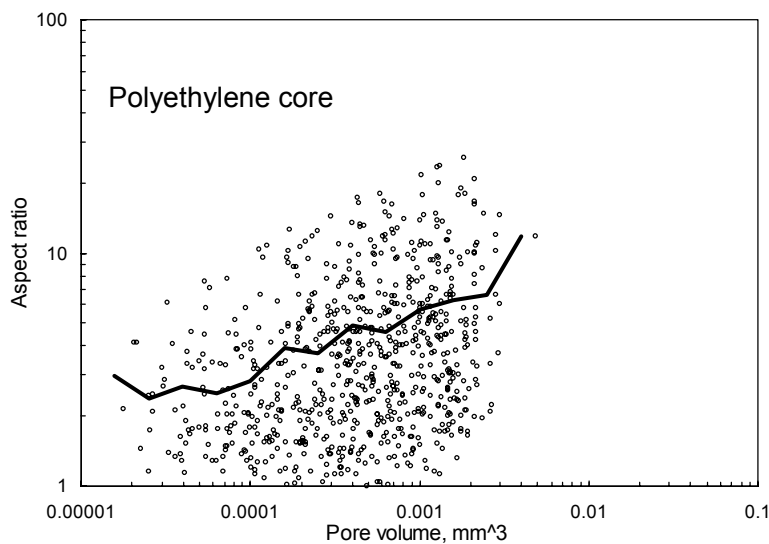
Fig. 75—Aspect ratios in the polyethylene core.

High Coordination Numbers

The distributions of coordination numbers for our three imaged cores are shown in Fig. 76.[47] (The coordination number is the number of exits from a pore.) The y-axis plots the average coordination number in pores with a given size (indicated on the x-axis). The average coordination number was 3.9 for the first Berea core, 4.7 for the second Berea core, and 6.2 for the polyethylene core. For the smallest pores, the coordination number was around three for all three cores. As the pore size increased, the coordination numbers increased—with the polyethylene core experiencing a slightly more rapid increase than the Berea cores. Coordination numbers up to 74 were noted for the largest pores. For a given pore size, standard deviations were typically 20% to 40% of the mean values.
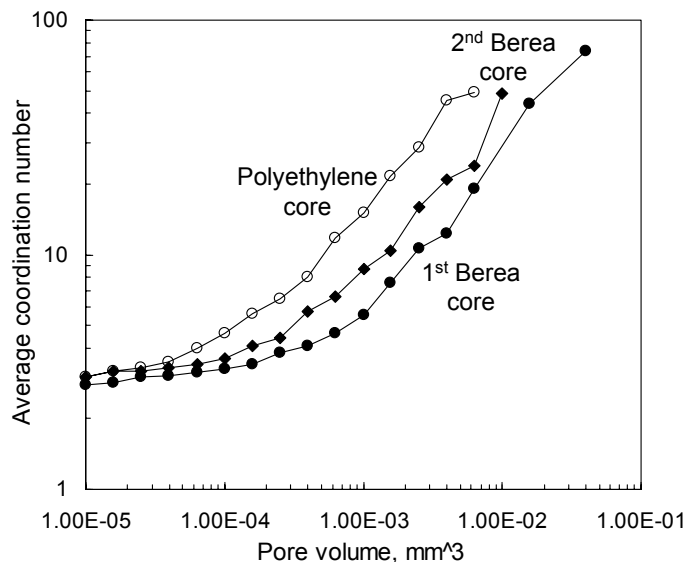
Fig. 76—Coordination number distributions.

Ioannidis *et al.*[47] reported comparable properties for Berea sandstone based on analyses of photomicrographs of 78 serial sections through a double pore cast of a Berea sample. Their analyses of 1,268 pores and 1,945 throats indicated that the average coordination number was 3.46—somewhat lower than our values. Their average throat area was 60% to 90% greater than our values, and their pore size distribution was weighted toward larger pores than our distributions.

Some reviewers of our work were skeptical that coordination numbers could be as high as some of the values that we reported. In particular, M. A. Ioannidis (personal communication, Andover, NH, August 8, 2002) felt that coordination numbers should rarely be greater than 10. In view of these comments, we are re-examining our data. Coordination numbers for individual pores in our first Berea core are shown in Fig. 77 (log scale for the *y*-axis) and Fig. 78 (normal scale for the *y*-axis). In Fig. 77, only three pores had coordination numbers greater than 22.

Upon re-examination of the image analysis software (3DMA), we found that many pores were assigned extra throats that did not appear to connect to other pores. When these throats were eliminated, the largest coordination number for any pore decreased from 74 to 22. However, the average coordination number decreased only slightly—from 3.9 to 3.8. Fig. 79 plots the coordination numbers from the new analysis.

In the new analysis, the largest coordination number was 22. Detailed examination of the pore with the highest coordination number revealed that several of the throats led to the same pore. In one case, five throats connected the same two pores. In two cases, three throats connected the same two pores, and in one case, two throats connected the same two pores. These observations emphasize that the irregular shapes of the pore bodies and pore throats can complicate the analyses. If only one connection is allowed between any two pores, the maximum coordination number in the first Berea core drops to 13.
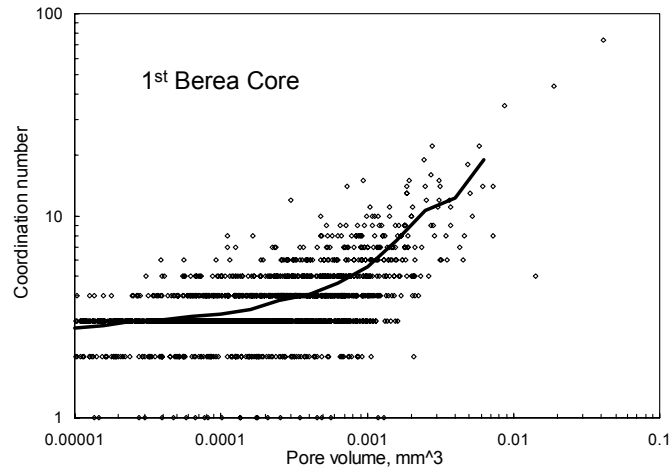
Fig. 77—Coordination numbers in the first Berea core: log scale.
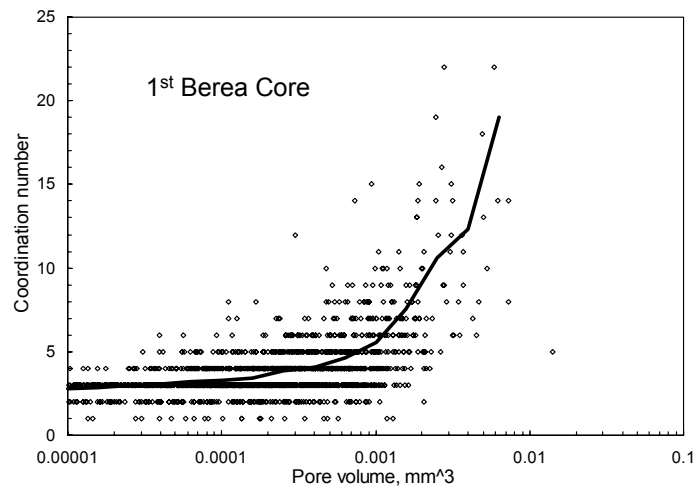
Fig. 78—Coordination numbers in the first Berea core: normal scale.
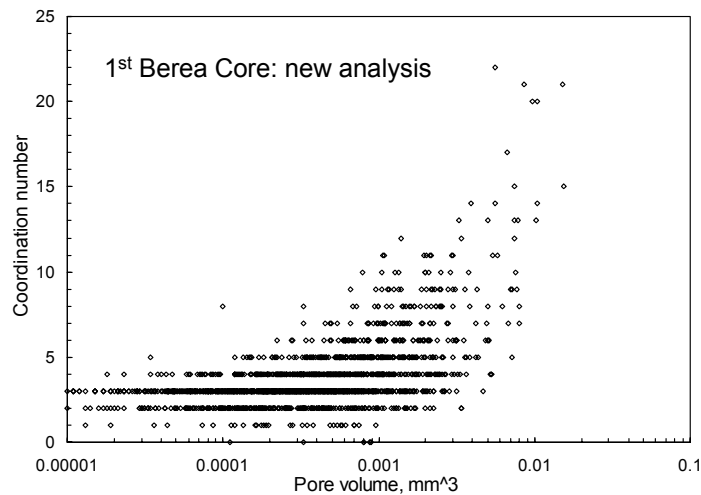

Fig. 79—Coordination numbers in the first Berea core: new analysis.

Also, in the new analysis, six pores were identified with a coordination number of zero (no connection to other pores.) The corrections associated with the new analysis will be incorporated into the analyses of our other images in future work.

Capillary End Effect And Saturation Gradients
Because our cores were small (30 mm in length), the capillary end effect could have created a saturation gradient through the core. Three factors worked in our favor to minimize this effect. First, the image volume was located near the center of the core—maximizing distance from the inlet and outlet faces. Second our cores were quite permeable (0.47 darcys for Berea and 8.8 darcys for polyethylene). Third, our floods were conducted using relatively high capillary numbers and pressure gradients (17-35 psi/ft). Examination of our images (which cover about 7% of the core length) revealed no obvious saturation trend in any direction. For the first Berea core, this finding is demonstrated in Figs. 80-82 for the conditions of (1) S_{wr} before gel placement, (2) at S_{or} immediately after gel placement, and (3) at S_{or} during the final water injection stage after gel placement. Each of these figures show saturation versus distance across the image volume in the x-, y-, and z-directions. The near-horizontal lines in each figure show the results of least squares regressions. The numbers in the legends indicate the slopes of these lines, while the numbers in parentheses indicate the variance in the last digit. These figures indicate no significant saturation trend across the image volume in any direction. Nevertheless, we cannot discount the possibility that a saturation gradient might have existed in the cores in the z-direction (the direction of flow) outside of the imaged volume.
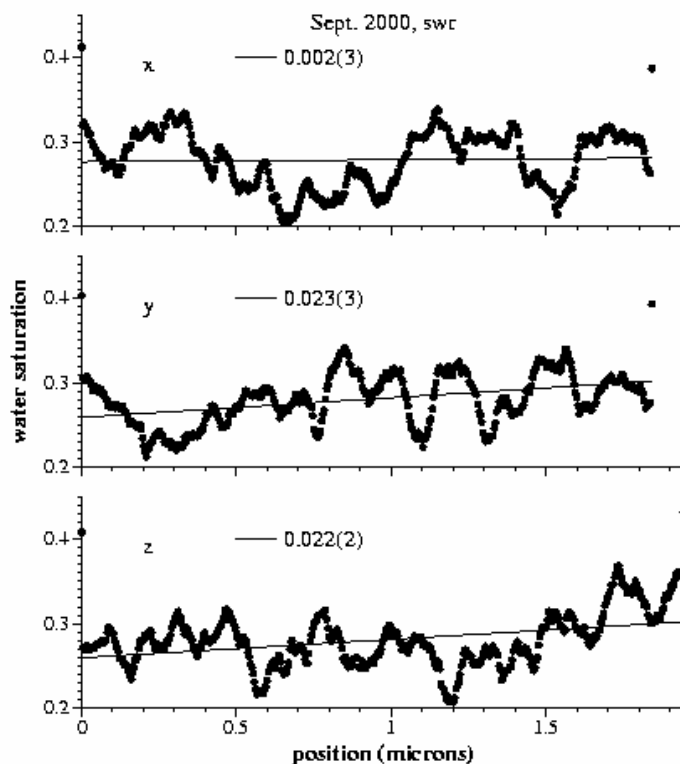

Fig. 80—Saturation gradients in the imaged volume at S_{wr}.

78
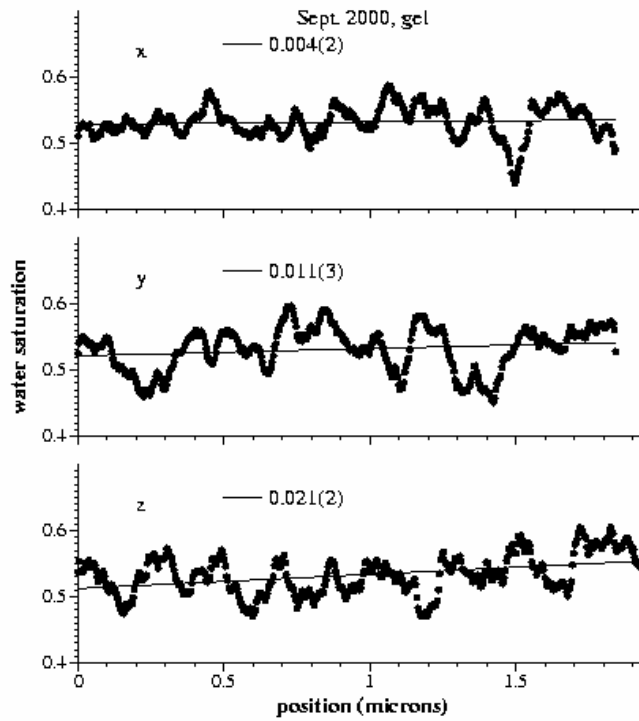
Fig. 81—Saturation gradients in the imaged volume just after gel placement.
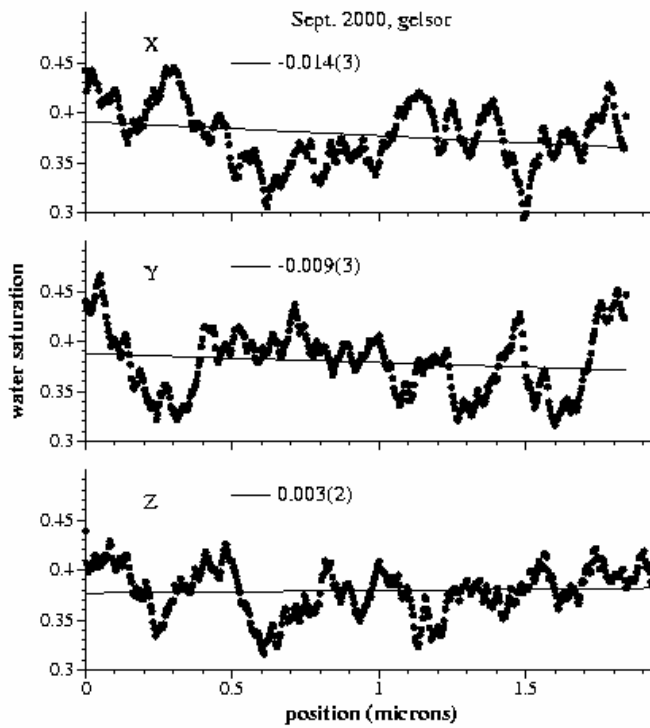
Fig. 82—Saturation gradients in the imaged volume at S_{or} after gel placement.

Representative Elementary Volume

One might also wonder whether our small image volume ($\sim$19 mm^3) was less than the representative elementary volume (REV) for this porous medium. We are unable to answer this question definitively. Our Berea images contained 1,700-1,800 pores that were larger than 10^{-5} mm^3. Those who advocate the REV concept might argue that at least one million pores (i.e., 100 grain diameters per side of the sample volume) are needed to form a representative elementary volume. Obviously, our image volume does not meet this criterion. On the other hand, the observations that we report in this paper appeared to be generally valid throughout the imaged volumes—i.e., we did not observe regions of exceptional behavior within a given image volume.

Tortuosity of Berea and Polyethylene

In our previous imaging studies, three-dimensional images of Berea sandstone and polyethylene cores were analyzed to determine pore size distributions, pore body/throat aspect ratios, and pore coordination numbers. These analyses were recently expanded to determine tortuosity values for the cores. The average tortuosity values for the porous media were 1.6 for Berea and 1.5 for polyethylene. These values reflect the shortest fluid pathways through the porous media relative to a straight-line connection, and apply to the case where the porous media is saturated with a single fluid. In future work, we plan to determine tortuosity values within a given phase (oil or water) when two phases are present, and also before versus after gel placement. Hopefully, these measurements will provide insight into the mechanism for disproportionate permeability reduction.

NOMENCLATURE

A_c = fractional area associated with concentrated gel

A_f = fracture area, ft^2 [m^2]

A_m = fractional area associated with mobile gel

B_o = oil formation volume factor, rb/stb [m^3/m^3]

B_w = water formation volume factor, rb/stb [m^3/m^3]

C = concentration of dehydrated gel, g/m^3

C_o = injected or original concentration, g/m^3

c_a = compressibility, ft^3/ft^3-psi [m^3/m^3-Pa]

D = diffusion coefficient, cm^2/s

F_{rro} = oil residual resistance factor

F_{rrw} = water residual resistance factor

G' = elastic modulus, psi [Pa]

h = height, ft [m]

h_f = fracture height, ft [m]

h_{oil} = height of the oil zone, ft [m]

h_{total} = total height of the net pay, ft [m]

h_{water} = height of the water zone, ft [m]

k = permeability, darcys [μm^2]

k_f = fracture permeability, darcys [μm^2]

k_{final} = final permeability, darcys [μm^2]

k_{gel} = gel permeability to water, darcys [μm^2]

k_m = matrix permeability, darcys [μm^2]

k_o = permeability to oil, darcys [μm^2]

k_{ro} = endpoint relative permeability to oil, darcys [μm^2]

k_{rw} = endpoint relative permeability to water, darcys [μm^2]

k_w = permeability to water, darcys [μm^2]

L = distance along a fracture, ft [m]

L_e = distance parameter defined by Eq. 28, ft [m]

L_f = fracture length, ft [m]

L_m = length of the mixing zone, ft [m]

L_p = distance of gelant penetration, ft [m]

L_{po} = distance of gelant penetration in oil zone, ft [m]

L_{pw} = distance of gelant penetration in water zone, ft [m]

n = exponent in Eq. 6

p_1 = pressure at Point 1, psi [Pa]

p_2 = pressure at Point 2, psi [Pa]

p_r = reservoir pressure, psi [Pa]

Δp = pressure drop, psi [Pa]

dp/dl = pressure gradient, psi/ft [Pa/m]

q = injection or production rate, BPD [m^3/d]

q_{max} = maximum acceptable leak rate, BPD [m^3/d]

R = aspect ratio

r = correlation coefficient

r_1 = radius at Point 1, ft [m]

r_2 = radius at Point 2, ft [m]

r_e = external drainage radius, ft [m]

r_w = wellbore radius, ft [m]

S_{or} = residual oil saturation

S_w = water saturation

S_{wr} = residual water saturation

T = temperature, °C

t = time, s

t_{exp} = time of first exposure, s

Δt = time change, s

u = leakoff rate or flux, ft/d [cm/s]

u_c = water leakoff rate associated with concentrated or immobile gel, ft/d [cm/s]

u_l = water leakoff rate, ft/d [cm/s]

u_m = water leakoff rate associated with fresh or mobile gel, ft/d [cm/s]

V_a = annular volume, ft^3 [m^3]

V_{gelant} = volume of gelant injected, ft^3 [m^3]

w_f = fracture width, in. [mm]

α = factor by which gel or particulates are concentrated

ϕ = porosity

μ = viscosity, cp [mPa-s]

μ_{gelant} = gelant viscosity, cp [mPa-s]

μ_o = oil viscosity, cp [mPa-s]

μ_w = water viscosity, cp [mPa-s]

REFERENCES

1. "Profile of the Oil and Gas Extraction Industry," EPA/310-R-99-006 (Oct. 1999) 38.
2. Petrusak, R.L., Freeman, B.D., and Smith, G.E.: "Baseline Characterization of U.S. Exploration and Production Wastes and Waste Management," paper SPE 63097 presented at the 2000 SPE Annual Technical Conference and Exhibition, Dallas, Oct. 1-4.
3. Bailey *et al.*: "Water Control," *Oilfield Review* **12** (Spring 2000) 30-51.
4. Seright, R.S. and Liang, J.: "A Survey of Field Applications of Gel Treatments for Water Shutoff," paper SPE 26991 presented at the 1994 SPE III Latin American & Caribbean Petroleum Engineering Conference, Buenos Aires, Argentina, April 27-29.
5. Sydansk, R.D. and Moore, P.E.: "Gel Conformance Treatments Increase Oil Production in Wyoming," *Oil & Gas J.* (Jan. 20, 1992) 40-45.
6. Borling, D.C.: "Injection Conformance Control Case Histories Using Gels at the Wertz Field CO_2 Tertiary Flood in Wyoming, USA," paper SPE 27825 presented at the 1994 SPE/DOE Symposium on Improved Oil Recovery, Tulsa, April 17-20.
7. Hild, G.P. and Wackowski, R.K.: "Reservoir Polymer Gel Treatments To Improve Miscible CO_2 Flood," *SPE Reservoir Engineering and Evaluation* (April. 1999) 196-204.
8. Lane, R.H. and Sanders, G.S.: "Water Shutoff Through Fullbore Placement of Polymer Gel in Faulted and in Hydraulically Fractured Producers of the Prudhoe Bay Field," paper SPE 29475 presented at the 1995 SPE Production Operations Symposium, Oklahoma City, April 2-4.
9. Lane, R.H., and Seright, R.S.: "Gel Water Shutoff in Fractured or Faulted Horizontal Wells," paper CIM/SPE 65527 presented at the 2000 SPE/Petroleum Society of CIM International Conference on Horizontal Well Technology held in Calgary, Alberta, Canada, Nov. 6-8.
10. Seright, R.S., Lane, R.H., and Sydansk, R.D.: "A Strategy for Attacking Excess Water Production," paper 70067 presented at the 2001 SPE Permian Basin Oil and Gas Recovery Conference, Midland, May 15-16.
11. Seright, R.S.: "Gel Placement in Fractured Systems," *SPE Production & Facilities* (Nov. 1995), 241-248.
12. Seright, R.S.: "Use of Preformed Gels for Conformance Control in Fractured Systems," *SPE Production & Facilities* (Feb. 1997) 59-65.
13. Seright, R.S: "Mechanism for Gel Propagation Through Fractures," paper SPE 55628 presented at the 1999 SPE Rocky Mountain Regional Meeting, Gillette, May 15-19.
14. Seright, R.S: "Polymer Gel Dehydration During Extrusion Through Fractures," *SPE Production & Facilities* (May 1999) 110-116.
15. Seright, R.S.: "Gel Propagation Through Fractures," paper SPE/DOE 59316 presented at the 2000 SPE/DOE Symposium on Improved Oil Recovery, Tulsa, April 2-5.
16. Liu, Jin, and Seright, R.S.: "Rheology of Gels Used For Conformance Control in Fractures," *SPE Journal* (June 2001) 120-125.
17. Howard, G.C. and Fast, C.R.: *Hydraulic Fracturing*, Monograph Series, SPE, Dallas, (1970) **2,** 32-42.
18. Howard, G.C. and Fast, C.R.: Optimum Fluid Characteristics for Fracture Extension," *Drill. and Prod. Prac.*, API (1957) 261.
19. Mack, M.G. and Warpinski, N.R.: "Mechanics of Hydraulic Fracturing," *Reservoir Stimulation, 3rd ed.*, John Wiley, New York (2000) Chapter 6.

20. Seright, R.S.: "An Alternative View of Filter Cake Formation in Fractures," paper SPE 75158 presented at the 2002 SPE/DOE Symposium on Improved Oil Recovery, Tulsa, April 13-17.
21. Seright, R.S.: "Using Chemicals to Optimize Conformance Control in Fractured Reservoirs," Annual Technical Progress Report (U.S. DOE Report DOE/BC/15110-4), U.S. DOE Contract DE-AC26-98BC15110 (Sept. 2000) 3-56.
22. Seright, R.S.: "Using Chemicals to Optimize Conformance Control in Fractured Reservoirs," Annual Technical Progress Report (U.S. DOE Report DOE/BC/15110-2), U.S. DOE Contract DE-AC26-98BC15110 (Sept. 1999) 21-28.
23. Bird, R.B., Stewart, W.E., and Lightfoot, E.N.: *Transport Phenomena*, John Wiley & Sons, New York (1960) 11, 42-63.
24. Seright, R.S.: "Using Chemicals to Optimize Conformance Control in Fractured Reservoirs," Annual Technical Progress Report (U.S. DOE Report DOE/BC/15110-6), U.S. DOE Contract DE-AC26-98BC15110 (Sept. 2001) 2-54.
25. Smith, D.K.: *Cementing*, SPE Mongraph Vol. 4, Society of Petroleum Engineers (1990).
26. Urdahl, H. *et al*.: "Experience with Temporarily Sealing Leaking Tubing Annuli With Extended-Life Polymer Gel Plugs in the Greater Ekofisk Area," paper SPE 24982 presented at the 1992 European Petroleum Conference, Cannes, France, Nov. 16-18.
27. Creel, P. and Crook, R.: "Gels, Monomer Solutions Fix Pinhole Casing Leaks," *Oil & Gas J.* (Oct. 13, 1997) 44-46.
28. Jurinak, J.J. and Summers, L.E.: "Oilfield Applications of Colloidal Silica Gel," *SPEPE* (Nov. 1991) 406-412.
29. Liang, J., Sun, H., Seright, R.S.: "Why Do Gels Reduce Water Permeability More Than Oil Permeability?," *SPE Reservoir Engineering* (Nov. 1995) 282-286.
30. Seright, R.S.: "Reduction of Gas and Water Permeabilities Using Gels," *SPE Production & Facilities* (May 1995) 103-108.
31. Seright, R.S.: "Effect of Rock Permeability on Gel Performance in Fluid-Diversion Applications," *In Situ* (1993) 17, No.4, 363-386.
32. Seright, R.S.: "Impact of Permeability and Lithology on Gel Performance," paper SPE 24190 presented at the 1992 SPE/DOE Symposium on Enhanced Oil Recovery, Tulsa, OK, April 22-24.
33. Seright, R.S. and Martin, F.D.: "Effect of Cr^{3+} on the Rheology of Xanthan Formulations in Porous Media: Before and After Gelation," *In Situ* (1992) **16**, No.1, 1-16.
34. Seright, R.S.: "Impact of Dispersion on Gel Placement for Profile Control," *SPE Reservoir Engineering* (Aug. 1991) 343-352.
35. Bryant, S.L., Bartosek, M., and Lockhart, T.P.: "Propagation of Cr(III) in Porous Media and Its Effect on Polymer Gelant Performance," *Journal of Petroleum Sciences and Engineering* (1996) **16**, 1-13.
36. Seright, R.S., Liang, J., and Seldal, M.: "Sizing Gelant Treatments in Hydraulically Fractured Production Wells," *SPE Production & Facilities* (Nov. 1998) 223-229.
37. Zaitoun A. and Kohler, N.: "Two-Phase Flow Through Porous Media: Effect of an Adsorbed Polymer Layer," paper SPE 18085 presented at the 1988 SPE Annual Technical Conference and Exhibition, Houston, Oct. 2-5.
38. Marin, A., Seright, R., Hernandez, M., Espinoza, M., Mejias, F.: "Connecting Laboratory and Field Results for Gelant Treatments in Naturally Fractured Production Wells," paper SPE

77411 presented at the 2002 SPE Annual Technical Conference and Exhibition, San Antonio, Sept. 29- Oct. 2.

39. Alvarez, I. *et al.*: "Water Control Experiences in the Motatan Field Using Specially Designed Gels," paper SPE 69545 presented at the 2001 SPE Latin American and Caribbean Petroleum Engineering Conference, Buenos Aires, Argentina, March 25-28.

40. Kakadjian, S., Rauseo, O., and Mejias, F.: "Dynamic Rheology as a Method to Quantify Gel Strength of Water Shutoff Systems," paper SPE 50751 presented at the 1999 International Symposium on Oilfield Chemistry, Houston, Feb. 16-19.

41. Hernandez, M.I. *et al.*: "Gel Systems Design, Formulation, and Evaluation for Water Control in Venezuelan Wells," presented at the 1998 PNEC 4th International Conference on Reservoir Conformance, Profile Control, and Water and Gas Shutoff, Houston, Aug. 10-12.

42. Marin, A. *et al.*: "Lake Maracaibo Experience Using a New Gel System for Water Control in Oil Producing Wells," presented at the 1998 PNEC 4th International Conference on Reservoir Conformance, Profile Control, and Water and Gas Shutoff, Houston, Aug. 10-12.

43. Liang, J., Lee, R.L., and Seright, R.S.: "Placement of Gels in Production Wells," *SPE Production & Facilities* (Nov. 1993) 276-284; *Transactions* AIME **295**.

44. Aguilera. R.: *Naturally Fractured Reservoirs*, PennWell, Tulsa (1980) 449.

45. Seright, R.S.: "Placement of Gels to Modify Injection Profiles," paper SPE/DOE 17332 presented at the 1988 SPE/DOE Enhanced Oil Recovery Symposium, Tulsa, April 17-20.

46. Sorbie, K.S. and Seright, R.S.: "Gel Placement in Heterogeneous Systems with Crossflow," paper SPE 24192 presented at the 1992 SPE/DOE Symposium on Enhanced Oil Recovery, Tulsa, OK, April 22-24.

47. Seright, R.S, Liang J., Lindquist, B.W., and Dunsmuir, J.H.: "Characterizing Disproportionate Permeability Reduction Using Synchrotron X-Ray Computed Microtomography," *SPE Reservoir Engineering and Evaluation*, Oct. 2002.

48. Ioannidis, M.A. *et al.*: "Comprehensive Pore Structure Characterization Using 3D Computer Reconstruction and Stochastic Modeling," paper SPE 38713, presented at the 1997 SPE Annual Technical Conference and Exhibition, San Antonio, Oct. 5-8.

49. Liang, J., Sun, H., Seright, R.S.: "Reduction of Oil and Water Permeabilities Using Gels," paper SPE 24195 presented at the 1992 SPE/DOE Symposium on Enhanced Oil Recovery, Tulsa, April 22-24.

50. Seright, R.S., Liang, J., and Sun, H.: "Gel Treatments in Production Wells with Water Coning Problems," *In Situ* (1993) **17**(3) 243-272.

51. Seright, R.S.: "Improved Techniques for Fluid Diversion In Oil Recovery," final report, DOE/BC/14880-15, U.S. DOE (Jan. 1996) 97-108.

APPENDIX A: Technology Transfer

Presentations
On October 10, 2002, we held a project review at Shell's offices in Rijswijk, Netherlands.

On October 8, 2002, we presented "Treatment of Fracture Problems Using Gels," at the SPE Applied Technology Workshop, "Emerging Chemical Solutions for Water Control," in Copenhagen, Denmark.

On September 30, 2002, we presented SPE paper 77411, "Connecting Laboratory and Field Results for Gelant Treatments in Naturally Fractured Production Wells," at the 2002 SPE Annual Technical Conference and Exhibition, in San Antonio.

On August 5, 2002, we presented "Permeability Reduction Mechanisms using Microtomography," at the Gordon Research Conference, "Flow & Transport In Permeable Media" at the Proctor Academy in Andover, NH.

On June 12, 2002, we held a project review at BP's offices in Houston.

On April 16, 2002, we presented SPE paper 75158, "An Alternative View of Filter Cake Formation in Fractures," at the 2002 SPE/DOE Symposium on Improved Oil Recovery, in Tulsa.

On April 14, 2002, we presented the Short Course, "Water Shutoff," at the 2002 SPE/DOE Improved Oil Recovery Symposium in Tulsa, OK.

On March 11, 2002, we presented "Use of X-Ray Computed Microtomography to Understand Why Gels Reduce Permeabilty to Water More Than That to Oil," at the 7th International Symposium on Reservoir Wettability in Freycinet, Tasmania, Australia.

On March 8, 2002, we presented "A New Model for Filter Cake Formation in Fractures" at the University of Tulsa, Department of Petroleum Engineering graduate seminar.

On December 19, 2001, we held a project review at Shell's offices in Rijswijk, Netherlands.

On October 1, 2001, we presented the talk, "Characterizing Disproportionate Permeability Reduction Using Synchrotron X-Ray Computed Microtomography," at the 2001 SPE Annual Technical Conference and Exhibition in New Orleans, Louisiana.

Internet Postings On The Project And Software To Download
A description of our research group can be found at the following New Mexico PRRC web site: http://baervan.nmt.edu/randy. The site lists the publications of our group and allows downloads of several papers, reports, and presentations.

This web site also allows downloading of software, Version 2.0 of "Gel Design," for sizing gelant treatments in hydraulically fractured production wells.

Papers And Publications

Seright, R.S, Liang J., Lindquist, B.W., and Dunsmuir, J.H.: "Characterizing Disproportionate Permeability Reduction Using Synchrotron X-Ray Computed Microtomography," *SPE Reservoir Engineering and Evaluation*, Oct. 2002.

Marin, A., Seright, R., Hernandez, M., Espinoza, M., Mejias, F.: "Connecting Laboratory and Field Results for Gelant Treatments in Naturally Fractured Production Wells," paper SPE 77411 presented at the 2002 SPE Annual Technical Conference and Exhibition, San Antonio, Sept. 29-Oct. 2.

Seright, R.S.: "An Alternative View of Filter Cake Formation in Fractures," paper SPE 75158 presented at the 2002 SPE/DOE Symposium on Improved Oil Recovery, Tulsa, April 13-17.

Seright, R.S, Liang J., Lindquist, B.W., and Dunsmuir, J.H.: "Use of X-Ray Computed Microtomography to Understand Why Gels Reduce Permeabilty to Water More Than That to Oil," 7th International Symposium on Reservoir Wettability in Freycinet, Tasmania, Australia, March 12-15, 2002.

Seright, R.S.: "Gel Propagation Through Fractures," *SPE Production & Facilities* (Nov. 2001) 225-232.

Seright, R.S, Liang J., Lindquist, B.W., and Dunsmuir, J.H.: "Characterizing Disproportionate Permeability Reduction Using Synchrotron X-Ray Computed Microtomography," paper SPE 71508 presented at the 2001 SPE Annual Technical Conference and Exhibition, New Orleans, Sept. 30- Oct. 3.

Liang, J., and Seright, R.S.: "Wall-Effect/Gel Droplet Model of Disproportionate Permeability Reduction," *SPE Journal* (September 2001) 268-272.